

The University of Maine

DigitalCommons@UMaine

Electronic Theses and Dissertations

Fogler Library

Summer 8-23-2019

Neuromuscular Development and Phenotypic Variation in Zebrafish Models of Dystroglycanopathy

Erin Bailey

University of Maine, erin.bailey1@maine.edu

Follow this and additional works at: <https://digitalcommons.library.umaine.edu/etd>



Part of the [Cell and Developmental Biology Commons](#)

Recommended Citation

Bailey, Erin, "Neuromuscular Development and Phenotypic Variation in Zebrafish Models of Dystroglycanopathy" (2019). *Electronic Theses and Dissertations*. 3089.

<https://digitalcommons.library.umaine.edu/etd/3089>

This Open-Access Thesis is brought to you for free and open access by DigitalCommons@UMaine. It has been accepted for inclusion in Electronic Theses and Dissertations by an authorized administrator of DigitalCommons@UMaine. For more information, please contact um.library.technical.services@maine.edu.

NEUROMUSCULAR DEVELOPMENT AND PHENOTYPIC VARIATION IN ZEBRAFISH

MODELS OF DYSTROGLYCANOPATHY

By

Erin Bailey

B.S. University of Maine, 2013

A DISSERTATION

Submitted in Partial Fulfillment of the

Requirements for the Degree of

Doctor of Philosophy

(in Biomedical Science)

The Graduate School

The University of Maine

August 2019

Advisory Committee:

Clarissa Henry, Associate Professor of Biological Sciences, University of Maine, Advisor

Gregory Cox, Associate Professor, The Jackson Laboratory

Melissa Maginnis, Assistant Professor of Microbiology, University of Maine

Roger Sher, Research Associate Professor of Neurobiology, Stony Brook University

Robert Wheeler, Associate Professor of Microbiology, University of Maine

Copyright 2019 Erin Bailey

All Rights Reserved

NEUROMUSCULAR DEVELOPMENT AND PHENOTYPIC VARIATION IN ZEBRAFISH

MODELS OF DYSTROGLYCANOPATHY

By Erin Bailey

Dissertation Advisor: Dr. Clarissa Henry

An Abstract of the Dissertation Presented
in Partial Fulfillment of the Requirements for the
Degree of Doctor of Philosophy
(in Biomedical Science)
August 2019

Skeletal muscle is highly conserved among vertebrates and is essential for strength and locomotion. This tissue becomes integrated with the skeletal system via tendons at the myotendinous junction and with the nervous system at the neuromuscular junction. Both of these specialized junctions are rich in extracellular matrix, a protein scaffold that occupies the extracellular space of cells. Skeletal muscle is also highly plastic and can grow in size (hypertrophy) or lose mass (atrophy) in response to genetic or environmental cues. Muscle atrophy is found in individuals battling a number of neuromuscular conditions, including muscular dystrophy.

Muscular dystrophies are a suite of incurable genetic diseases characterized by progressive muscle wasting and weakness. Secondary dystroglycanopathies are a subset of muscular dystrophies that result from mutations in genes that participate in Dystroglycan glycosylation. This process is necessary in order for muscle fibers to interact with the extracellular matrix and connect to nearby tendons and/or nerves. Patients battling secondary dystroglycanopathies experience a wide array of symptoms and severities, even when the

molecular basis of their condition is identical. This prevents doctors and clinicians from providing patients and their families with accurate prognoses.

Multiple roadblocks in our understanding of secondary dystroglycanopathies exist. We previously determined that improving muscle-extracellular matrix adhesion with NAD⁺ supplementation is sufficient to improve muscle structure in primary dystroglycanopathy. However, it is unknown whether this strategy is applicable to secondary dystroglycanopathies. It is also unknown how identical molecular variants of an allele can result in phenotypic variation among individuals with these conditions. Here, we leverage the zebrafish model system to address these gaps. We find that NAD⁺ supplementation prior to muscle development improves muscle structure in an established zebrafish model of secondary dystroglycanopathy, as well as myotendinous junctions and neuromuscular junctions. Additionally, we show that a new zebrafish model of secondary dystroglycanopathy exhibits phenotypic variation and plasticity throughout the first several days of life and is not improved by NAD⁺ supplementation. These studies highlight the importance of viewing secondary dystroglycanopathies as individual conditions at both the basic and clinical levels.

ACKNOWLEDGEMENTS

Thank you to my committee members—Drs. Rob Wheeler, Greg Cox, Roger Sher, and Melissa Maginnis—for your valuable feedback, flexibility, and support throughout graduate school. I especially thank Dr. Greg Cox for insight regarding the molecular biology of the *gmppb* mutant. I owe a special thank you to Dr. Rob Wheeler: thank you for accepting me into your lab as an undergraduate student, igniting my passion and curiosity for the biomedical sciences through your outstanding mentorship, and for encouraging me to pursue a PhD.

I feel incredibly grateful and honored to have been advised by Dr. Clarissa Henry during my doctoral training. Thank you Dr. Henry for taking me on as a PhD student. It was an honor to learn from you and grow as a researcher—both in terms of experimental design and science communication. Thanks to your unique mentoring style with a special emphasis on effective communication and mindset, I have become comfortable with setbacks, venturing into the unknown, and embracing these as part of the scientific process. I am thankful to have spent several years in an interactive lab environment that values both independent thought and collaboration. Perhaps one day we will figure out which one of us is more accident prone...

I also thank all members of the Henry lab, past and present, for their support, friendship, and making the lab a wonderful place to work. I am very fortunate to have worked in such an interactive and collaborative environment. I thank Dr. Michelle Goody for patiently working with me through many day-to-day lab activities, including manuscript editing, experimental advice, effectively communicating my work in writing, and practicing research seminars multiple times in one week. I thank Mary Astumian for advice on many experiments and for keeping the Henry lab running smoothly for many years. Special thanks to all Henry lab graduate students whose time overlapped with mine—Sarah, Beth, Elisabeth, Maggie, and Matt—for your support throughout the years. I thank Michelle, Mary, Sarah, Beth, and Elisabeth

for their contributions to these projects. I thank all undergraduate and high school students I had the pleasure of mentoring, past and present—Joe B., Maggie, Chaya, Ethan, Daisy, Amneh, and Emma. Thank you all for your hard work in the lab and for helping with experiments, deyolking, and image analysis.

Additionally, I thank Dr. Andre Khalil for muscle architecture analysis, Dr. Josh Kelley for the semi-automated NMJ segmentation analysis, and Dr. Ben King and his research team, especially Kodey Silkknitter, for RNA-seq and splicing analysis on the *gmppb* mutants. It was a pleasure to collaborate with all of you and gain a better understanding (or as much of an understanding as a cell/developmental biologist can gain) of the world of bioinformatics and computational biology. I also thank Mark Nilan for exceptional zebrafish care and maintenance. Without your meticulous care of the zebrafish housed in the fish facility, I would not have the experiments described within this dissertation.

I thank the Graduate School of Biomedical Science and Engineering (GSBSE) for fostering an interactive graduate program that has enriched my growth as a scientist. I especially thank former directors Dr. Carol Kim and Dr. Dave Neivandt for their hard work developing the GSBSE into the wonderful, student-centered program that it is today. I also thank my advisor, Dr. Clarissa Henry, for recently taking on the role as program director. I thank Zhen Zhang, Kristen Freeman, and Tammy Crosby for their administrative support throughout my time as a PhD student. Additionally, I thank the School of Biology and Ecology (SBE) for their professional and administrative support, especially Trish Costello, Tracey Walls, Dr. Ann Dieffenbacher-Krall, and Dr. Farahad Dastoor. I am especially thankful for the teaching opportunities provided by SBE that allowed me to develop my teaching and communication skills, and I thank Kevin Tracewski and Dr. Michelle Goody for their mentorship throughout my time as a teaching assistant.

I wish to thank all of my family and friends who have supported me throughout the years. I thank my parents, Michael and Donna Carter, and my grandmother, Joan Carter, for their unconditional love and support, and for encouraging me to follow whichever path in life I wish. Mom—thank you for introducing me to your friend, Dr. Susan Smith. Sue—thank you for presenting your conference poster to me all of those years ago, for providing me with a flavor of what it means to be a scientist, and for inspiring me to pursue a career in developmental and cell biology research. I also thank my family in-law. Lisa, Jason, John, Pam, Spencer, Stephan, Meaghan, Samantha, and Kyle: thank you for your encouragement and for welcoming me into your family. Special thanks to Sam, Holly, Joe M., Iris, Griffin, Charles, Mallory, Kathleen, and Scott for your close friendship and support over the years.

Finally, I thank my husband, Tyson, and our cat, Dusty for their immeasurable love and support throughout this entire process. Dusty, thank you for your endless cuddles and love, even when I am trying to analyze data. Tyson—you mean the world to me. Thank you for your patience, humor, willingness to sit in lab at night or on a weekend during an experiment, and for endlessly challenging me to be the best person that I can possibly be. I couldn't have done this without you. I am excited for our new adventures in Massachusetts that await us!

The projects described in this dissertation were financially sponsored through March of Dimes Award Number: #1-FY14-284 to Dr. Clarissa Henry, NIH R15HD088217 to Dr. Clarissa Henry, a University of Maine Interdisciplinary Undergraduate Research Collaborative Program Grant to Dr. Benjamin King and Dr. Clarissa Henry, University of Maine Graduate Student Government Grants to Erin Bailey, and a University of Maine Chase Distinguished Research Assistantship to Erin Bailey.

TABLE OF CONTENTS

ACKNOWLEDGEMENTS.....	iii
LIST OF TABLES.....	xi
LIST OF FIGURES.....	xii
Chapter	
1. MECHANISMS OF MUSCLE DEVELOPMENT AND DISEASE	1
1.1. Introduction	1
1.2. Structure and function of the myomatrix	3
1.2.1. May the force be with you: ECM components of the myotendinous junction.....	7
1.2.2. Communication breakdown: ECM components of the neuromuscular junction.....	8
1.3. Post-translational modification of Dystroglycan.....	10
1.4. The many faces of dystroglycanopathies	12
1.4.1. Fukutin-related protein (FKRP)	13
1.4.2. GDP-mannose pyrophosphorylase B (GMPPB)	14
1.5. Zebrafish as a model organism for neuromuscular development and disease	16
1.5.1. Zebrafish neuromuscular development.....	16
1.5.2. Modeling muscle disease in zebrafish	18
1.5.3. CRISPR/Cas9 mutagenesis	20
1.6. Concluding remarks	21

2. NAD ⁺ IMPROVES NEUROMUSCULAR DEVELOPMENT IN A ZEBRAFISH MODEL OF FKRP-ASSOCIATED DYSTROGLYCANOPATHY.....	22
2.1. Introduction	22
2.2. Results.....	28
2.2.1. NAD ⁺ supplementation prior to muscle development improves muscle and MTJ structure.....	28
2.2.2. NAD ⁺ /EmergenC are not sufficient to improve vascularization, midbrain-hindbrain development, or the increased unfolded protein response in <i>fkrp</i> morphants	31
2.2.3. Paxillin overexpression does not significantly reduce muscle degeneration	37
2.2.4. NAD ⁺ supplementation after initial muscle development improves MTJs, but not muscle structure	40
2.2.5. NMJ development is disrupted and partially improved with NAD ⁺ supplementation in <i>fkrp</i> morphants.....	40
2.2.6. Muscle specific FKRP expression is not sufficient to rescue <i>fkrp</i> morphants	46
2.3. Discussion.....	49
2.3.1. Cell-matrix adhesion and secondary dystroglycanopathy	49
2.3.2. Benefits of NAD ⁺ supplementation may be restricted to the neuromusculoskeletal system	53
2.3.3. Timing of NAD ⁺ intervention is critical	54

2.3.4. <i>Dag1</i> and <i>fkrp</i> are required for proper NMJ development.....	55
2.3.5. Muscle-specific overexpression of <i>Fkrp</i> is not sufficient to rescue <i>fkrp</i> morphants	56
2.4. Conclusion.....	57
3. PHENOTYPIC VARIATION AND PLASTICITY IN A ZEBRAFISH MODEL OF GMPPB- ASSOCIATED DYSTROGLYCANOPATHY.....	58
3.1. Introduction	58
3.2. Results.....	62
3.2.1 Characterization of <i>gmppb</i> mutants.....	62
3.2.2. NAD ⁺ is not sufficient to improve muscle phenotypes in <i>gmppb</i> mutants.....	65
3.2.3. <i>Gmppb</i> mutants exhibit phenotypic variation in muscle.....	65
3.2.4. <i>Gmppb</i> mutants exhibit neural phenotypes.....	68
3.2.5. <i>Gmppb</i> mutants can be quantitatively separated into mild and severe phenotypes.....	70
3.2.6. A portion of severe <i>gmppb</i> mutants recover to milder phenotypes.....	73
3.3. Discussion.....	73
3.3.1. Alternative splicing in <i>gmppb</i> mutants.....	75
3.3.2. Cell-matrix adhesion and GMPPB-associated dystroglycanopathy.....	78
3.3.3. Primary motoneuron disruption in GMPPB-associated dystroglycanopathy.....	79
3.3.4. Phenotypic variation and plasticity in <i>gmppb</i> mutants.....	81
3.4. Conclusion.....	82

4. FUTURE DIRECTIONS	83
4.1. Introduction	83
4.2. New zebrafish models of FKRP-associated dystroglycanopathy	83
4.3. What are the tissue-specific requirements of Fkrp?	84
4.4. Functional rescue of <i>gmppb</i> mutants	85
4.5. Elucidating the mechanisms underlying phenotypic variation in <i>gmppb</i> mutants	86
4.5.1. Do levels of RNA mis-splicing correlate between mild and severe <i>gmppb</i> mutant phenotypes?	87
4.5.2. Examining differences in muscle regeneration in <i>gmppb</i> mutants	90
4.5.3. Does early motor axon pathfinding influence phenotypic severity?	91
4.5.4. Investigating differences in cell adhesion strength	92
4.6. Concluding remarks	93
5. MATERIALS AND METHODS	94
5.1. Zebrafish husbandry and lines	94
5.1.1. Zebrafish husbandry	94
5.1.2. Construction of new transgenic lines	94
5.1.3. Construction of <i>gmppb</i> mutants	94
5.2. Morpholino injections	95
5.3. NAD ⁺ and EmergenC supplementation	96
5.4. Expression of constructs with the heat shock promoter	96
5.5. Mobility assays	96
5.6. Immunohistochemistry	97
5.7. Myofiber purification and staining	98

5.8. Imaging.....	98
5.9. Statistical analyses	99
5.10. Image Analyses.....	99
5.10.1. Birefringence image analysis	99
5.10.2. Phenotypic classification.....	100
5.10.3. Myotome scoring.....	100
5.10.4. MTJ angles	100
5.10.5. Anisotropy analysis	100
5.10.6. Fluorescence intensity	101
5.10.7. Intersegmental vessel and motoneuron lengths	101
5.10.8. NMJ analysis	101
5.10.9. Myofiber analysis.....	102
BIBLIOGRAPHY	103
APPENDIX A: CATEGORICAL SCORING OF MTJ STAINING INTENSITY	119
APPENDIX B: PRELIMINARY RNA-SEQ DATA OF <i>GMPPB</i> MUTANTS.....	120
BIOGRAPHY OF THE AUTHOR	122

LIST OF TABLES

Table 5.1.	Sequences used to construct <i>gmppb</i> mutants via CRISPR/Cas9 mutagenesis.....	95
Table B.1.	RNA-seq reads of <i>gmppb</i> transcripts in <i>gmppb</i> mutants	120

LIST OF FIGURES

Figure 1.1.	Structure of the myomatrix.....	5
Figure 1.2.	Post-translational modification of alpha-Dystroglycan.....	11
Figure 1.3.	Visualization of zebrafish muscle phenotypes.	19
Figure 2.1.	NAD ⁺ or EmergenC supplementation at gastrulation improves muscle structure and function in <i>fkrp</i> morphants.....	30
Figure 2.2.	NAD ⁺ and EmergenC supplementation at gastrulation do not significantly improve the UPR or vascularization in <i>fkrp</i> morphants	33
Figure 2.3.	Paxillin overexpression does not improve muscle structure in <i>fkrp</i> morphants.....	36
Figure 2.4.	Later NAD ⁺ supplementation improves MTJ structure, but NAD ⁺ and EmergenC are required prior to initial muscle development to improve motility, fiber resilience, and fiber organization	39
Figure 2.5.	<i>Fkrp</i> morphants exhibit NMJ defects and NAD ⁺ and EmergenC treatment prior to muscle development improves NMJ development.....	42
Figure 2.6.	Skeleton length is less disrupted in <i>dag1</i> morphants than in <i>fkrp</i> morphants and is not significantly improved with NAD ⁺ supplementation.....	45
Figure 2.7.	Supplementation with NAD ⁺ or EmergenC after muscle development does not improve NMJ morphology in <i>fkrp</i> morphants.....	48
Figure 2.8.	Muscle-specific overexpression of Fkrp improves MTJ angles, but not motility or fiber resiliency.....	51
Figure 3.1.	Characterization of <i>gmppb</i> mutant zebrafish embryos	64
Figure 3.2.	<i>Gmppb</i> mutants are not rescued by NAD ⁺ supplementation and have abnormal beta-DG localization.....	67
Figure 3.3.	<i>Gmppb</i> mutants exhibit phenotypic variation in muscle	69

Figure 3.4.	<i>Gmppb</i> mutants exhibit neural phenotypes	72
Figure 3.5.	<i>Gmppb</i> mutants can be quantitatively separated into mild and severe phenotypes at 2 dpf	74
Figure 3.6.	A portion of severe <i>gmppb</i> mutants recover to mild phenotypes by 7 dpf.....	77
Figure 4.1.	Potential mechanisms underlying phenotypic variation in <i>gmppb</i> mutant zebrafish	89
Figure A.1.	Scoring of relative MTJ staining intensity.....	119
Figure B.1.	Examples of RNA-seq reads of <i>gmppb</i> transcripts	121

CHAPTER 1

MECHANISMS OF MUSCLE DEVELOPMENT AND DISEASE

1.1 Introduction

Many of the organisms inhabiting planet Earth possess muscle, a highly conserved tissue that contributes to strength and locomotion. Muscle can be divided into three subtypes: cardiac, smooth, and skeletal. In vertebrates, skeletal muscle is associated with organismal locomotion and connects to bones via tendons. It is composed of multinucleated fibers that happen to be some of the largest cells in our bodies. While there are multiple forms of these fibers, the two primary types are slow-twitch muscle fibers that are responsible for endurance and fast-twitch fibers that are associated with speed. Regardless of subtype, all skeletal muscle fibers contain actin and myosin filaments that contribute to muscle contraction (Goody et al., 2017; Hinitz and Hughes, 2007).

Skeletal muscle relies on other tissues in the body in order to properly develop, function, and maintain homeostasis. It becomes integrated with the skeletal system via tendons at myotendinous junctions (MTJs) and with the nervous system at neuromuscular junctions (NMJs). These specialized junctions help achieve proper architecture, function, and homeostasis in skeletal muscle and are rich in extracellular matrix (ECM) (reviewed by (Goody et al., 2015)). The ECM is a scaffold of proteins that occupies the extracellular space of cells and associates with muscle fibers through cell-matrix adhesion complexes. Additionally, skeletal muscle is highly plastic, meaning that it is susceptible to change based on genetic and/or environmental input. Skeletal muscle has the ability to grow in size (hypertrophy) in response to exercise and diet. Conversely, muscle atrophy—or wasting—can occur as a consequence of aging, cachexia, a lack of exercise, or neuromuscular diseases. Additionally, the degree to which individuals battling conditions that affect muscle tissue can regenerate skeletal muscle is highly variable.

Neuromuscular diseases are disorders that impair muscle and/or peripheral nerve function. These conditions are prevalent in humans, and some notable examples include congenital myasthenic syndrome, a genetic disorder of the NMJ, and muscular dystrophies, a suite of heritable diseases associated with progressive muscle wasting and weakness. Muscular dystrophies vary remarkably in terms of the genetic basis, age of onset, severity, and muscle groups affected. Patients battling the same subtype of muscular dystrophy sometimes experience drastically different symptoms and severities, even when the molecular basis of their condition is identical.

Several roadblocks in our understanding of muscle development and disease currently exist. The adhesion of muscle fibers to the ECM is disrupted in several forms of muscular dystrophy. Recent work suggests that improving muscle cell-matrix adhesion is beneficial for some of these conditions. In particular, it has been shown that increasing levels of functionally redundant receptors can compensate in the absence of others (Goody et al., 2012; Sarathy et al., 2017). However, it is necessary to determine the breadth at which this strategy is applicable. Chapter 2 describes a study that addresses this in a zebrafish muscular dystrophy model that has not been examined in this context. We determined that one previously described method of enhancing cell-ECM adhesion improves muscle structure and function, as well as MTJ and NMJ morphology. However, another previously described method of improving muscle structure has a neutral effect in this model. These studies provide insight into how these specialized junctions are affected in dystroglycanopathies and highlight the importance of viewing different types of muscular dystrophies as individual conditions.

An additional gap in the field of muscle biology is understanding how phenotypic variation develops among individuals carrying the same disease-causing mutation. Although the disease-causing alleles of many forms of neuromuscular disease have been identified, the

unpredictable nature of some of these conditions prevents doctors and clinicians from providing patients and their families with accurate prognoses. Chapter 3 details a study that begins to address this gap. We engineered a zebrafish mutant by targeting a gene associated with neuromuscular phenotypic variation via CRISPR/Cas9 mutagenesis. These fish exhibit phenotypic variation and plasticity in muscle throughout the first several days of life. Given the idiosyncratic nature of many neuromuscular diseases, understanding the mechanisms behind phenotypic variation and plasticity can provide a valuable perspective on how to approach these conditions from a clinical lens.

Throughout my graduate training in biomedical science, I learned that understanding the basic biology of muscle homeostasis is key to creating an environment conducive to optimal muscle health. Although it is important to consider how muscle development and homeostasis relates to muscle disease, providing a baseline for translational research requires an understanding of the proteins, cellular structures, and neighboring tissues that work in concert to orchestrate muscle homeostasis. The overarching goal of my doctoral dissertation research was to leverage the zebrafish model system to answer questions regarding cell-matrix adhesion, neuromuscular development, and phenotypic variation in zebrafish models of muscle disease.

1.2. Structure and function of the myomatrix

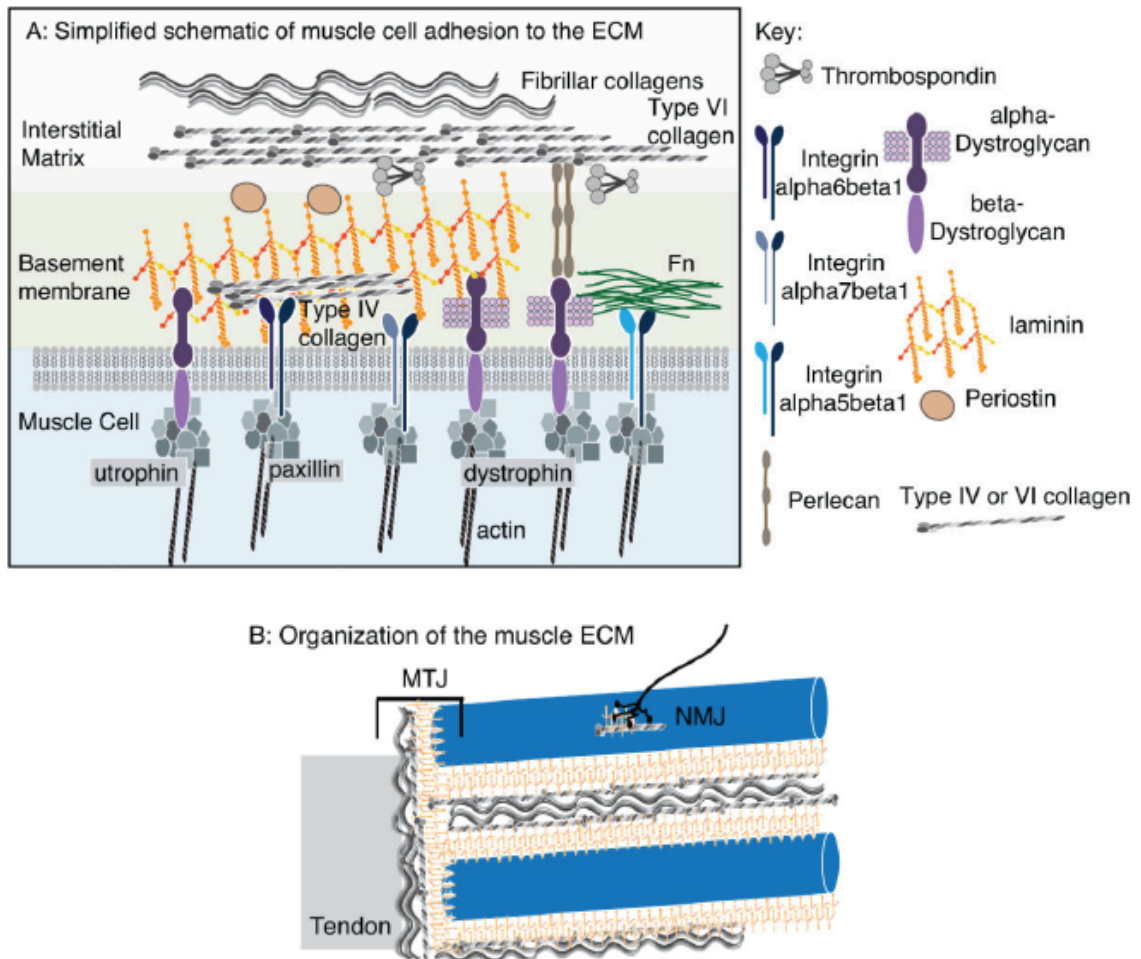
Skeletal muscle is necessary for strength and locomotion and is comprised of bundles of individual muscle fibers. Although the muscle fibers themselves are critical for homeostasis of this organ, they must adhere to their surrounding extracellular matrix (ECM) to achieve homeostasis. Muscle-associated ECM, or the myomatrix, is composed of a vast array of extracellular proteins that link to structures within the muscle cell via transmembrane receptors (Fig. 1.1A). The myomatrix provides structure and mediates bidirectional signaling between cells

and their microenvironments (Goody et al., 2015). These attributes are important for skeletal muscle, given its recurrent cycles of tension, contraction, and relaxation.

One specialized myomatrix component that is important for structural integrity and signaling is the basement membrane. Basement membranes surround muscle fibers and contain the fibrous proteins collagen-IV and laminin (Goody and Henry, 2010; Goody et al., 2015). Laminin is composed of three types of chains that trimerize to form a complete heterotrimeric protein (Miner and Yurchenco, 2004). The specific chains include five alpha, four beta, and three gamma chains (Miner and Yurchenco, 2004). Different combinations of laminin heterotrimers associated with different developmental stages and/or physiological structures. For example, laminin-111 (lamininalpha1beta1gamma1) is primarily expressed during early muscle development (Gullberg et al., 1999) and is later replaced by laminin-211 (lamininalpha2beta1gamma1) (Sasaki et al., 2002). Mutations in *LAMA2*, which encodes the lamininalpha2 chain, are associated with merosin-deficient muscular dystrophy (MDC1A) (Helbling-Leclerc et al., 1995). Therefore, lamininalpha2 is important for muscle homeostasis and cell-matrix adhesion.

But how do laminins interact with muscle? Laminin interacts with two types of transmembrane receptor complexes that connect muscle fibers to their surrounding microenvironments. The integrin heterodimers are one of these receptor complexes. Integrin heterodimers are composed of alpha and beta subunits and possess three distinct conformations—active, inactive, and ligand-bound (Askari et al., 2009). Extracellularly, integrin complexes have different ligands within the myomatrix, depending on the specific heterodimer. For example, integrinalpha5beta1 serves as a receptor for fibronectin, whereas integrinalpha6beta1 and integrinalpha7beta1 are receptors for laminin (Fig. 1.1A) (Goody et al., 2015). Different integrin complexes are more prevalent at different stages of an organism's life.

Figure 1.1. Structure of the myomatrix. (A) Schematic depicting adhesion complexes that link the actin cytoskeleton of muscle fibers with basement membranes that are rich in laminin and collagen IV. **(B)** The myomatrix (tan chains) surrounds the entirety of muscle tissue, bundles of muscle fibers, and individual fibers (blue). The myotendinous junction (MTJ) and neuromuscular junction (NMJ) link muscle fibers to tendons (gray) and nerves (black) respectively. The MTJ and NMJ interact with muscle fibers via cell-ECM interactions. Originally from *Goody et al., 2015*.



Integrinalpha6beta1 is the prevailing isoform throughout early muscle development and interacts with laminin-111 (Bajanca et al., 2006; Bronner-Fraser et al., 1992), whereas integrinalpha7beta1 is the major laminin-binding integrin isoform in mature skeletal muscle (Burkin and Kaufman, 1999) and interacts with laminin-211 (Holmberg and Durbeej, 2013). Loss

of integrin α 7 is associated with muscular dystrophy (Hayashi et al., 1998; Mayer et al., 1997); thus, functional integrin α 7 β 1 heterodimers are essential for muscle homeostasis.

In addition to integrin receptor complexes, the dystrophin and utrophin glycoprotein complexes (DGC and UGC) also connect the actin cytoskeleton of muscle fibers to the laminin-rich basement membrane in the myomatrix (Fig. 1.1A) (Ervasti and Campbell, 1993). The DGC contains dystrophin and is predominantly at the myotendinous junction (Ervasti and Campbell, 1993), whereas the UGC is predominantly found at the neuromuscular junction (Deconinck et al., 1997). These complexes also contain Sarcoglycan, Sarcospan, and Dystroglycan (Michele and Campbell, 2003). Dystroglycan (DG) is a major component of this complex and contains a transmembrane beta subunit and an extracellular alpha subunit. This alpha subunit serves as a receptor for laminin, perlecan, neurexin, and agrin (Michele and Campbell, 2003). The alpha subunit of DG binds to these ECM proteins when it is glycosylated by a team of enzymes that synthesize a glycan ligand for these proteins (detailed in Section 1.3). Given that the DGC is necessary for muscle fibers to anchor to their extracellular environments, proper assembly of the DGC is critical for muscle development and homeostasis.

The adhesion complexes that establish connections between muscle fibers and their extracellular environments are functionally redundant in their role of indirectly connecting the actin cytoskeleton of the myomatrix (Goody et al., 2012). These complexes are also critical for linking muscle fibers to two specialized junctions—the myotendinous junction (MTJ) and the neuromuscular junction (NMJ). These specialized junctions are rich in ECM and connect muscle tissue to nearby tendons and nerves respectively (Goody et al., 2015) (Fig. 1.1B). The following subsections will describe both of these regions in greater detail.

1.2.1. May the force be with you: ECM components of the myotendinous junction

Tendons provide an essential connection between skeletal muscle and bone that facilitates locomotion. While tendons themselves serve a bridge between muscle and bone, the region connecting muscle to tendons is known as the myotendinous junction (MTJ). This specialized junction is a structural unit that consists of extracellular matrix proteins, transmembrane receptors, and sarcolemma (the transmembrane region of muscle fibers) and extends to the cytoskeleton. On the muscle end, the actin cytoskeleton is indirectly linked to transmembrane proteins that interact with ECM components (Goody et al., 2017). On the tendon side, tenocytes (tendon cells) produce collagen fibers that connect to the rest of the ECM (Charvet et al., 2012). The MTJ is a critical structural component of muscle and is the major site of force transmission (Charvet et al., 2012) that helps muscle contraction drive movement.

Several well-known ECM components are enriched at the MTJ. Collagen-I and tenascin are highly concentrated on the tendon side of the junction, collagen-VI is distributed throughout the myomatrix and provides structural stability of the sarcolemma during muscle contraction, and laminin and collagen-IV are abundant in the muscle basement membrane (Charvet et al., 2012; Goody et al., 2015). Throughout development, MTJ undergoes changes in composition, especially in zebrafish. For example, fibronectin is initially present at somite boundaries, but eventually becomes downregulated (Snow and Henry, 2009). An increase in laminin-111 at the MTJ correlates with fibronectin downregulation (Jenkins et al., 2016; Snow et al., 2008a). A shift from laminin-111 expression to laminin-211 expression also occurs at the MTJ in zebrafish, mice, and humans, and laminin-211 then remains the prevailing laminin isoform at the MTJ (Charvet et al., 2012; Goody et al., 2017).

Several additional ECM components play important roles in MTJ maintenance. Collagen-VI is distributed throughout the myomatrix and provides the sarcolemma with structural

stability throughout muscle contraction (Telfer et al., 2010). Thrombospondins bind to transmembrane receptors and ECM proteins to mediate cell-matrix adhesion (Charvet et al., 2012). In *Drosophila*, thrombospondin is synthesized and secreted by tenocytes and binds to muscle-specific integrin receptors (Subramanian et al., 2007). Zebrafish *thrombospondin4b* (*tsp4b*) is critical for basement membrane assembly in tendons and for muscle attachment during MTJ development and repair (Subramanian and Schilling, 2014). Deficiencies of ECM components that participate in MTJ development and homeostasis are linked to aberrant muscle development (Hall et al., 2007; Odenthal et al., 1996; Snow et al., 2008a; Subramanian and Schilling, 2014; Telfer et al., 2010; Welser et al., 2009). Therefore, appropriate timing and expression of these proteins is critical for MTJ development and homeostasis.

1.2.2. Communication breakdown: ECM components of the neuromuscular junction

In addition to muscle tissue and MTJs, locomotion also depends on the initiation and regulation of muscle contraction from nerves. This occurs via the neuromuscular junction (NMJ), a synapse that lies at the interface of motoneurons and muscle fibers. Motoneurons that innervate muscle fibers serve as the presynaptic component and release neurotransmitters. In vertebrates, acetylcholine is the neurotransmitter that is released, which travels to postsynaptic acetylcholine receptors (AChRs) on the surface of muscle cells (Singhal and Martin, 2011). Formation of the vertebrate NMJ relies on careful crosstalk of initial muscle and motoneuron development. Embryonic muscle fibers are prepatterned with aneural AChRs in the medial regions of muscle prior to innervation, the motoneuron migrates to the muscle fiber for innervation, and synaptogenesis occurs (reviewed by (Burden et al., 2018; Tintignac et al., 2015; Wu et al., 2010)). This process in zebrafish can be studied in the context of slow-twitch and fast-twitch muscle fibers (discussed in Section 1.5.1).

Vertebrate NMJ development and homeostasis also relies on myomatrix components and their receptors. Muscle fibers secrete and deposit laminin and collagen IV, the two primary basement membrane proteins, into the synaptic cleft to form a basement membrane that provides a barrier between the presynaptic motoneuron and the postsynaptic muscle fiber (Singhal and Martin, 2011). The synaptic laminins that are prevalent at the NMJ are distinct from those that are prevalent at the MTJ and include the laminin β 2 chain. These laminins include laminin-221 (laminin α 2 β 2 γ 1), laminin-421 (laminin α 4 β 2 γ 1), and laminin-521 (laminin α 5 β 2 γ 1) (Singhal and Martin, 2011). The NMJ also contains several additional and transmembrane components that are indispensable for NMJ development and maintenance and have been nicely reviewed (Pilgram et al., 2010; Singhal and Martin, 2011; Tintignac et al., 2015; Wu et al., 2010). Agrin is a heparin sulfate proteoglycan (HSPG) protein in the ECM that contributes to AChR clustering and NMJ stabilization, and neural agrin is secreted by motoneurons and released into the basement membrane (Pilgram et al., 2010; Singhal and Martin, 2011; Tintignac et al., 2015; Wu et al., 2010). Agrin interacts with several receptors on the post-synaptic membrane, including α -DG, muscle-specific receptor tyrosine kinase (MuSK), and the agrin co-receptor Lrp4 (Pilgram et al., 2010; Singhal and Martin, 2011; Tintignac et al., 2015; Wu et al., 2010). MuSK is necessary for AChR prepatterning and post-synaptic differentiation, is activated by the protein Dok7, and interacts with rapsyn, leading to MuSK signaling (Singhal and Martin, 2011; Tintignac et al., 2015). Thus, MuSK is an especially critical contributor to NMJ development and homeostasis.

Proper coordination between muscle, motoneurons, and the signaling components that contribute to AChR clustering and maintenance is key for NMJ assembly and function. Autoantibodies against AChRs, MuSK, and Lrp4 are associated with autoimmune myasthenia gravis, a progressive NMJ disease, in human populations (Pevzner et al., 2012). Studies have also

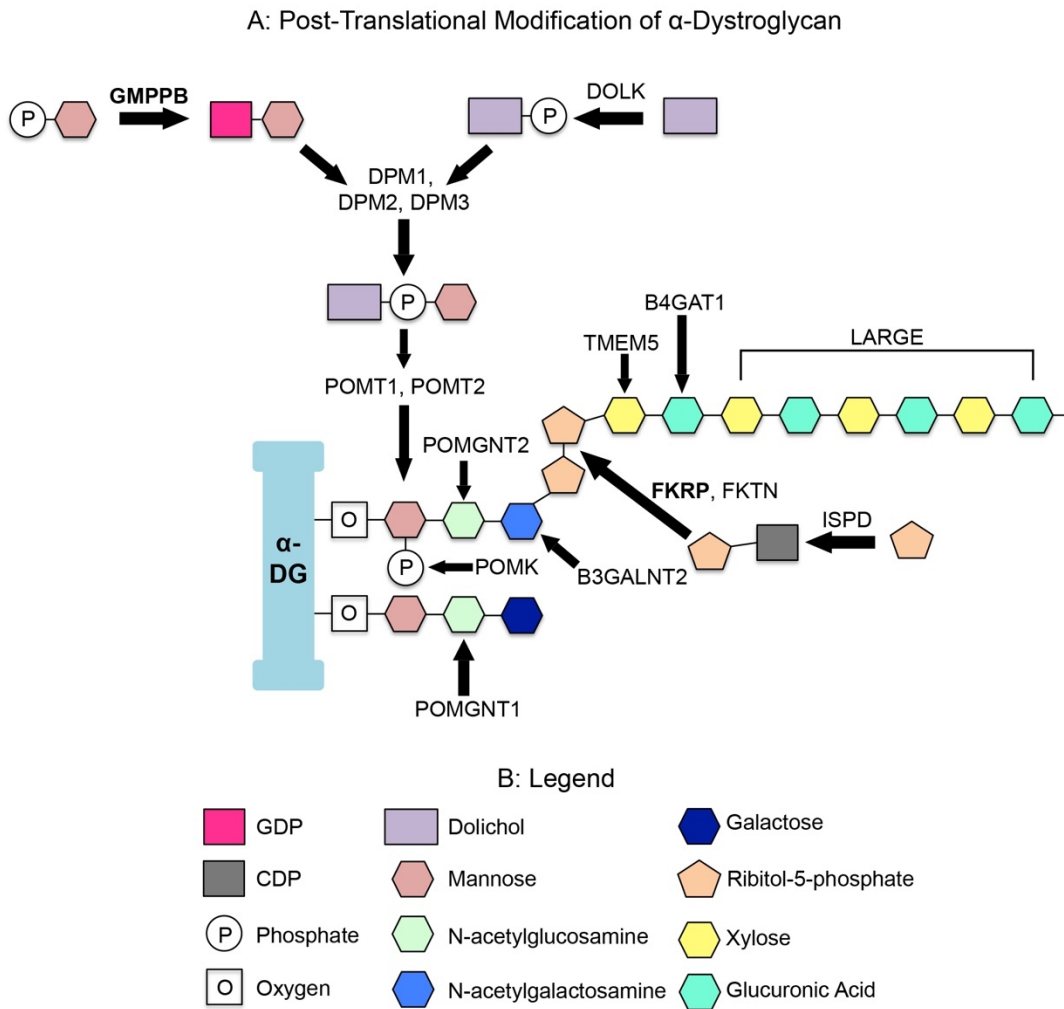
detected NMJ abnormalities in mouse models of muscular dystrophies. These include Duchenne Muscular Dystrophy (Pratt et al., 2015), the most well-known form of the disease, as well as muscular dystrophies associated with compromised DG (Herbst et al., 2009; Saito et al., 2007). Chapters 2 and 3 will discuss how the NMJ is disrupted in zebrafish models of dystroglycanopathy.

1.3. Post-translational modification of Dystroglycan

As detailed in Section 1.2, the dystrophin glycoprotein complex (DGC) is a major receptor complex that connects the actin cytoskeleton of muscle fibers to the laminin-rich basement membrane in the myomatrix (Ervasti and Campbell, 1993). Major components of this complex include dystrophin that is linked to f-actin and DG. Several muscular dystrophies are associated with mutated components of the DGC. Mutations in Dystrophin, the intracellular component of the DGC, are associated with Duchenne and Becker Muscular Dystrophies. Compromised DG is associated with a broad suite of muscular dystrophies known as dystroglycanopathies.

DG serves as a major receptor for a number of ECM proteins, including laminin. Like many other components of the ECM and/or the neuromusculoskeletal system, α -DG is heavily glycosylated. This process is necessary in order for interact with laminin and other ECM proteins that are involved in cell-matrix adhesion. Multiple enzymes work in concert to synthesize this glycan (Fig. 1.2) (reviewed by (Nickolls and Bönnemann, 2018; Taniguchi-Ikeda et al., 2016). DOLK, GMPPB, DPM1, DPM2, and DPM3 help synthesize dolichol phosphate mannose precursors used in o-mannosylation reactions (Carss et al., 2013; van Tol et al., 2019). When co-expressed, POMT1 and POMT2 use these precursors to add mannose (o-linked) directly

Figure 1.2. Post-translational modification of alpha-Dystroglycan. (A) Multiple enzymes work together to synthesize a glycan chain that links alpha-DG (light blue) to ECM proteins such as laminin. This process is important for muscle-ECM adhesion. FKRP and GMPPB (bold font) will be the focus of subsequent chapters in this dissertation. **(B)** Legend for molecules depicted in (A). Adapted from Carss et al. (2013), Nickolls and Bönnemann (2018), Taniguchi-Ikeda et al., 2016, and van Tol et al. (2019).



to alpha-DG (Manya et al., 2004). N-acetylglucosamine is subsequently added to mannose via POMGNT1 and POMGNT2 (Ogawa et al., 2013; Yoshida et al., 2001), and the mannose modified by POMGNT2 is phosphorylated by POMK (Yoshida-Moriguchi et al., 2013). B3GALNT2 adds N-acetylgalactosamine to the N-acetylglucosamine synthesized by POMGNT2 (Yoshida-Moriguchi et al., 2013). ISPD then supplies CDP-ribitol that is used by FKRP and FKTN to produce a tandem

ribitol 5-phosphate repeat (Gerin et al., 2016; Kanagawa et al., 2016). TMEM5 then catalyzes the addition of xylose (Praisman et al., 2016), followed by the addition of glucuronic acid by B4GAT1 (Willer et al., 2014). Finally, LARGE synthesizes a repeating unit of xylose and glucuronic acid that serves as the ligand for laminin (Inamori et al., 2012). Completion of this process in the appropriate steps is necessary for muscles to adhere to their extracellular environments and achieve homeostasis. Failure of DG to undergo glycosylation is associated with a complex subset of muscular dystrophies known as secondary dystroglycanopathies.

1.4. The many faces of dystroglycanopathies

The dystroglycanopathies are a group of molecularly distinct muscular dystrophies that are associated with compromised DG function. Primary dystroglycanopathy occurs with mutations in DG (Frost et al., 2010; Hara et al., 2011), whereas secondary dystroglycanopathies occur due to mutations in genes that encode enzymes that participate in alpha-DG glycosylation (Muntoni et al., 2011). A number of molecularly distinct secondary dystroglycanopathies have been identified (Nickolls and Bönnemann, 2018); however, the clinical presentation of these conditions is highly variable, even when the disease-causing allele is known. While some individuals with secondary dystroglycanopathies experience limb-girdle muscular dystrophies that are more likely to develop in adolescence, others experience severe congenital muscular dystrophies (CMDs) (Muntoni et al., 2011). Individuals with CMDs associated with dystroglycanopathy often experience eye and/or brain involvement in the form of Muscle-Eye Brain Disease, Walker-Warburg Syndrome, or Cobblestone Lissencephaly (Nickolls and Bönnemann, 2018). This level of variation prevents clinicians from providing their patients with accurate prognoses. Poor understanding of the basic biological mechanisms of phenotypic variation and plasticity in neuromuscular diseases are a major roadblock to understanding

phenotypic variation in the dystroglycanopathies. Chapter 3 describes a study regarding phenotypic variation in new zebrafish dystroglycanopathy model.

1.4.1. Fukutin-related protein (FKRP)

Fukutin-related protein (FKRP) participates in Dystroglycan (DG) glycosylation and is associated with dystroglycanopathy in humans (Brockington et al., 2001). As previously mentioned, FKRP is a ribitol-5 phosphate transferase that, along with Fukutin (FKTN), uses CDP-ribitol to form a tandem ribitol-5-phosphate (Gerin et al., 2016; Kanagawa et al., 2016) that links N-acetylgalactosamine with xylose (Taniguchi-Ikeda et al., 2016). Failure of this linkage to form prevents completion of alpha-DG glycosylation, reducing its affinity to bind to ECM ligands such as laminin.

Like other dystroglycanopathies, patients harboring FKRP mutations present with phenotypic variability. Individuals with FKRP-associated dystroglycanopathy may develop limb-girdle muscular dystrophy 2I (LGMD2I) or congenital muscular dystrophy with or without eye and brain involvement, depending on the specific molecular variant (Stensland et al., 2011; Van Reeuwijk et al., 2010). Although some genotype-phenotype correlation is present in patients with *FKRP* mutations (Beltran-Valero de Bernabé et al., 2004; de Bernabé et al., 2003; Stensland et al., 2011; Van Reeuwijk et al., 2010), there is sometimes phenotypic variation among individuals with identical mutations, particularly in regard to muscle pathology, levels of glycosylated alpha-DG, and age of onset (Stensland et al., 2011). This suggests genetic or environmental cues could contribute to disease progression in FKRP-associated dystroglycanopathy, as well as features other than muscle pathology and levels alpha-DG glycosylation.

Several animal models of FKRP-associated dystroglycanopathy have been engineered. These include *Fkrp* mutant mice (Ackroyd et al., 2009; Blaeser et al., 2013; Chan et al., 2010),

fkrrp morphant zebrafish, (Kawahara et al., 2010; Lin et al., 2011; Thornhill et al., 2008), and *fkrrp* mutant zebrafish (Serafini et al., 2018). Previous animal models have focused on levels of alpha-DG glycosylation, regenerative capacity, and functional rescue. Gene therapy (Qiao et al., 2014; Thomas et al., 2016; Tucker et al., 2018; Vannoy et al., 2017) estrogen receptor modulators (Wu et al., 2018), and exogenous ribitol supplementation (Cataldi et al., 2018) improve muscle in mouse models. However, the efficacy of some therapies decreases if administered later in the mouse's lifespan (Cataldi et al., 2018; Vannoy et al., 2017). This suggests that early intervention is most beneficial for these conditions. However, little is known regarding how MTJs and/or NMJs are affected in the context of FKRP deficiency. Chapter 2 describes the involvement of the MTJ and NMJ in a zebrafish model of FKRP-associated dystroglycanopathy and implicates early improvement of cell-matrix adhesion as a mechanism for improving muscle structure, function, and specialized muscle junctions.

1.4.2. GDP-mannose pyrophosphorylase B (GMPPB)

GDP-Mannose Pyrophosphorylase B (GMPPB) is an enzyme that synthesizes GDP-mannose, a molecule used in several glycosylation reactions. In addition to O-mannosylation of alpha-DG, GMPPB also participates in GPI-anchor formation, N-glycosylation, and C-mannosylation (Carss et al., 2013). Given that multiple myomatrix and NMJ proteins are also glycosylated, it is possible that GMPPB may have additional effects on neuromuscular skeletal system beyond alpha-DG modification. Unsurprisingly, mutations in *GMPPB* are associated with dystroglycanopathies that vary drastically in their clinical presentation.

Similar to FKRP-associated dystroglycanopathy, cases of congenital muscular dystrophies and limb-girdle muscular dystrophies (specifically Limb-Girdle Muscular Dystrophy Type 2T (LGMD2T)) have been documented in individuals harboring *GMPPB* mutations (Balcin et al., 2017; Cabrera-Serrano et al., 2015; Carss et al., 2013; Jensen et al., 2015; Montagnese et al.,

2017; Oestergaard et al., 2016; Raphael et al., 2014). Although molecular variants that specifically correlate with LGMD2T or congenital muscular dystrophies have been detected (Jensen et al., 2015), there is still a great deal of phenotypic variation in GMPPB-associated dystroglycanopathy. Additional conditions have been observed in patients with *GMPPB* mutations. Congenital myasthenic syndrome, a disease of the NMJ, has been detected in individuals harboring mutations with the same molecular basis as LGMD2T (Belaya et al., 2015; Luo et al., 2017; Montagnese et al., 2017; Rodríguez Cruz et al., 2016). Patients with the most common *GMPPB* mutation, c.79 G>C, have ranged between 2 and 62 years old at the age of symptomatic onset (Bharucha-Goebel et al., 2015; Montagnese et al., 2017). Cases of epilepsy and one case of autism spectrum disorder (Astrea et al., 2018; Raphael et al., 2014) have also been documented. These studies highlight the need to elucidate the mechanisms underlying phenotypic variation in GMPPB-associated dystroglycanopathy in order to accurately predict the course of the disease.

Given the poor genotype-phenotype correlation observed in these conditions, the fact that new individuals with *GMPPB* mutations are often identified (Sun et al., 2019), and the lack of genomic animal models for GMPPB-associated dystroglycanopathy, it is critical to study these conditions outside of the clinic. In terms of model systems, *GMPPB* mutations are linked with GMPPB mislocalization in cultured myoblasts, and *gmppb* morphant zebrafish have been superficially characterized and exhibit hypoglycosylated alpha-DG and muscle phenotypes (Carss et al., 2013). There are currently no published genomic models for this disorder in any model organism. Chapter 3 documents a study where a *gmppb* mutant was engineered to study the mechanisms underlying phenotypic variation in the dystroglycanopathies.

1.5. Zebrafish as a model organism for neuromuscular development and disease

Mammalian model systems have played a key role in elucidating the molecular and cellular biology of neuromuscular disorders. However, zebrafish (*Danio rerio*) offer many advantages for studying neuromuscular development and disease. Zebrafish embryos are externally fertilized and develop at a faster time scale than rodents. Embryonic and larval zebrafish are also optically transparent (Gibbs et al., 2013), which allows individuals to easily visualize their internal tissues under a fluorescence microscope, either through live imaging transgenics or with fixed immunostaining. This attribute allows one to easily image zebrafish muscle fibers, motoneurons, myotendinous junctions, and neuromuscular junctions throughout the embryonic and early larval stages. Other advantages of zebrafish as a model include high fecundity, low maintenance cost, and the ability to perform high-throughput screening in large numbers (Gibbs et al., 2013). Herein, the processes of neuromuscular development in zebrafish will be described, as well as current zebrafish models of muscular dystrophy and the emergence of CRISPR/Cas9 genome editing technology.

1.5.1. Zebrafish neuromuscular development

Zebrafish muscle is organized into chevron-shaped segments called myotomes, which are derived from somites. Like mammals, zebrafish possess slow-twitch muscle fibers that are associated with endurance and fast-twitch muscle fibers linked to speed. Zebrafish muscle fibers can be divided into subtypes that can be identified by specific genetic markers: superficial slow-twitch muscle fibers, slow-twitch muscle pioneers, medial fast-twitch muscle fibers, and fast-twitch fibers (Wolff et al., 2003). In contrast to mammals, zebrafish subtypes of zebrafish muscle fibers spatially occupy distinct regions in the myotome (Goody et al., 2017). This allows for easy identification of each fiber type, as well as how it is affected in the context of muscle development and disease.

But how does a zebrafish muscle segment with multiple fiber types develop? The paraxial mesoderm is initially segmented into somites. Somites are composed of four cell types—epithelial, mesenchymal, adaxial (slow-twitch fiber precursors), and anterior border cells—and give rise to multiple tissues, including muscle fibers, skeleton and tendon components, hematopoietic stem cells, and dermis of the skin (Goody et al., 2017). When muscle begins to develop, adaxial cells located in the medial plane of muscle elongate and subsequently migrate to the lateral surface of muscle (Devoto et al., 1996). This slow-twitch fiber migration induces fast-twitch muscle fiber morphogenesis (Henry and Amacher, 2004). These fast-twitch fibers elongate, and the terminal ends attach to the somite boundaries and form myotubes (Snow et al., 2008b). Muscle cell fusion occurs to form multinucleated muscle fibers (Powell and Wright, 2011). Finally, sarcomeres composed of thick myosin filaments and thin actin filaments are assembled into a myofibril that is essential for muscle contraction (Goody et al., 2017; Hinitz and Hughes, 2007). All of these components must be actively maintained in order to achieve proper muscle homeostasis.

Motoneuron development and NMJ formation in zebrafish occurs simultaneously with muscle morphogenesis. Initially, fish muscle is innervated by the caudal (CaP), middle (MiP) and rostral (RoP) primary motoneurons (Myers et al., 1986). Secondary motoneurons follow similar innervation paths several hours later in development (Beattie, 2000; Fashena and Westerfield, 1999). Medial slow-twitch muscle cells secrete ECM proteins that facilitate primary motoneuron guidance and exit from the neural tube (Guillon et al., 2016; Schweitzer et al., 2005). The medial slow muscle fiber precursors (adaxial cells) are prepatterned with aneural AChR clusters prior to the motoneurons reaching the choice point (Flanagan-Steet et al., 2005; Panzer et al., 2005). When the primary motoneurons leave the choice point, the CaP extends ventrally, the MiP extends dorsally, and the RoP remains in the middle of the myotome (Lewis and Eisen, 2003).

Initially, synapses form on muscle fibers located in close proximity to the choice point, followed by the medial muscle fibers, and are present in the lateral muscle by 48 hours post-fertilization (hpf) (Panzer et al., 2005). Chapters 2 and 3 both describe studies where fast-twitch muscle fiber innervation was quantified in zebrafish models of dystroglycanopathy.

1.5.2. Modeling muscle disease in zebrafish

Over the past two decades, zebrafish have emerged as a valuable model for studying muscular dystrophies and other neuromuscular diseases. The optical transparency of zebrafish embryos allows one to easily observe zebrafish muscle through transgenic zebrafish or immunohistochemistry. Staining embryos for f-actin with fluorescently tagged phalloidin visualizes the zebrafish muscle fibers (Fig. 1.3A-C) and can detect several muscle abnormalities (Goody et al., 2017). Typically, zebrafish muscle fibers are organized into chevron-shaped muscle segments. When muscle undergoes appropriate development and maintenance, these fibers remain attached to the MTJ (Fig. 1.3A). In some cases, muscle fibers fail to be captured by the myotome boundary and extend past the MTJ. This phenomenon is known as MTJ failure (Fig. 1.3B) (Goody et al., 2017). At other times, muscle fibers detach from the boundaries, which is indicative of dystrophy (Fig. 1.3C). Damage to the sarcolemma may or may not accompany this fiber detachment (Goody et al., 2017). Therefore, both muscle and MTJ phenotypes at high magnification can be readily quantified in zebrafish models of muscle disease. This allows researchers to analyze muscle and MTJ abnormalities and delve into the mechanisms contributing to these phenotypes.

Compromised zebrafish muscle can also be detected via live, non-invasive birefringence imaging. This technique uses polarized light to detect muscle fibers that are in-tact and have maintained their integrity (Berger et al., 2012; Gibbs et al., 2013). Such fibers retain their birefringence and appear as well organized, bright muscle segments under polarized light

Figure 1.3. Visualization of zebrafish muscle phenotypes. (A-C) Anterior left, dorsal top, side-mounted 48 hpf embryos stained for f-actin (phalloidin, gray) to visualize muscle fibers. **(A)** Control embryo. **(B)** Zebrafish embryo with fibers crossing the MTJ (MTJ failure, yellow arrowhead). **(C)** Zebrafish embryo with fiber detachment (dystrophy, white arrowhead). **(D-E)** Anterior left, dorsal top, side-mounted 4 dpf zebrafish imaged live for birefringence. **(D)** Control embryo with normal birefringence. **(E)** Embryo with muscle degeneration indicated by a patchy area of birefringence (blue arrowhead).

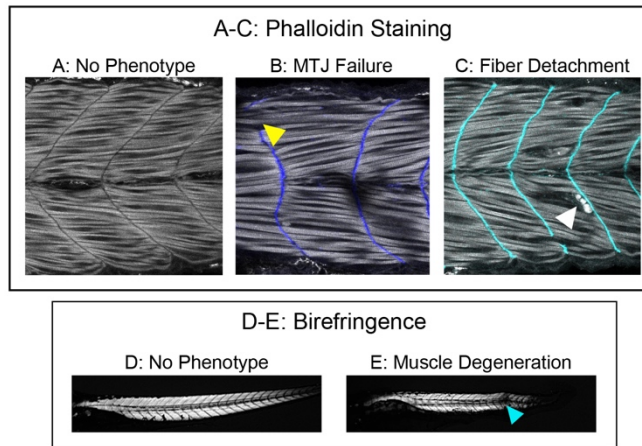


(Fig. 1.3D). In contrast, patchy areas of birefringence are indicative of muscle damage (Fig. 1.3E) and reduced brightness indicates muscle fiber disorganization (Gibbs et al., 2013). This technique allows for rapid screening and quantification of muscle phenotypes (Berger et al., 2012), particularly in regard to “mild,” “moderate,” or “severe” abnormalities in muscle development and homeostasis.

In addition to their visual advantages, zebrafish are also a suitable model for muscle disease at the genetic level. Many genes associated with the muscular dystrophies and other muscle diseases are conserved in zebrafish (Gibbs et al., 2013; Goody et al., 2017), making them an appropriate molecular model for the disease. A number of muscular dystrophies have been modeled in the fish by impairing expression of these genes, both with genomic manipulation and morpholino technology. Morpholinos are oligonucleotides that bind to RNA to block gene expression. Numerous morpholinos have been developed to target the transcripts of muscular

dystrophy genes (Carss et al., 2013; Guyon et al., 2003; Kawahara et al., 2010; Marchese et al., 2016; Moore et al., 2008; Parsons et al., 2002; Postel et al., 2008; Roscioli et al., 2012; Stevens et al., 2013; Thornhill et al., 2008). However, there are disadvantages to using morpholinos. In particular, the effects of morpholinos often fade by 5 days post-fertilization (dpf) (Gibbs et al., 2013). An alternative approach is to use zebrafish harboring genomic mutations for a gene of interest. Several zebrafish models of muscular dystrophy, including *sapje* (*dystrophin* mutants), *candyfloss* (*lamininalpha2* mutants), and *patchytail* (*dystroglycan* mutants) were identified from ENU mutagenesis screens (Bassett and Currie, 2004; Gupta et al., 2011; Hall et al., 2007). Additionally, recent genome editing technology, including CRISPR/Cas9 mutagenesis, has yielded opportunities for researchers to generate mutations in the zebrafish genome with high specificity that can be used to generate new zebrafish muscular dystrophy mutants.

1.5.3. CRISPR/Cas9 mutagenesis

Three prominent genome editing techniques—zinc finger nucleases (ZFNs), transcription activator-like effector nucleases TALENs, and CRISPR/Cas9—are commonly used in zebrafish and allow scientists to specifically target a region of genomic DNA. Although ZFNs and TALENs have been used extensively to generate mutant lines of interest (Rafferty and Quinn, 2018; Simone et al., 2018), CRISPR/Cas9 mutagenesis has recently gained popularity in the zebrafish community. CRISPR/Cas9 has garnered much attention—and some controversy—over the past several years. This technique emerges from the adaptive immune system of bacteria and archaea. Cas9 enzyme derived from *Streptococcus pyogenes* or *Streptococcus thermophilus* accompanies clustered regulatory interspaced short palindromic repeat (CRISPR) RNAs (crRNAs) or single guide RNAs (sgRNAs) to target sites to cleave DNA (Cong et al., 2013; Gasiunas et al., 2012; Jinek et al., 2012; Mali et al., 2013). Specifically, the sgRNA-Cas9 complex is guided to a DNA sequence complementary to the sgRNA, and this sequence neighbors a protospacer adjacent motif (PAM)

sequence (Rafferty and Quinn, 2018). Double stranded breaks are induced that can later be repaired via two mechanisms: non-homologous end joining (NHEJ) and homology-directed repair (HDR) (Cornet et al., 2018; Liu et al., 2019). Over the past several years, multiple techniques for engineering CRISPR/Cas9 mutants in zebrafish have emerged and this technology continues to evolve (reviewed by (Cornet et al., 2018; Liu et al., 2019)). Chapter 3 describes a study where CRISPR/Cas9 mutagenesis was used to engineer a zebrafish model of GMPPB-associated dystroglycanopathy.

1.6. Concluding remarks

Skeletal muscle is important for strength and locomotion in vertebrate organisms. These muscle fibers adhere to surrounding ECM to form cell-matrix adhesion complexes. These connections help link muscle to nearby tendons and nerves, which contribute to its overall function. One of these complexes, the DGC is disrupted in secondary dystroglycanopathies, which are muscular dystrophies associated with progressive muscle wasting and weakness and phenotypic variation. It is currently unknown whether improving muscle cell-ECM adhesion is sufficient to improve muscle structure in secondary dystroglycanopathies. Chapter 2 describes a study that demonstrates that one of these strategies is sufficient prior to muscle development. It is also unknown how identical molecular variants of a *GMPPB* allele can result in phenotypic variation. Chapter 3 documents how we engineered an animal model of GMPPB-associated dystroglycanopathy that exhibits phenotypic variation and plasticity throughout the first several days of life. Both of these studies leverage the advantages of the zebrafish model system to answer questions regarding neuromuscular development and phenotypic variation in secondary dystroglycanopathies.

CHAPTER 2

NAD⁺ IMPROVES NEUROMUSCULAR DEVELOPMENT IN A ZEBRAFISH MODEL OF FKRP-ASSOCIATED DYSTROGLYCANOPATHY

2.1. Introduction

Muscle is a highly conserved tissue that part of the neuromusculoskeletal system and is essential for strength, locomotion, and health. The neuromuscular junction (NMJ) initiates muscle contraction, whereas the myotendinous junction (MTJ) is the major site of force transmission from muscle to the skeletal system. Muscle fibers adhere to their surrounding extracellular matrix (ECM), the MTJ, and the NMJ; and these adhesion complexes are critical for muscle development and homeostasis (reviewed by (Goody et al., 2015)). The muscle extracellular matrix and adhesion complexes at MTJs and NMJs are specialized and allow the muscle to adhere to and interact with neurons and tendons during development and homeostasis. Thus, regulation of cell-ECM adhesion is essential for development and homeostasis of the neuromusculoskeletal system.

The dystrophin-glycoprotein complex (DGC) is an essential component of muscle-ECM adhesion. The DGC is a multi-protein complex that indirectly links the actin cytoskeleton of muscle fibers to the laminin-rich basement membrane in the ECM (Ervasti and Campbell, 1993). The DGC is thought to provide mechanical stabilization during muscle contraction (Ervasti and Campbell, 1993; Rybakova et al., 2000) in addition to its role as a signaling complex (Constantin, 2014). Different variants of the DGC are present at the MTJ versus the NMJ. Whereas Dystrophin is the predominant protein that connects the actin cytoskeleton to the transmembrane protein Dystroglycan (DG) at the MTJ (Ervasti and Campbell, 1993), Utrophin mainly establishes this connection at the NMJ (Deconinck et al., 1997). Despite these differences, DG is present and highly glycosylated at both the MTJ and the NMJ. DG glycosylation is required for DG binding to

basement membrane proteins such as laminin, agrin, and perlecan (Briggs et al., 2016; Gee et al., 1994; Martin, 2006). Dystroglycanopathies result from mutations in genes responsible for glycosylation of alpha-DG (DG contains two subunits: a transmembrane beta subunit and an extracellular alpha subunit) (Godfrey et al., 2011; Inamori et al., 2012; Muntoni et al., 2011). Thus far, 16 gene products that participate in DG glycosylation have been identified (Nickolls and Bönnemann, 2018). In addition to muscle degeneration, dystroglycanopathies are frequently associated with central nervous system defects such as intellectual disability and brain malformation (Nickolls and Bönnemann, 2018). The role of DG glycosylation in the peripheral nervous system is less understood although abnormal NMJs have been reported after birth in a couple dystroglycanopathy mouse models (Côté et al., 1999; Herbst et al., 2009; Levedakou et al., 2005; Pratt et al., 2015; Saito et al., 2007). Because NMJ defects have been observed after embryonic development, the most prevalent hypothesis is that post-synaptic DG does not play a role in NMJ formation, but is important for NMJ stabilization (Nickolls and Bönnemann, 2018). For example, patients with mutations in *GMPPB* (required for GDP-mannose formation (Jensen et al., 2015)), show decreased action potentials with repeated nerve stimulation (Johnson et al., 2018). Given the plethora of glycosylated proteins at the NMJ, it is possible that a subset of dystroglycanopathy genes may be required outside of muscle tissue for NMJ development.

FKRP-associated dystroglycanopathy results from mutations in *FKRP*, which encodes an enzyme critical for DG glycosylation. FKRP works in concert with Fukutin to use CDP-ribitol synthesized by Isoprenoid Synthase Domain-Containing (ISPD) protein to form a tandem ribitol-5-phosphate (Gerin et al., 2016; Kanagawa et al., 2016) that links xylose with N-acetylgalactosamine (Taniguchi-Ikeda et al., 2016). This process is necessary for DG glycosylation. Patients with FKRP-associated dystroglycanopathy present with phenotypic

variability; however, muscle weakness and elevated serum creatine kinase are consistently present (Johnson et al., 2018). Depending on the molecular basis of the *FKRP* mutation, individuals with this condition may develop limb-girdle muscular dystrophy 2I (LGMD2I) or congenital muscular dystrophy with or without eye and brain involvement (Stensland et al., 2011; Van Reeuwijk et al., 2010). There is some genotype-phenotype correlation in patients with C-terminal *FKRP* mutations tending to be more severe (Beltran-Valero de Bernabé et al., 2004; de Bernabé et al., 2003; Stensland et al., 2011; Van Reeuwijk et al., 2010). However, there is remarkable phenotypic variation among individuals with the same mutation (Stensland et al., 2011). For example, a study of 25 patients homozygous for c826C/A found significant variation in muscle pathology, and levels of glycosylated DG (Stensland et al., 2011). Neither the histopathological alterations nor levels of DG glycosylation correlated with age of onset or walking function. Interestingly, whereas one set of siblings presented with similar clinical and histopathological features, a second set of siblings had dramatic variation in the age of onset (12 vs 27 years old) (Stensland et al., 2011). These data suggest that there are modifying factors - environmental and/or genetic - that affect progression of *FKRP*-associated dystroglycanopathy. These data also suggest that it is imperative to study features other than muscle pathology and/or levels of DG glycosylation. Mouse (Ackroyd et al., 2009) and zebrafish models of *FKRP* deficiency have been used to study mechanisms associated with *FKRP*-associated dystroglycanopathy. Zebrafish models of *FKRP*-associated dystroglycanopathy include morpholino (MO) models (Kawahara et al., 2010; Thornhill et al., 2008) and a more recently generated *fkrp* mutant (Serafini et al., 2018). These studies indicate that the *fkrp* morphants phenocopy the *fkrp* mutant, *fkrp* deficiency results in impaired muscle development and wasting, and that laminin deposition at the MTJ is disrupted in *Fkrp*-deficient zebrafish.

Laminin is a major component of the basement membrane that surrounds muscle. Laminin is a heterotrimeric protein with an alpha, beta, and gamma chain. Adhesion of muscle fibers to laminin is necessary for muscle development and homeostasis (Bajanca et al., 2006; Gupta et al., 2012; Hall et al., 2007; Smith et al., 2017; Snow et al., 2008b; Yurchenco et al., 2018). The principle laminin isoform in mature vertebrate skeletal muscle is laminin-211 (alpha2 beta1 gamma1). Mutations in the human *laminin alpha2* gene result in MDC1A, a common congenital muscular dystrophy (Helbling-Leclerc et al., 1995). A different laminin isoform, laminin-111, is the major isoform expressed during muscle development and laminin-111 is required for muscle development in mouse and zebrafish (Bajanca et al., 2006; Snow et al., 2008b). Laminin-111 can partially compensate for laminin-211. Overexpression of laminin alpha1 slows the progression of dystrophy in *laminin alpha2* mutant mice (Gawlik et al., 2004; Rooney et al., 2012). Injection of laminin-111 protein directly into muscle of *mdx* mice modeling Duchenne muscular dystrophy (DMD) improves muscle structure and function (Rooney et al., 2009). These data indicate that understanding mechanisms that mediate laminin-111 expression and polymerization during muscle development could provide information for future therapeutic development. We identified a novel pathway required for laminin-111 organization at the zebrafish MTJ during muscle development. We found that Nicotinamide Riboside Kinase 2b (previously called muscle Integrin binding protein (Li et al., 1999; Li et al., 2003)) is necessary for normal laminin-111 organization (Goody et al., 2010). Yeast and human Nrk2s function in an alternative salvage pathway that generates Nicotinamide Adenine Dinucleotide (NAD⁺) (Bieganowski and Brenner, 2004; Tempel et al., 2007). Exogenous NAD⁺ rescues MTJ morphogenesis in Nrk2b-deficient zebrafish, indicating that zebrafish Nrk2b also functions to generate NAD⁺ (Goody et al., 2010). Given that NAD⁺ biosynthesis is necessary for normal laminin-111 organization during muscle development, we asked whether exogenous NAD⁺

would be sufficient to improve muscle structure and function in zebrafish modeling muscular dystrophies. We showed that NAD⁺ supplementation increases laminin organization and reduces muscle degeneration in zebrafish deficient for either of the laminin-211 receptors (DG or Integrin alpha7 (*Itga7*)) (Goody et al., 2012). As vitamin B3 is a precursor for NAD⁺, we asked whether vitamin supplementation would increase NAD⁺ and improve muscle structure and function in DG-deficient zebrafish. Indeed, we found that supplementation with EmergenC packets that contain B vitamins (chosen because they are water soluble) improves muscle structure and motility in DG-deficient zebrafish.

The two major transmembrane receptors that anchor muscle cells to laminin in their ECM are DG (described above) (Ervasti and Campbell, 1993; Gee et al., 1994) and Integrin alpha7 (*Itga7*) (Cohn et al., 1999; Song et al., 1993). *Itga7* is also required for muscle homeostasis: mutations in *Itga7* lead to congenital muscular dystrophy with *Itga7* deficiency (Hayashi et al., 1998). These two cell adhesion complexes display some degree of functional redundancy in both zebrafish and mouse models. Pharmacologically increasing levels of *Itga7* compensates for the loss of Dystrophin in a mouse model of DMD (Sarathy et al., 2017; Van Ry et al., 2015). Given that NAD⁺ is sufficient to improve muscle structure in zebrafish deficient for either laminin receptor complex (DG or *Itga7*), we hypothesized that NAD⁺ increases laminin organization by increasing clustering of the remaining receptor (Goody et al., 2012). Our model is that in the absence of *Itga7*, NAD⁺ increases DG clustering, thus improving muscle-ECM adhesion. Similarly, we hypothesize that in the absence of DG, NAD⁺ increases *Itga7* clustering, thus improving muscle-ECM adhesion. This model leads to the question of whether, if DG is present but hypoglycosylated, NAD⁺ would be sufficient to improve muscle structure in a zebrafish secondary dystroglycanopathy model. Our previous data showed beneficial effects of NAD⁺

when administered prior to muscle development (Goody et al., 2012). Whether NAD⁺ is beneficial after initial muscle development in this context has not yet been determined.

Paxillin is an Integrin-associated adaptor protein that concentrates at the MTJ during muscle development (Crawford et al., 2003). Paxillin is an essential signaling nexus that regulates cell adhesion, morphology, and migration (Deakin and Turner, 2008). Paxillin participates in the Nr2b-laminin pathway. Nr2b is cell-autonomously required for subcellular concentration of Paxillin at the MTJ; and Paxillin overexpression rescues muscle development Nr2b-deficient zebrafish (Goody et al., 2010). DG is required for normal Paxillin concentration at the MTJ: DG-deficient zebrafish show reduced concentration of Paxillin at the MTJ. Addition of NAD⁺ improves Paxillin concentration at the MTJ and Paxillin overexpression reduces muscle degeneration in DG-deficient zebrafish (Goody et al., 2012). In contrast, Paxillin overexpression does not rescue zebrafish deficient for *Itga7* (Goody et al., 2012). These data suggest that Paxillin functions downstream of NAD⁺ to improve muscle resilience in DG-deficient zebrafish. However, whether Paxillin concentration at the MTJ is disrupted in zebrafish models of secondary dystroglycanopathy and whether Paxillin overexpression ameliorates muscle degeneration in zebrafish models of secondary dystroglycanopathy have not been investigated.

We used the *fkrp* morphant model of FKR- associated dystroglycanopathy (Kawahara et al., 2010; Thornhill et al., 2008) to address unanswered questions regarding NAD⁺ regulation of the ECM in a secondary dystroglycanopathy. In addition, given the data indicating that there is not a strict correlation between DG glycosylation levels and phenotype, we investigated neuromuscular junction development in *fkrp* morphants. We found that supplementing *fkrp* morphants with NAD⁺ at gastrulation improves laminin polymerization at the MTJ, muscle structure, and muscle function. Despite the fact that Paxillin localization is disrupted in *fkrp* morphants, Paxillin overexpression failed to rescue any of these phenotypes. Early NMJ

development was disrupted in *fkrp* morphants and improved with NAD⁺. To our knowledge, this is the first report of initial NMJ development being disrupted in an animal model of secondary dystroglycanopathies. As initial NMJ development has not been investigated in an animal model of DG deficiency, we analyzed early NMJ development in *dag1* morphants. We found that NMJ development is disrupted in *dag1* morphants, although to a lesser extent than *fkrp* morphants. In contrast to *fkrp* morphants, NAD⁺ supplementation did not improve NMJ development in *dag1* morphants. Finally, we show that muscle-specific overexpression of *fkrp* improved MTJ morphology but was not sufficient to improve muscle structure or function. Taken together, these data indicate that, at least in the zebrafish, FKR-associated dystroglycanopathy does not phenocopy DG-deficiency. Furthermore, these data show that *Fkrp* is required for normal NMJ development and is required in tissues other than muscle.

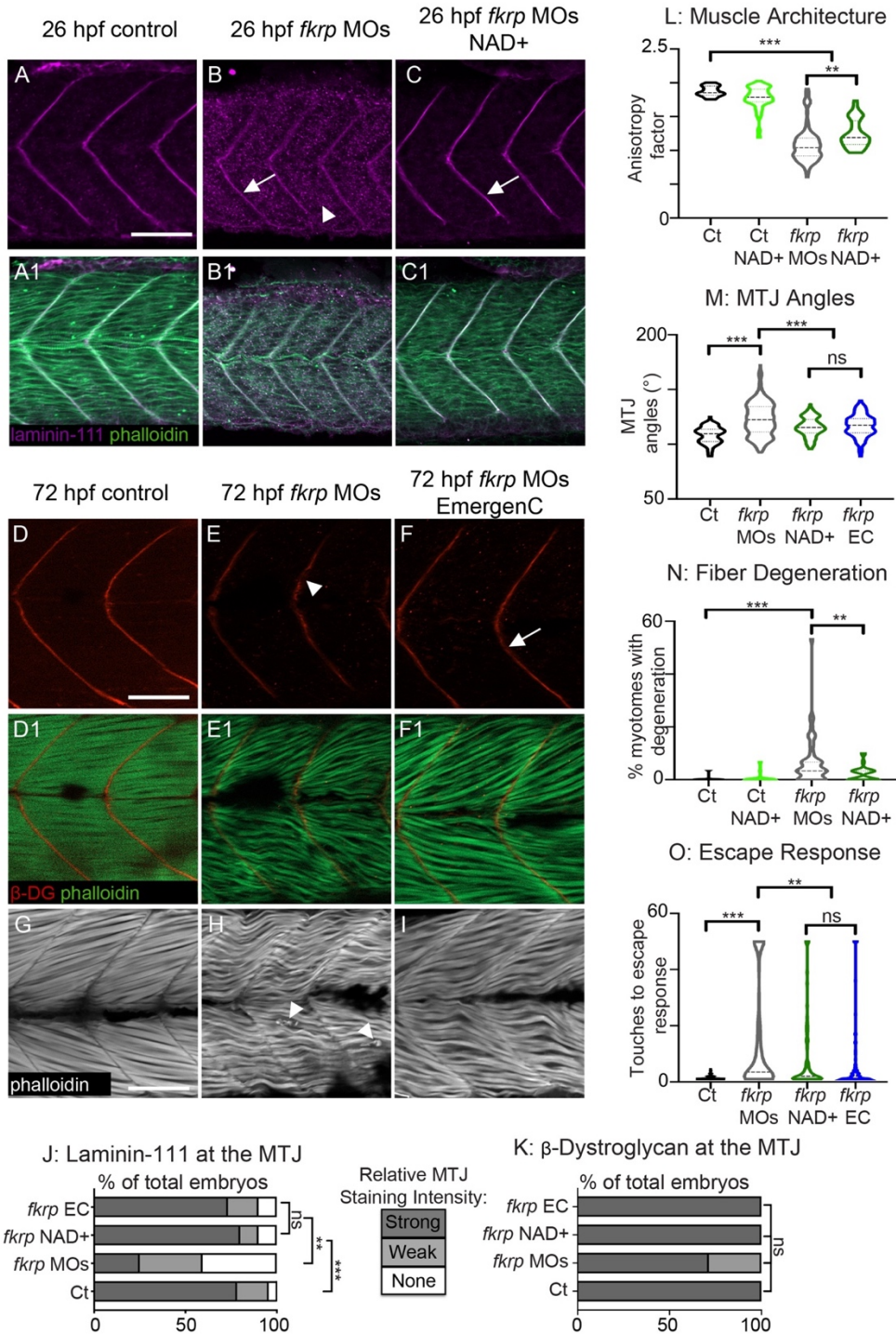
2.2. Results

2.2.1. NAD⁺ supplementation prior to muscle development improves muscle and MTJ structure

Injection of previously published *fkrp* MOs recapitulated the previously described phenotype of *fkrp* morphants (Kawahara et al., 2010; Thornhill et al., 2008) and the recently described *fkrp* mutant (Serafini et al., 2018). In agreement with previous findings, multiple aspects of muscle development are disrupted in *fkrp* morphants: MTJs are significantly wider than in control embryos (Fig. 2.1M), muscle fibers are disorganized (Fig. 2.1L), and muscle degeneration is observed (Fig. 2.1H, N). Muscle fiber adhesion to the MTJ and ECM organization at the MTJ are disrupted in *fkrp* morphants (Kawahara et al., 2010; Lin et al., 2011; Thornhill et al., 2008). We also found that laminin (Fig. 2.1A-B, J) is reduced in *fkrp* morphants compared to controls and that beta-DG is concentrated at the MTJ, although sometimes slightly reduced (Fig. 2.1D-E, K). We next asked whether muscle function was disrupted by quantifying the number of

Figure 2.1. NAD⁺ or EmergenC supplementation at gastrulation improves muscle structure and function in *fkrp* morphants. (A-C) Anterior left, dorsal top, side-mounted embryos at 26 hpf stained for laminin-111 (purple) and actin (phalloidin, green). **(A, A1)** Control embryo. Laminin is concentrated at the MTJ. **(B, B1)** *fkrp* morphant. Although laminin is present at the MTJ (white arrow), it is also present within the myotome (white arrowhead). **(C, C1)** *fkrp* morphant treated with NAD⁺ at 6 hpf. Laminin is concentrated at the MTJ (white arrow) as in control embryos. **(D-F1)** Anterior left, dorsal top, side-mounted embryos at 72 hpf stained for beta-DG (red) and f-actin (phalloidin, green). **(D, D1)** Control embryo. **(E, E1)** *fkrp* morphant. Beta-DG staining appears weaker at the MTJ (white arrowhead). **(F, F1)** *fkrp* morphant treated with EmergenC at 6 hpf. Beta-DG staining appears stronger at the MTJ (white arrow). **(G-I)** Anterior left, dorsal top, side-mounted embryos at 72 hpf stained for f-actin (phalloidin, gray). **(G)** Control embryo. **(H)** *fkrp* morphant. White arrowheads indicate single detached fibers. **(I)** *fkrp* morphant treated with EmergenC at 6 hpf. Note the improved muscle fiber structure. **(J)** Relative staining intensity of laminin-111 at the MTJ in 26 hpf embryos, based on no staining/localization (none, white), weak staining/localization (weak, light gray), and strong staining/localization (strong, dark gray) (images were blinded prior to analysis, see methods). Controls (n=23 embryos) have greater laminin intensity staining than *fkrp* morphants (n=32 embryos). NAD⁺ (n=10 embryos) and EmergenC (n=30 embryos) supplementation improve laminin-111 concentration at the MTJ in *fkrp* morphants. **(K)** Relative staining intensity of beta-DG at the MTJ in 72 hpf embryos, based on weak staining (weak, light gray) and strong staining (strong, dark gray). Although *fkrp* morphants have more embryos with weaker beta-DG staining at the MTJ (n=7 embryos), there is no significant difference in beta-DG at the MTJ between untreated morphants, morphants treated with NAD⁺ (n=7 embryos), EmergenC (n=7 embryos), or control morphants (n=5 embryos). **(L)** Quantification of muscle organization at 72 hpf. The anisotropy factor in embryos injected with *fkrp* MOs (n=96 half-myotomes) is reduced compared to uninjected controls (n=16 half-myotomes), and NAD⁺ (n=40 half-myotomes) significantly increases the anisotropy factor in *fkrp* morphants. **(M)** Quantification of MTJ angles at 72 hpf. Injection of *fkrp* MOs (n=343 MTJs) significantly increases MTJ angles compared to uninjected controls (n=98 MTJs). Either NAD⁺ (n=105 MTJs) or EmergenC (n=158 MTJs) treatment significantly reduces MTJ angles compared to untreated morphants. **(N)** Untreated *fkrp* morphants (n=54 embryos) have a significantly higher percent of myotomes per embryo with fiber detachments than controls (n=40 embryos) at 72 hpf. NAD⁺ (n=31 embryos) supplementation significantly reduces the percent of

myotomes with dystrophy per embryo. **(O)** Injection of *fkrp* MOs (n=184 embryos) significantly increases the number of touches required to induce an escape response compared to uninjected controls (n=185 embryos). NAD⁺ (n=84 embryos) or EmergenC (n=111 embryos) treatment significantly reduces the number of touches to invoke an escape response. Scalebars are 50 micrometers. **p*<0.05, ***p*<0.01, ****p*<0.001, ns non-significant.



touches required to induce an escape response. We found that *fkrp* morphants have reduced muscle function in that they require significantly more touches to induce an escape response (Fig. 2.1O). These data indicate that *fkrp* is necessary for normal muscle development and function.

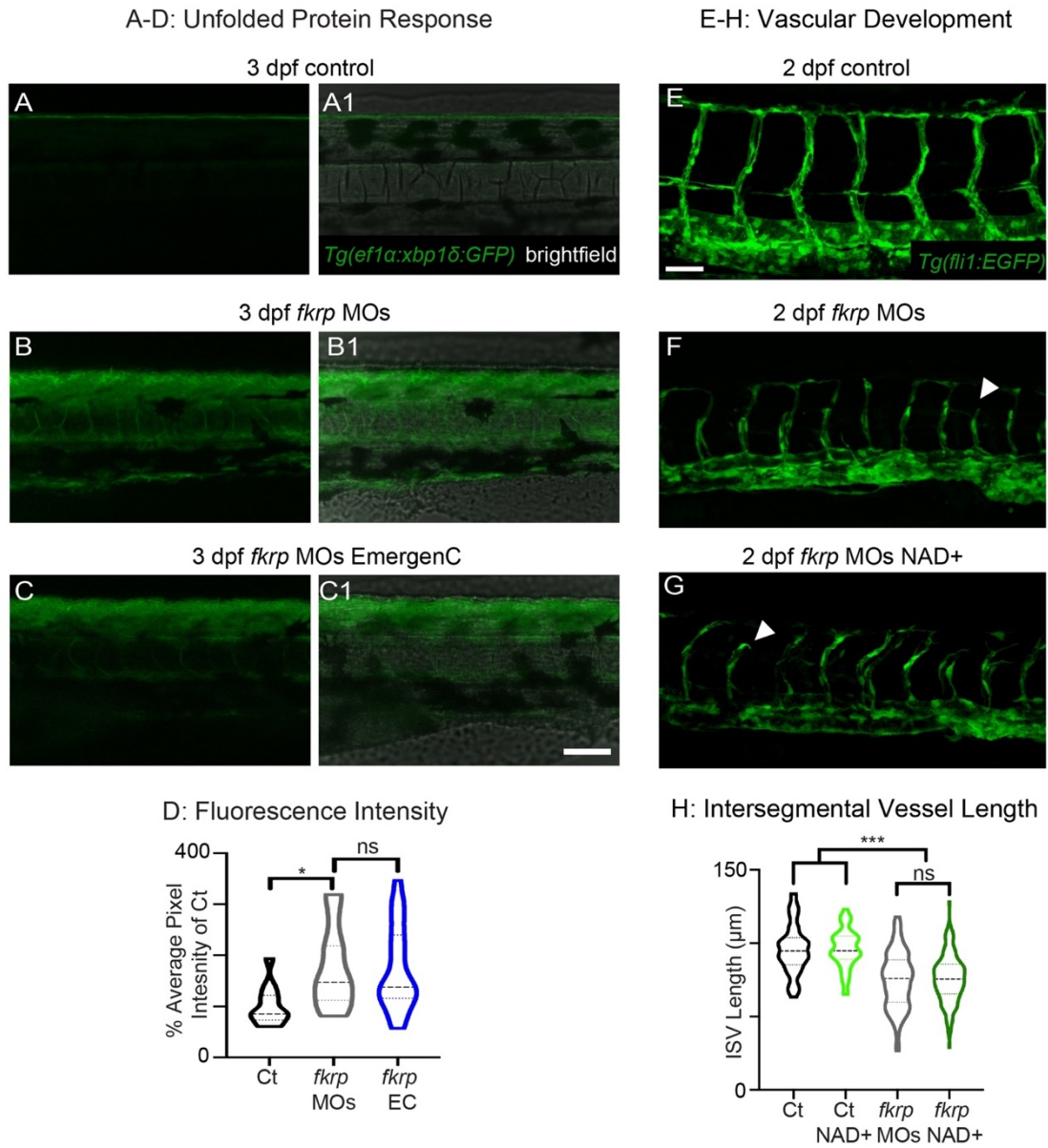
We previously showed that either NAD⁺ or EmergenC supplementation at gastrulation is sufficient to improve ECM organization, reduce muscle degeneration, and improve motility in *dag1* morphants (Goody et al., 2012). We hypothesized that NAD⁺/EmergenC increased laminin organization by potentiating clustering of the other major laminin receptors in muscles, Integrins alpha6/beta1 and alpha7/beta1. We asked if NAD⁺/EmergenC is sufficient to improve laminin organization in the context of impaired DG glycosylation because hypoglycosylated DG could hinder increased laminin organization. We found that NAD⁺ or EmergenC supplementation at gastrulation increased the concentration of laminin at the MTJ (Fig. 2.1C, J), decreased MTJ angles (Fig. 2.1M), decreased muscle degeneration (Fig. 2.1N), improved muscle fiber organization (Fig. 2.1L), and significantly reduced the touches required to evoke an escape response (Fig. 2.1O). These data indicate that NAD⁺ or EmergenC supplementation during gastrulation is sufficient to improve muscle development and function in *Fkrp*-deficient zebrafish.

2.2.2. NAD⁺/EmergenC are not sufficient to improve vascularization, midbrain-hindbrain development, or the increased unfolded protein response in *fkrp* morphants

Fkrp is required for normal zebrafish vascularization: *fkrp* morphants and the recently described *fkrp* mutant exhibit shorter intersegmental vessel (ISV) lengths compared to wild-type embryos (Serafini et al., 2018; Wood et al., 2011). *Fli1:EGFP* transgenics injected with *fkrp* MOs exhibited shorter ISV lengths (including truncated vessels) than uninjected controls (Fig. 2.2E-F,

Figure 2.2. NAD⁺ and EmergenC supplementation at gastrulation do not significantly improve the UPR or vascularization in *fkrp* morphants. (A-C1) Anterior left, dorsal top, side-mounted 3 dpf (72 hpf) embryos expressing *Tg(ef1α:xbp1δ-GFP)*. Fluorescence intensity was kept constant within an experiment (see methods). Numbered panels are merged with the brightfield channel. **(A-A1)** Control embryo. Note low relative expression of Xbp1 compared to morphants. **(B-B1)** *fkrp* morphant. **(C-C1)** *fkrp* morphant treated with EmergenC at gastrulation. Note that fluorescence intensity is similar to that of untreated morphant. **(D)** Quantification of Xbp1 fluorescence intensity normalized to control fluorescence intensity for all groups imaged. Fluorescence intensity is significantly increased in morphants. There is no significant difference in fluorescence intensity between untreated morphants (n=15 embryos) and morphants receiving EmergenC (n=21 embryos). **(E-G)** Anterior left, dorsal top, side-mounted 2 dpf embryos expressing *Tg(fli1:EGFP)* focused on the ISVs. **(E)** Control embryo. **(F)** *fkrp* morphant embryo. Note that some ISVs are truncated (white arrowhead). **(G)** *fkrp* morphant embryo treated with NAD⁺ at gastrulation. Truncated ISVs are still present in NAD⁺ treated morphants (white arrowhead). **(H)** Quantification of ISV length. ISV length is reduced in *fkrp* morphants (n=201 vessels) compared with uninjected controls (n=84 vessels). NAD⁺ supplementation (n=166 vessels) does not rescue ISV length in *fkrp* morphants. Scalebars are 50 micrometers. **p*<0.05, ***p*<0.01, ****p*<0.001, ns non-significant.

Figure 2.2.

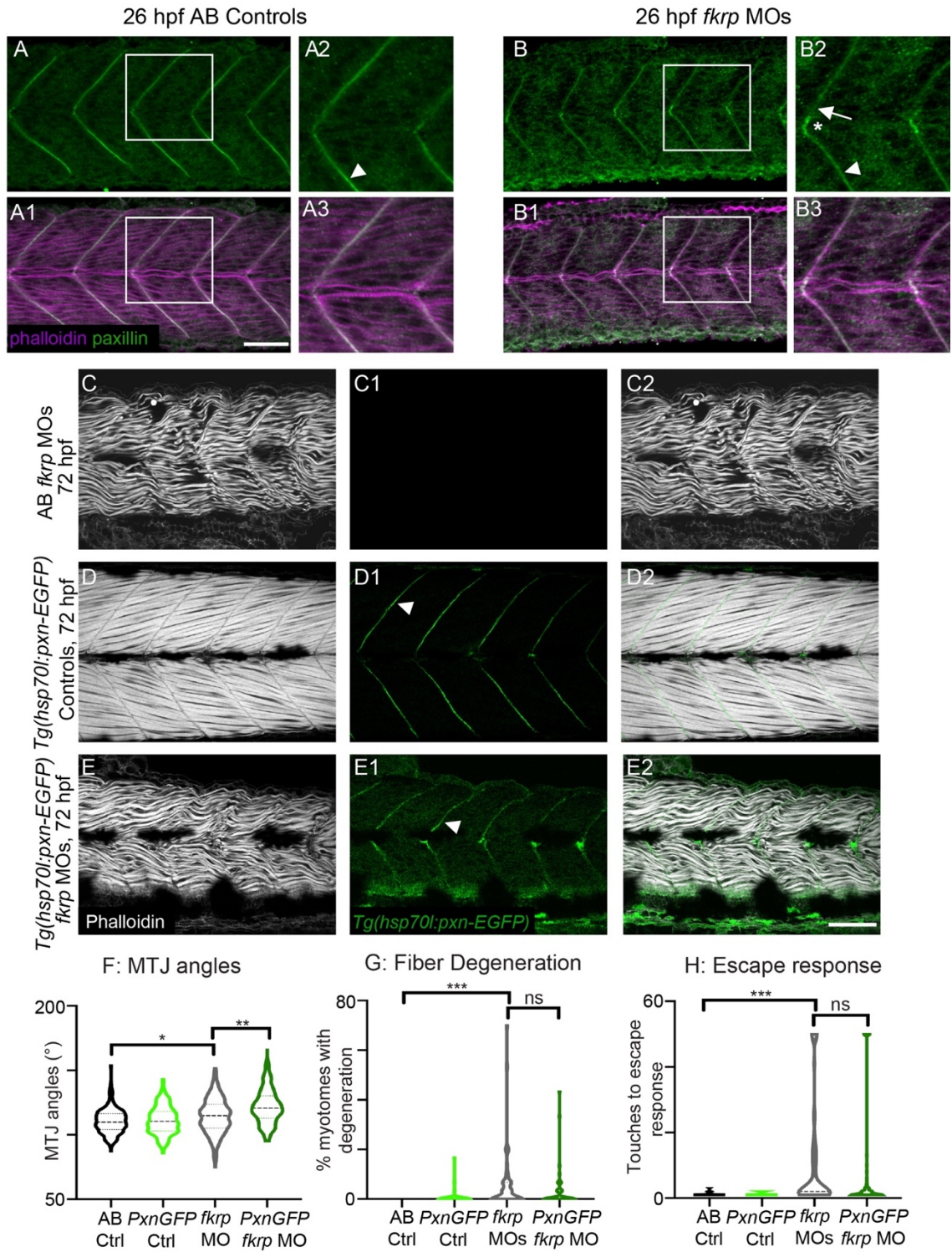


H). NAD⁺ supplementation had no significant effect on ISV length in *fkrp* morphants (Fig. 2.2G-H). We also analyzed ISV length when normalized to the width of the embryos because muscle development is disrupted in *fkrp* morphants. The same result was observed with normalized data (not shown). These data suggest that: (1) NAD⁺ supplementation is not sufficient to improve vascularization in *fkrp* morphants, and (2) the vascularization defects observed in *fkrp* morphants are likely a consequence of *fkrp* knockdown and not aberrant muscle development and/or homeostasis.

Zebrafish deficient for Fkrp exhibit abnormal midbrain-hindbrain boundary formation that has been likened to cobblestone lissencephaly (Thornhill et al., 2008). We also observed abnormal midbrain-hindbrain boundary formation in *fkrp* morphants at 26 hpf (n = 8 embryos) compared with uninjected controls. NAD⁺ was not sufficient to rescue midbrain-hindbrain boundary formation (n = 8 embryos, data not shown). Zebrafish models of FKRP-associated dystroglycanopathy are also associated with endoplasmic reticulum (ER) stress and activation of the unfolded protein response (UPR) (Lin et al., 2011). One marker of the UPR is increased activation of the *xbp1* transcript, which is upregulated in *fkrp* morphants (Lin et al., 2011) and the recently described *fkrp* mutant (Serafini et al., 2018). To determine whether EmergenC could improve ER stress in *fkrp* morphants, we injected *fkrp* MOs into the *Tg(ef1α:xbp1δ-GFP)* line that allows visualization of *xbp1* activation (Li et al., 2015). Injection of *fkrp* MOs increased the UPR (Fig. 2.2B) compared with controls (Fig. 2.2A). However, untreated and EmergenC treated *fkrp* morphants did not significantly differ in relative fluorescence intensity (Fig. 2.2C-D). Taken together, these results suggest that the benefits of NAD⁺ supplementation may be limited to muscle in Fkrp-deficient zebrafish.

Figure 2.3. Paxillin overexpression does not improve muscle structure in *fkrp* morphants. (A-B3) Anterior left, dorsal top, side-mounted embryos at 26 hpf stained for Paxillin (green) and f-actin (purple). Paxillin concentrates at the MTJ (white arrowhead) in control embryos. There are some gaps in Paxillin localization in *fkrp* morphants (B2, white arrow) and Paxillin accumulates at the muscle pioneers (B2, white asterisk). **(C-E2)** Anterior left, dorsal top, side-mounted embryos at 72 hpf stained for f-actin (phalloidin, gray) in lettered and even numbered panels and expressing Paxillin-EGFP (green) in numbered panels. **(C-C2)** A *fkrp* morphant with disorganized muscle fibers. **(D-D2)** Control *Tg(hsp70l:pxna-EGFP)* embryo expressing Paxillin which concentrates at the MTJ (white arrowhead). **(E-E2)** *Tg(hsp70l:pxna-EGFP)* *fkrp* morphant. **(F)** MTJ angle quantification. *Fkrp* morphants with (n=241 MTJs) and without (n=170 MTJs) Paxillin-EGFP expression have a significant increase in average MTJ angle width compared with uninjected controls (n=189, 191 MTJs). Paxillin overexpression in *fkrp* morphants significantly increases MTJ angles compared to morphants that do not overexpress Paxillin. **(G)** Fiber degeneration quantification. *Fkrp* morphants with (n=55 embryos) and without (n=60 embryos) Paxillin-EGFP expression have a significant increase in the percent of myotomes with degeneration per embryo compared to uninjected controls (n=57, 54 embryos). Although there is a trend, Paxillin overexpressing morphants do not have a significant reduction in dystrophy compared to control *fkrp* morphants. **(H)** Escape response quantification. *Fkrp* morphants with (n=88 embryos) and without (n=70 embryos) Paxillin-EGFP expression require significantly more touches to induce an escape response compared with uninjected controls (n=66, 80 embryos). *Fkrp* morphants overexpressing Paxillin do not exhibit a significant improvement in escape response compared with *fkrp* morphants that do not overexpress Paxillin. Scalebars are 50 micrometers. * $p < 0.05$, ** $p < 0.01$, *** $p < 0.001$, ns non-significant.

Figure 2.3.

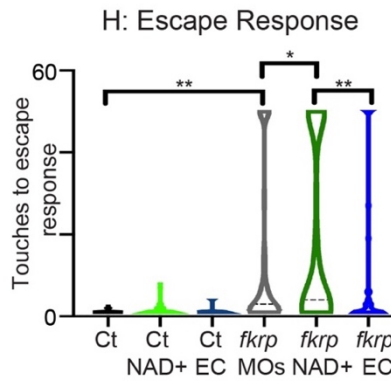
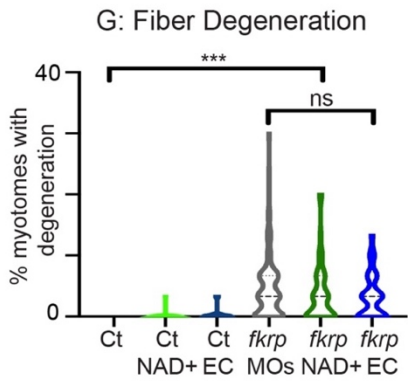
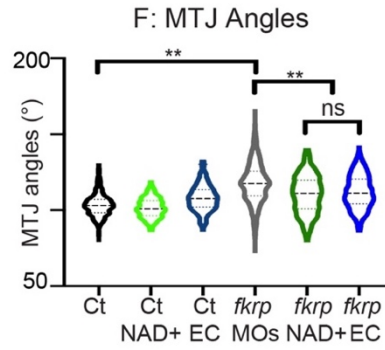
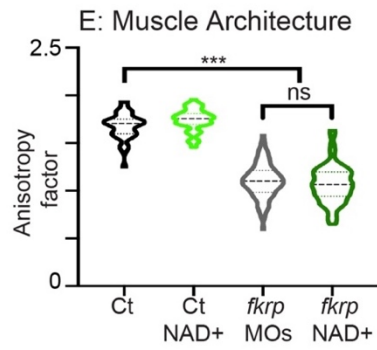
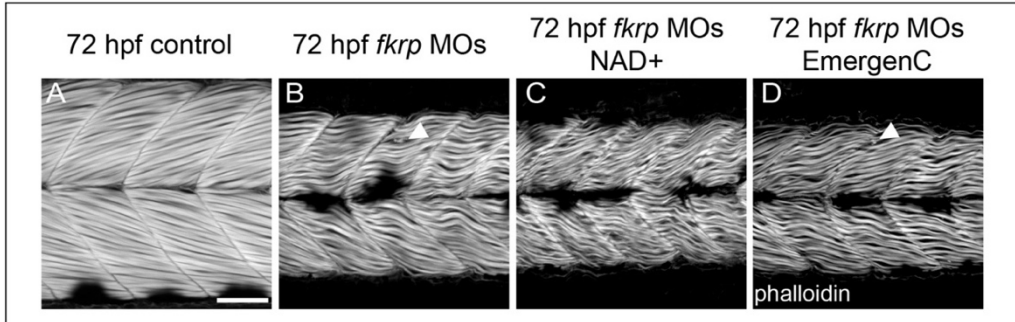


2.2.3. Paxillin overexpression does not significantly reduce muscle degeneration

Paxillin is an Integrin-associated protein that is required for cell adhesion to the ECM (Turner et al., 1990). Paxillin concentrates at MTJs in wild-type muscle ((Crawford et al., 2003), Fig. 2.3). Paxillin plays a role in the Nr2b-NAD⁺-laminin cell adhesion pathway. Paxillin concentration at the MTJ is disrupted in *nrk2b* morphants and rescued with NAD⁺ (Goody et al., 2010). Paxillin overexpression rescues *nrk2b* morphants (Goody et al., 2010). Similarly, concentration of Paxillin at the MTJ is disrupted in *dag1* morphants and is improved with NAD⁺. Paxillin overexpression improves muscle structure in *dag1* morphants (Goody et al., 2012). It is not known if either Paxillin concentration at the MTJ is disrupted in animal models of secondary dystroglycanopathy or if Paxillin overexpression improves muscle structure in these models. We found that Paxillin concentration at the MTJ was disrupted in 26 hpf *fkrp* morphants (Fig. 2.3B) compared with controls (Fig. 2.3A). Paxillin does concentrate at the center of the MTJ adjacent to muscle pioneers that are slow-twitch fibers (Fig. 2.3B at the crux of the v-shaped MTJ, this was observed in 14/16 *fkrp* morphants). However, Paxillin concentration at the MTJ adjacent to fast-twitch muscle is disrupted (Fig. 2.3B2, arrow). These data suggest that Fkrp is required for normal development of the MTJ adjacent to fast-twitch muscle. Overexpression of Paxillin was sufficient for Paxillin to concentrate at the fast-muscle MTJ in *fkrp* morphants (Fig. 2.3E1 arrowhead). However, in contrast to what we previously observed in *dag1* morphants (Goody et al., 2012), Paxillin overexpression did not reduce muscle degeneration or improve the escape response in *fkrp* morphants (Fig. 2.3G-H). Paxillin overexpression actually increased MTJ angles (Fig. 2.3F). These data indicate that, in contrast to *dag1* morphants, Paxillin overexpression is not sufficient to improve muscle structure in *fkrp* morphants.

Figure 2.4. Later NAD⁺ supplementation improves MTJ structure, but NAD⁺ and EmergenC are required prior to initial muscle development to improve motility, fiber resilience, and fiber organization. (A-D) Anterior left, dorsal top, side-mounted embryos at 72 hpf stained for f-actin (phalloidin, gray). (A) Control embryo. (B) *fkrp* morphant. (C) *fkrp* morphant treated with NAD⁺ at 24 hpf. (D) *fkrp* morphant treated with EmergenC at 24 hpf. White arrowheads indicate single fiber detachments. (E) Fiber organization quantification. The anisotropy factor in embryos injected with *fkrp* MOs (n=104 half-myotomes) is reduced compared to controls (n=48 half-myotomes) and not improved with NAD⁺ supplementation at 24 hpf (n=96 half-myotomes). (F) MTJ angle quantification. *Fkrp* morphants treated with NAD⁺ (n=381 MTJs) or EmergenC (n=318 MTJs) at 24 hpf have significantly decreased MTJ angles compared to untreated morphants (n=651 MTJs). (G) Fiber detachment quantification. Although there is a trend towards reduced muscle degeneration, *fkrp* morphants receiving NAD⁺ (n=55 embryos) or EmergenC (n=41 embryos) at 24 hpf do not have a significant reduction in the percent of myotomes with dystrophy compared to untreated morphants (n=98 embryos). (H) Escape response quantification. The number of touches required to induce an escape response is elevated in embryos injected with *fkrp* MOs (n=128 embryos) compared to controls (n=114 embryos). Morphants treated with NAD⁺ at 24 hpf (n=81 embryos) have a worsened escape response compared to untreated morphants. Morphants treated with EmergenC at 24 hpf (n=52 embryos) do not exhibit a significant change in escape response compared to untreated morphants, but significantly differ from NAD⁺ treated morphants. Scalebars are 50 micrometers. * $p < 0.05$, ** $p < 0.01$, *** $p < 0.001$, ns non-significant.

Figure 2.4.



2.2.4. NAD⁺ supplementation after initial muscle development improves MTJs, but not muscle structure

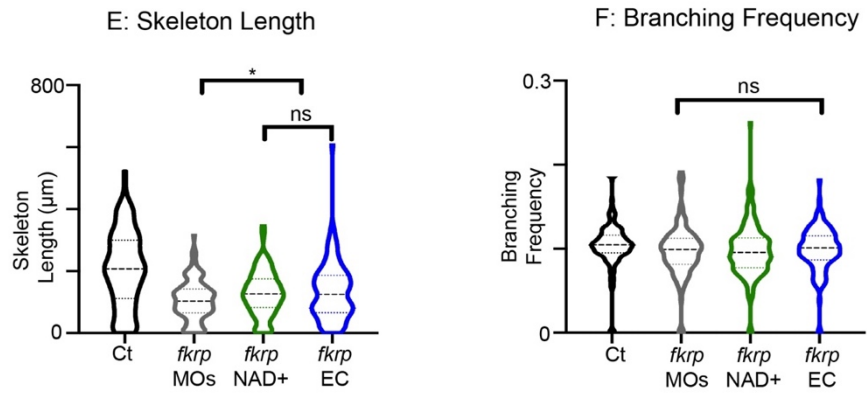
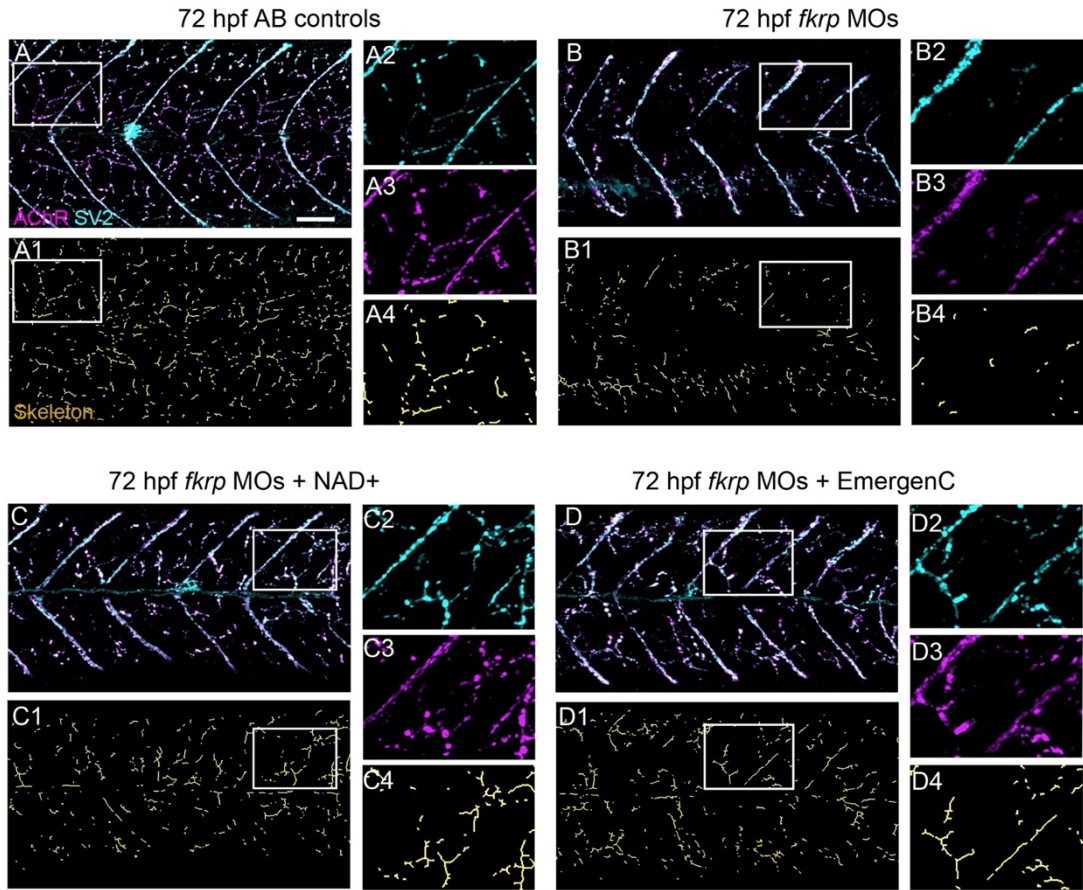
NAD⁺/EmergenC supplementation prior to muscle development is sufficient to improve muscle structure and function in *dag1* (Goody et al., 2012) and *fkrp* morphant embryos (Fig. 2.1). It is not known whether NAD⁺ or EmergenC can improve muscle structure and function after initial muscle development. We supplemented *fkrp* morphants with NAD⁺ or EmergenC at 24 hpf (after initial muscle development). Both NAD⁺ and EmergenC supplementation significantly improved MTJ angles (Fig. 2.4F). In contrast, neither NAD⁺ nor EmergenC supplementation at 24 hpf was sufficient to improve muscle fiber organization, reduce muscle degeneration, or improve the escape response (Fig. 2.4A-D, E, G, H). Thus, NAD⁺/EmergenC supplementation after initial muscle development is not sufficient to ameliorate muscle degeneration and improve muscle function in *Fkrp*-deficient zebrafish embryos.

2.2.5. NMJ development is disrupted and partially improved with NAD⁺ supplementation in *fkrp* morphants

The DGC is necessary for NMJ maturation after birth in mouse (Herbst et al., 2009; Jayasinha et al., 2003; Levedakou et al., 2005). DG glycosylation is also necessary for normal NMJ formation during muscle regeneration (Goddeeris et al., 2013). It is generally thought that DG is not required for NMJ development but is required for NMJ maturation/stabilization/regeneration (Gumerson et al., 2013). We asked whether initial NMJ development is disrupted in secondary dystroglycanopathies. We analyzed NMJ structure at 72 hpf by staining for SV2 and postsynaptic AChRs (alpha-bungarotoxin). We focused on analysis of innervation of fast-twitch fibers (distributed innervation, see skeletons Fig. 2.5). There is an extensive network of distributed NMJs in 72 hpf control embryos (Fig. 2.5A). This network is qualitatively disrupted in *fkrp* morphants where there appeared to be shorter chains of NMJs (Fig. 2.5B). Supplementation

Figure 2.5. *Fkrp* morphants exhibit NMJ defects and NAD⁺ and EmergenC treatment prior to muscle development improves NMJ development. (A-D4) Anterior left, dorsal top, side-mounted embryos at 72 hpf with labeled AChR and SV2. **(Lettered panels)** Merged channels of AChR and SV2. **(1)** Skeletonized images. **(2)** Magnification of SV2 channel. **(3)** Magnification of AChR channel. **(4)** Magnification of skeleton channel. **(A-A4)** Control embryo. **(B-B4)** *fkrp* morphant embryo exhibiting reduced distributed innervation within the myotome. **(C-C4)** *fkrp* morphant embryo treated with NAD⁺ at 6 hpf shows increased NMJs. **(D-D4)** *fkrp* morphant embryo treated with EmergenC at 6 hpf also shows increased NMJs. **(E)** Length of skeletons. Skeleton length is reduced in *fkrp* morphants (n=153 half-myotomes) compared to controls (n=144 half-myotomes), but significantly increased in *fkrp* morphants receiving NAD⁺ (n=183 half-myotomes) or EmergenC (n=127 half-myotomes) at 6 hpf. **(F)** Degree of branching within the myotome in control embryos (n=141 half-myotomes), *fkrp* morphants (n=147 half-myotomes), and *fkrp* morphants receiving NAD⁺ (n=179 half-myotomes) or EmergenC (n=126 half-myotomes) at 6 hpf. Scalebars are 50 micrometers. **p*<0.05, ns non-significant.

Figure 2.5.



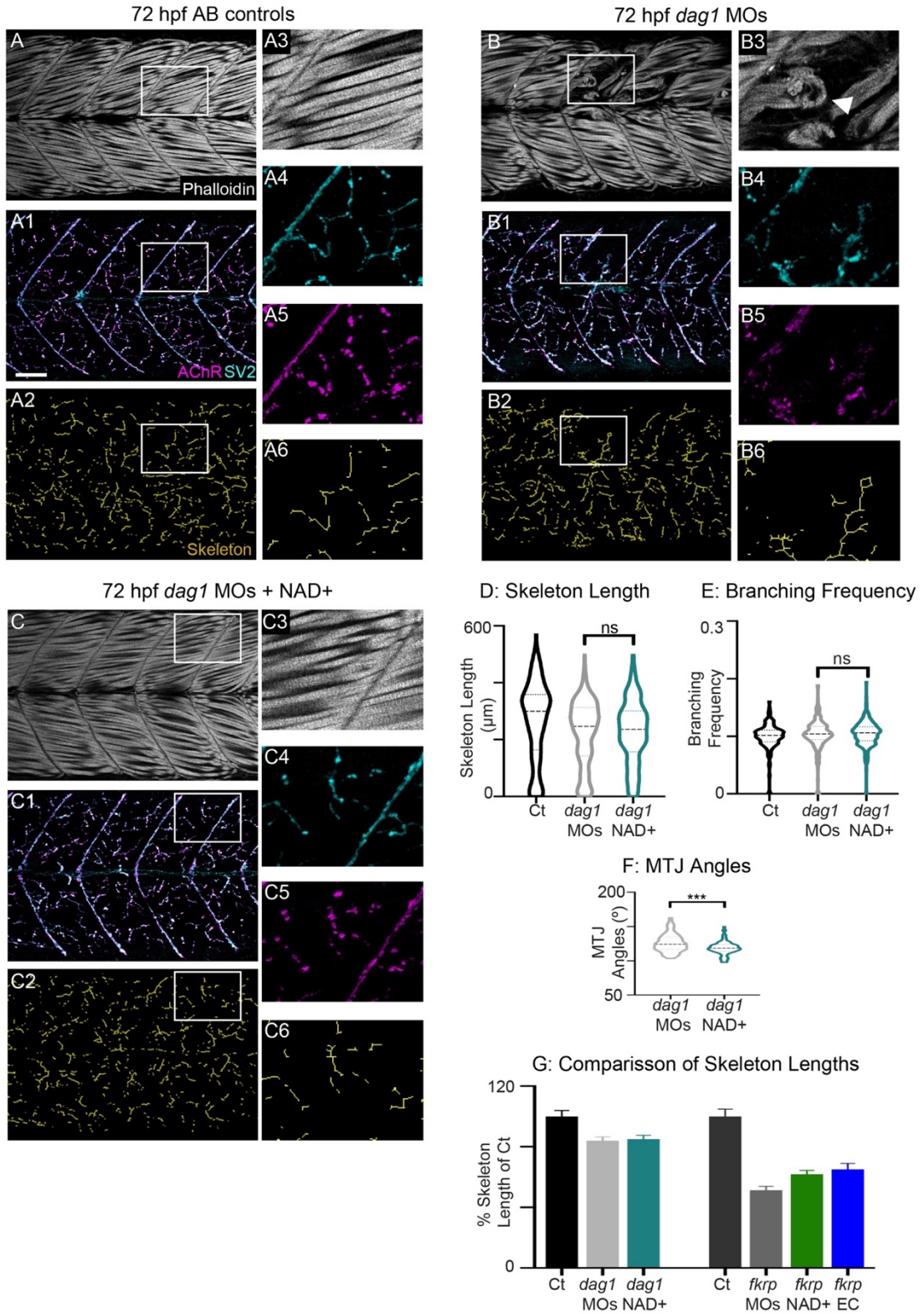
of NAD⁺ or EmergenC improved NMJ length, although NMJs were not fully restored (Fig. 2.5C-D). In order to quantify innervation, we developed a semi-automated technique in MATLAB to skeletonize NMJs (see Chapter 5, Section 5.10.8). This analysis showed that although branching frequency was normal, skeleton length was reduced in *fkrp* morphants (Fig. 2.5E, F). NAD⁺ or EmergenC supplementation at 6 hpf slightly, but significantly, improved skeleton length in *fkrp* morphants (Fig. 5E). These results suggest that Fkrp is necessary for innervation, but not branching.

As mentioned above, DG contributes to NMJ maturation and stabilization (Gumerson et al., 2013). Given the above data showing that initial NMJ development is disrupted in *fkrp* morphants, we asked whether DG is also required for NMJ development. We found that skeleton length was slightly, but significantly, reduced in *dag1* morphants (Fig. 2.6B) compared to controls (Fig. 2.6A). However, NAD⁺ supplementation at gastrulation did not significantly increase skeleton length in *dag1* morphants despite rescuing other aspects of the phenotype (Fig. 2.6C-D, F). This result contrasts with what we observed in *fkrp* morphants supplemented with NAD⁺. Thus, we compared the relative severity of NMJ skeleton length defects in *fkrp* morphants versus *dag1* morphants. On average, *dag1* morphant skeleton length was 83.9% of that of uninjected controls. In contrast, *fkrp* morphant skeleton length on average was 51.4% of that of uninjected controls (Fig. 2.6G). Thus, NMJs are more severely disrupted in *fkrp* morphants compared to *dag1* morphants.

Somewhat surprisingly, we found that NAD⁺ supplementation at 24 hpf actually significantly worsened the escape response in *fkrp* morphants (Fig. 2.4, $p < 0.05$) despite the fact that we did not observe a significant deterioration of muscle structure. Thus, we asked how NAD⁺ supplementation at 24 hpf affected NMJ structure (Fig. 2.7). We found that the effects of NAD⁺ on NMJ structure correlated with the motility defects: NAD⁺ at 24 hpf resulted in

Figure 2.6. Skeleton length is less disrupted in *dag1* morphants than in *fkrrp* morphants and is not significantly improved with NAD⁺ supplementation. (A-C6) Anterior left, dorsal top, side-mounted embryos at 72 hpf with labeled actin, AChRs, and SV2. **(Lettered panels)** Phalloidin stained embryos. **(1)** Merged channels of AChR and SV2. **(2)** Skeletonized images. **(3)** Magnification of phalloidin channel. **(4)** Magnification of SV2 channel. **(5)** Magnification of AChR channel. **(6)** Magnification of skeleton channel. **(A-A6)** Control embryo. **(B-B6)** *dag1* morphant embryo. **(C-C6)** *dag1* morphant embryo treated with NAD⁺ at 6 hpf. **(D)** Length of skeletons per myotome in control embryos (n=186 half-myotomes), *dag1* morphants (n=260 half-myotomes), and *dag1* morphants receiving NAD⁺ (n=252 half-myotomes) at 6 hpf. Skeleton length is not significantly different between untreated and NAD⁺ treated *dag1* morphants. **(E)** Degree of branching within the myotome in control embryos (n=180 half-myotomes), *dag1* morphants (n=254 half-myotomes), and *dag1* morphants receiving NAD⁺ (n=249 half-myotomes) at 6 hpf. NAD⁺ treatment made no significant difference. **(F)** MTJ angle quantification. MTJ angles are significantly reduced in *dag1* morphants receiving NAD⁺ (n=98 MTJs) compared to untreated *dag1* morphants (n=97 MTJs). **(G)** Bar graph of the percent skeleton length of control embryos per myotome. Note that the average percent skeleton length is more drastically reduced in *fkrrp* morphants (51.4%, n=153 half-myotomes) than in *dag1* morphants (83.9%, n=260 half-myotomes). NAD⁺ supplementation increased this percentage in *fkrrp* morphants (61.9%, n=183 half-myotomes), but has little effect on *dag1* morphants (85.0%, n=252 half-myotomes) Scalebars are 50 micrometers. Error bars in (G) are standard error of the mean. **p*<0.05, ***p*<0.01, ****p*<0.001, ns non-significant.

Figure 2.6.



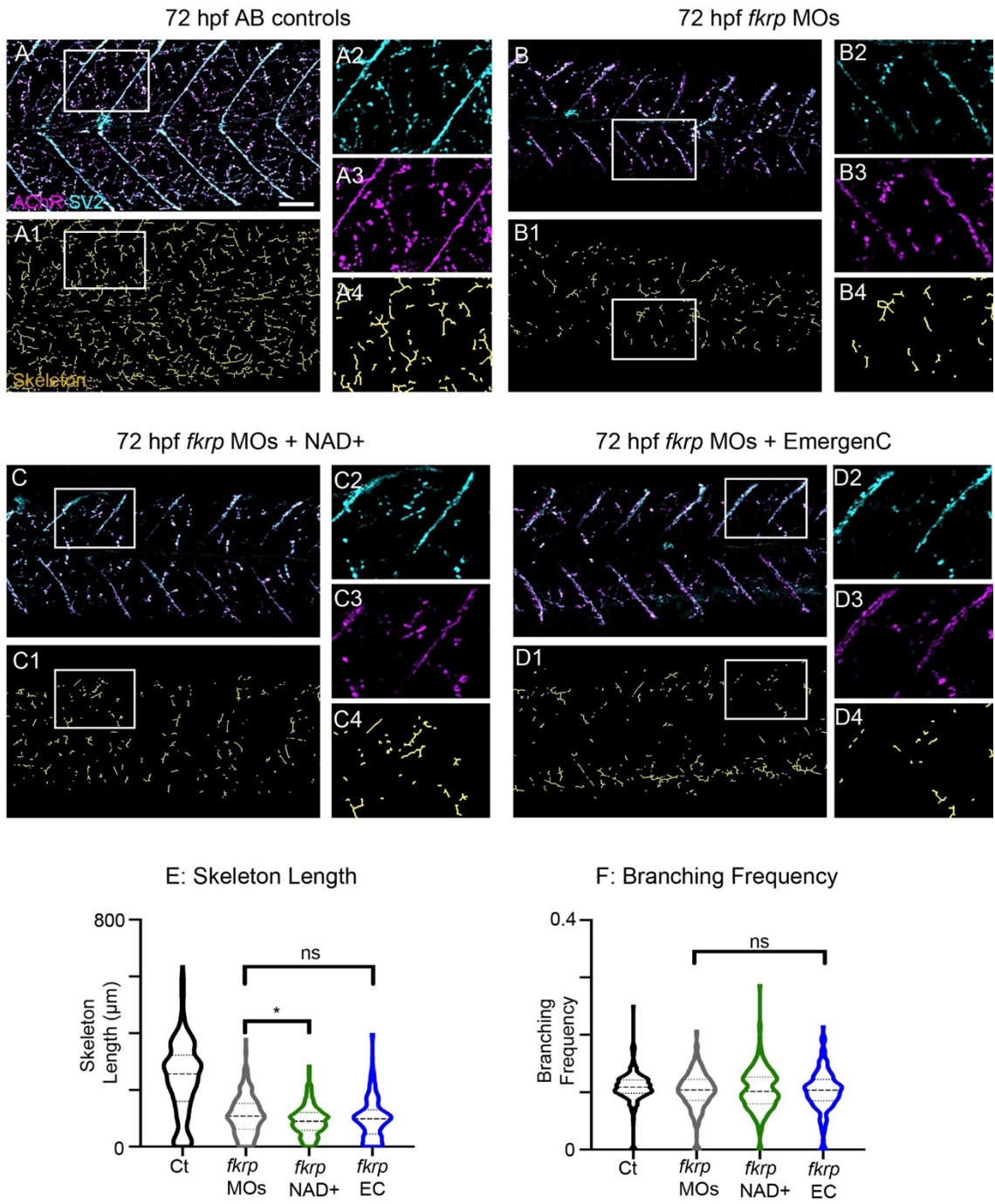
significantly shorter skeleton lengths (Fig. 2.7E). There was no significant difference between 24 hpf treated and untreated morphants in terms of branching frequency (Fig. 2.7F).

2.2.6. Muscle specific FKRP expression is not sufficient to rescue *fkrp* morphants

The above data indicate that Fkrp is necessary for early NMJ development and that disruption in NMJ morphology with 24 hpf NAD⁺ treatment correlates with worse motility. These results raise the possibility that Fkrp function is required in non-muscle tissues. We tested this hypothesis by expressing Fkrp in a muscle-specific manner. To confirm that constitutive Fkrp overexpression could rescue *fkrp* morphants, we injected *fkrp* MOs into a *Tg(hsp70l:fkrp-EGFP)* line we generated (Fig. 2.8A). Previous data suggest that overexpression of *fkrp* can be deleterious (Vannoy et al., 2017). Although we observed a slight increase in MTJ angles (Fig. 2.8C), we did not observe any significantly adverse effects of Fkrp-EGFP on fiber degeneration or the escape response in control embryos (expression was induced at the 15 somite stage) (Fig. 2.8A, D-E). Global overexpression of Fkrp-EGFP in *fkrp* morphants improved fiber resiliency, MTJ angles, and the escape response compared to control morphants (Fig. 2.8B-E). These data indicate that: (1) overexpression of Fkrp is not toxic under these conditions, and (2) EGFP does not deleteriously affect Fkrp function. We next asked whether muscle-specific expression was sufficient to rescue the phenotype. We generated a transgenic line expressing Fkrp-EGFP under control of the *-503unc* promoter (Berger and Currie, 2013). Muscle-specific overexpression of Fkrp did not affect muscle morphology in control embryos (Fig. 2.8F-F2). Muscle-specific overexpression of Fkrp in *fkrp* morphants decreased MTJ angles compared to EGFP negative control morphants (Fig. 2.8I). However, no other metrics of muscle structure/function were improved. Muscle specific overexpression neither ameliorated fiber detachment (Fig. 2.8G-H, J) nor reduced touches required to induce an escape response (Fig. 2.8K). These data indicate that expression of Fkrp in muscle is not sufficient to rescue muscle morphology or function.

Figure 2.7. Supplementation with NAD⁺ or EmergenC after muscle development does not improve NMJ morphology in *fkrp* morphants. (A-D4) Anterior left, dorsal top, side-mounted embryos at 72 hpf with labeled AChRs and SV2. **(Lettered panels)** Merged channels of AChR and SV2. **(1)** Skeletonized images. **(2)** Magnification of SV2 channel. **(3)** Magnification of AChR channel. **(4)** Magnification of skeleton channel. **(A-A4)** Control embryo. **(B-B4)** *fkrp* morphant embryo exhibiting a reduced degree of distributed innervation within the myotome. **(C-C4)** *fkrp* morphant embryo treated with NAD⁺ at 24 hpf also has reduced innervation. **(D-D4)** *fkrp* morphant embryo treated with EmergenC at 24 hpf has reduced NMJs. **(E)** Length of skeletons per myotome in control embryos (n=288 half-myotomes), *fkrp* morphants (n=303 half-myotomes), and *fkrp* morphants receiving NAD⁺ (n=225 half-myotomes) or EmergenC (n=225 half-myotomes) at 24 hpf. Note that skeleton length is actually significantly decreased in *fkrp* morphants receiving NAD⁺ at 24 hpf. **(F)** Degree of branching within the myotome in control embryos (n=283 half-myotomes), *fkrp* morphants (n=295 half-myotomes), and *fkrp* morphants receiving NAD⁺ (n=221 half-myotomes) or EmergenC (n=210 half-myotomes) at 24 hpf. Scalebars are 50 micrometers. **p*<0.05, ns non-significant.

Figure 2.7.



2.3. Discussion

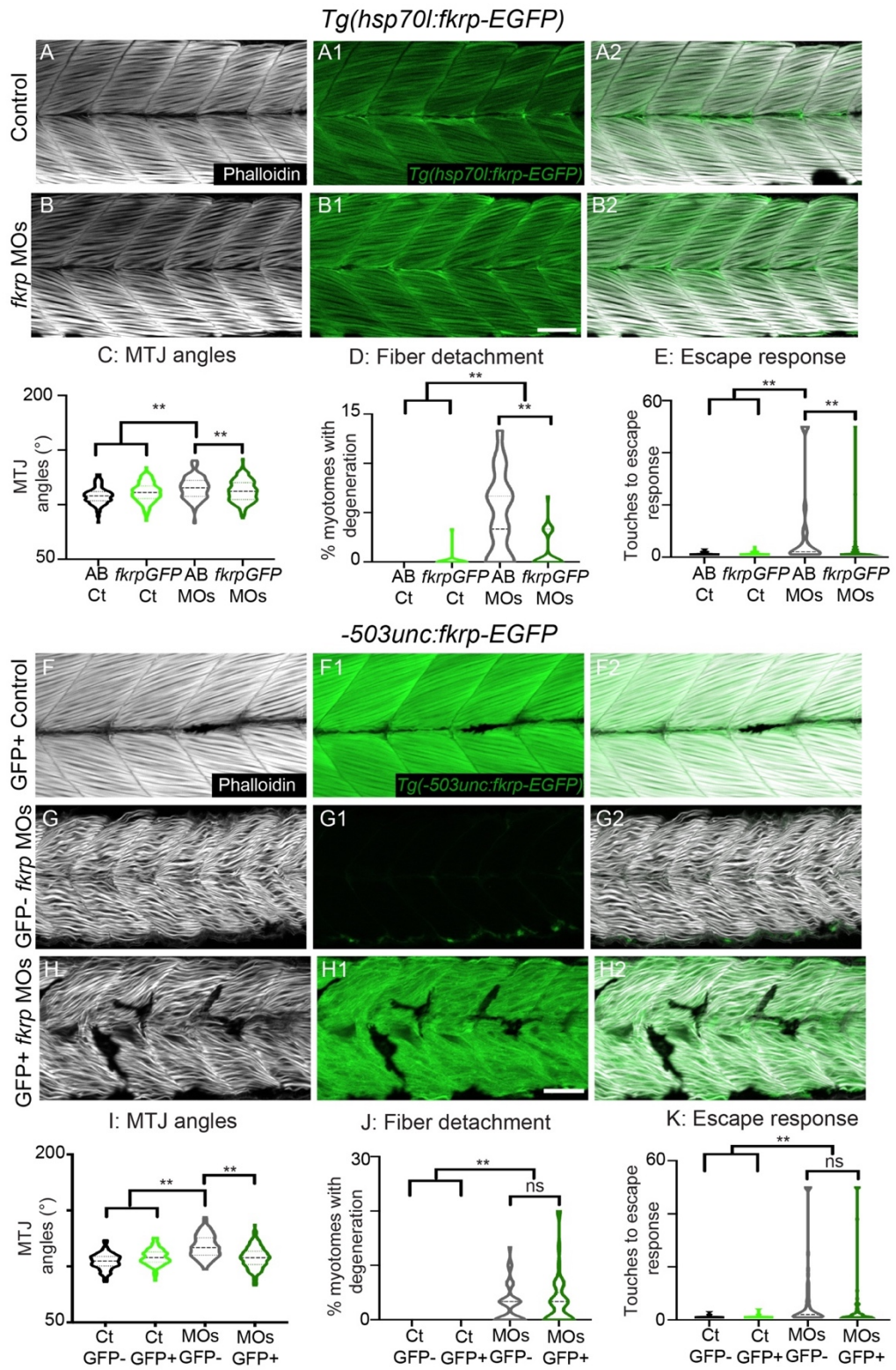
Dystroglycanopathies are a relatively understudied subset of muscular dystrophies. One aspect of dystroglycanopathies that is not well understood is how the myomatrix is impacted. Whether strategies that improve the myomatrix and muscle structure in a primary dystroglycanopathy (DG deficiency) are efficacious in secondary dystroglycanopathies are also not known. We previously showed that either NAD⁺ supplementation or overexpression of an Integrin-associated adaptor protein (Paxillin) are sufficient to improve muscle structure and function in DG-deficient zebrafish. Here we show that muscle phenotypes in a zebrafish model of FKR^P-associated dystroglycanopathy are improved with NAD⁺ supplementation but not Paxillin overexpression. Although the mechanisms are not known, these data clearly indicate that primary and secondary dystroglycanopathies show some differences. Our data also suggest that there are differences even within secondary dystroglycanopathies. Whereas muscle-specific expression of *Large* is sufficient to rescue muscle structure and function in *Large/myd* mutant mice (Gumerson et al., 2013), we found that muscle-specific expression of *fkrp* is not sufficient to improve muscle structure/function in *fkrp* morphant zebrafish. Finally, our data show that NMJ formation is disrupted earlier in development than has previously been observed in a primary and secondary dystroglycanopathy model. Taken together, these data indicate that it is necessary to study the secondary dystroglycanopathies individually within the context of the group as a whole.

2.3.1. Cell-matrix adhesion and secondary dystroglycanopathy

Adhesion of muscle fibers to the MTJ is necessary for muscle development and homeostasis. We previously identified a cell adhesion pathway that contributes to laminin organization at the MTJ: Nr^k2b-mediated NAD⁺ production potentiates laminin organization at the MTJ during zebrafish muscle development (Goody et al., 2010). We then demonstrated that

Figure 2.8. Muscle-specific overexpression of Fkrp improves MTJ angles, but not motility or fiber resiliency. **(A-B2)** Anterior left, dorsal top, side-mounted embryos at 72 hpf stained for f-actin (phalloidin, gray) and expressing Fkrp-EGFP (green). **(A-A2)** Control *Tg(hsp70l:fkpr-EGFP)* embryo expressing Fkrp in the fibers. **(B-B2)** *fkpr* morphant *Tg(hsp70l:fkpr-EGFP)* embryo expressing Fkrp in fibers. **(C)** MTJ angles of *Tg(hsp70l:fkpr-EGFP)* control (n=264 MTJs) and *fkpr* morphant (n=340 MTJs) embryos and AB controls and morphants (n=141, 194 MTJs) at 72 hpf. Constitutive expression of Fkrp improves MTJ angles in morphants. **(D)** Constitutive expression of Fkrp in morphants (n=72 embryos) significantly reduces the number of myotomes with fiber degeneration compared with control morphants (n=35 embryos). **(E)** The escape response is significantly reduced in *fkpr* morphants constitutively overexpressing Fkrp (n=82 embryos) compared to control morphants (n=44 embryos). **(F-H2)** Anterior left, dorsal top, side-mounted embryos at 72 hpf stained for f-actin (phalloidin, gray) and expressing Fkrp-EGFP under control of the muscle-specific *-503unc* promoter (green). **(F)** Control *Tg(-503unc:fkpr-EGFP)* embryo expressing Fkrp specifically in muscle fibers. **(G)** *fkpr* morphant embryo on *Tg(-503unc:fkpr-EGFP)* background lacking Fkrp expression in muscle fibers. **(H)** *fkpr* morphant *Tg(-503unc:fkpr-EGFP)* embryo expressing Fkrp specifically in muscle fibers does not show improved muscle organization. **(I)** Muscle specific expression of FKRP in *fkpr* morphants (n=158 MTJs) significantly improves MTJ angles compared to control morphants (n=153 MTJs). **(J)** Muscle-specific overexpression of Fkrp (n=45 embryos) does not significantly lower the percent of myotomes with muscle degeneration in control *fkpr* morphants (n=47 embryos). **(K)** There is not a significant difference in the number of touches required to induce an escape response in *fkpr* morphants that overexpress Fkrp (n=73 embryos) in muscle versus those that do not (n=79 embryos). Scalebars are 50 micrometers. * $p < 0.05$, ** $p < 0.01$, ns non-significant.

Figure 2.8.



exogenous NAD⁺ is sufficient to improve laminin organization, muscle structure, and muscle function in zebrafish deficient for either DG or Itga7 (Goody et al., 2012). DG and Itga7 are both transmembrane receptors for laminin. We hypothesized that NAD⁺ improved laminin organization, at least in part, by increasing clustering of the remaining receptor (DG in Itga7-deficient embryos, and Itga7 in DG-deficient embryos). Here, we asked whether laminin organization would be increased if DG is present but hypoglycosylated. The rationale was that it is possible that the presence of hypoglycosylated DG that cannot bind laminin could inhibit the improvement of laminin organization with NAD⁺. The ribitol 5-phosphate transferase FKR is necessary for proper glycosylation of DG (Gerin et al., 2016; Kanagawa et al., 2016). We asked if NAD⁺ was sufficient to improve cell-matrix adhesion in *fkp* morphant zebrafish embryos. We found that NAD⁺ supplementation prior to muscle development was sufficient to improve laminin polymerization, muscle structure, and the escape response.

Organization of laminin at the MTJ is disrupted in zebrafish deficient either for DG (Goody et al., 2012) or *Fkrp* (Kawahara et al., 2010; Lin et al., 2011; Thornhill et al., 2008) (Fig. 2.1). Laminin is required for concentration of the Integrin adaptor protein Paxillin to the MTJ (Goody et al., 2010). Paxillin is an intracellular protein that localizes to cell-ECM adhesion complexes (Deakin and Turner, 2008) and modulates ECM composition at the developing MTJ (Jacob et al., 2017). Previous data regarding the beneficial potential of Paxillin in the context of aberrant muscle development/homeostasis are contradictory. Paxillin overexpression worsens muscle damage in ethanol-treated zebrafish (Coffey et al., 2018). However, Paxillin overexpression is sufficient to improve MTJ morphology in *Nrk2b*-deficient zebrafish (Goody et al., 2010). Paxillin overexpression also improves laminin organization and reduces muscle degeneration in *dag1* morphant zebrafish (Goody et al., 2012). We hypothesized that Paxillin overexpression would improve muscle structure and function in *fkp* morphants where DG is

present but not properly glycosylated. Interestingly, we found that Paxillin expression trended towards reducing degeneration and improving the escape response, but the effects were not significant (Fig. 2.3). This result suggests the hypothesis that, in contrast to the situation where DG is absent, the presence of hypoglycosylated DG in the membrane prevents Paxillin-mediated stabilization of muscle fibers.

2.3.2. Benefits of NAD⁺ supplementation may be restricted to the neuromusculoskeletal system

Both *fkrp* morphants and mutants have an increased UPR. *Xpb1*, a marker of the UPR, is upregulated in both *fkrp* morphants and *fkrp* mutants (Lin et al., 2011; Serafini et al., 2018). Expression of *bip*, a marker of the UPR, is upregulated in *fkrp* morphants at 28 hpf, especially in the neural floor plate and the hatching gland (Lin et al., 2011). However, *glytl1b (large2)* morphants with hypoglycosylated DG, *dag1* morphants, and *sly/lam1c* mutants do not exhibit *bip* upregulation (Lin et al., 2011), suggesting that activation of the UPR may result directly from loss of Fkrp. We asked if EmergenC supplementation was sufficient to reduce the UPR in *fkrp* morphants. We found that 3 dpf *Tg(ef1a:xbp1δ-GFP)* embryos injected with *fkrp* MOs have increased *xbp1-GFP* fluorescence compared to control embryos. EmergenC supplementation at gastrulation was not sufficient to reduce *xbp1-GFP* fluorescence. Taken together, these data suggest that activation of the UPR occurs independently of muscle-cell matrix adhesion and DG glycosylation and is likely a direct consequence of Fkrp knockdown.

Fkrp morphants and *fkrp* mutants also exhibit aberrant vascular development, including reduced ISV lengths (Serafini et al., 2018; Wood et al., 2011). One study suggests that impaired vascularization directly results from loss of Fkrp and that muscle phenotypes and vascular phenotypes are independent of one another (Wood et al., 2011). Here, we demonstrate that NAD⁺ supplementation at gastrulation is not sufficient to rescue truncated ISVs in *fkrp*

morphants. Given that NAD⁺ improves muscle structure and function in *fkrp* morphants, our data suggest that vascular phenotypes observed in *fkrp* morphants are not dependent on muscle phenotypes. This supports the previous hypothesis that abnormal vascular development in zebrafish models of FKR- associated dystroglycanopathy is a direct result of loss of Fkrp.

2.3.3. Timing of NAD⁺ intervention is critical

Gene therapy (Qiao et al., 2014; Thomas et al., 2016; Tucker et al., 2018; Vannoy et al., 2017), estrogen receptor modulators (Wu et al., 2018), and exogenous ribitol supplementation (Cataldi et al., 2018) improve muscle structure in FKR- associated dystroglycanopathy models. The efficacy of adenoviral gene therapy and ribitol supplementation decreases if administered later in the mouse's lifespan (Cataldi et al., 2018; Vannoy et al., 2017), suggesting that early intervention is most beneficial. Our data regarding the timing of NAD⁺ and EmergenC supplementation in *fkrp* morphants are consistent with the data mentioned above. We found that NAD⁺ (or EmergenC) supplementation prior to muscle development increased laminin organization, reduced muscle degeneration, improved muscle function, and improved NMJ structure (Fig. 2.1). In contrast, NAD⁺ (or EmergenC) supplementation after initial muscle development only improved MTJs and not muscle structure/function (Fig. 2.4).

Our data do not resolve why MTJ morphology is improved with late NAD⁺ supplementation or muscle-specific overexpression of Fkrp. Improved MTJ morphology does not always correlate with fiber degeneration. *Itga7* morphants exhibit muscle fiber detachment but have normal MTJ morphology, and NAD⁺ supplementation improves MTJ angles, but not fiber degeneration in *dag1/itga7* double morphants (Goody et al., 2012). Movement is not necessary for MTJ chevron formation in zebrafish embryos (Rost et al., 2014). We show that motility is not improved in *fkrp* morphants receiving NAD⁺ or EmergenC after initial muscle development, further suggesting that improved MTJ morphology does not always correlate with mobility.

While this manuscript was in preparation, it was shown that administration of pentetic acid at 48 hpf improved muscle and pericardiac phenotypes in a *fkrp* zebrafish model of LGMD2I (Serafini et al., 2018). Pentetic acid is a chelating agent that binds Ca²⁺ and Mg²⁺. The mechanism by which this improves muscle phenotypes is currently unknown. However, abnormal Ca²⁺ levels have been implicated in DMD and inducing an influx of Ca²⁺ is sufficient to induce dystrophy (Millay et al., 2009). Together, these data suggest that different therapeutic avenues have different time windows of efficacy in multiple animal models.

2.3.4. *Dag1* and *fkrp* are required for proper NMJ development

NMJ development requires orchestrated interactions between muscle cells and motor neurons. The DGC is a major component of NMJs. Thus, it is not surprising that NMJ morphology is disrupted in multiple dystroglycanopathies. Fukutin-deficient chimeric mice have abnormal AChR clustering and NMJs at postnatal day 15 (Saito et al., 2007). Newborn pups homozygous for *Large/myd* mutations have altered NMJs as well (Herbst et al., 2009). These data clearly indicate that NMJs are abnormal after birth. What is not clear is at which point in embryonic development NMJ disruption occurs. Do NMJs develop normally and then degenerate or is initial NMJ development abnormal? Here, we provide evidence that early NMJ development is slightly disrupted in DG-deficient zebrafish, with NMJ chains that innervate fast-twitch muscle being approximately 84% of control chain length. To our knowledge, this is the earliest developmental stage at which NMJ disruption has been observed in a primary or secondary dystroglycanopathy. Interestingly, *fkrp* morphants exhibit more dramatic disruption of NMJ morphology, with NMJ chains about half of control chain length. We do not know the mechanisms underlying the more severe disruption in NMJ development in *fkrp* versus *dag1* morphants. One possibility is that hypoglycosylated *dag1* acts as a “dominant negative” and thus disrupts NMJ development more than when *dag1* is not present. Additionally, there are many glycosylated proteins at the MTJ,

such as Lrp2, Musk, and Agrin. Thus, the more severe disruption in *fkrp* morphants could also reflect a requirement of Fkrp for glycosylation of other NMJ resident proteins.

2.3.5. Muscle-specific overexpression of Fkrp is not sufficient to rescue *fkrp* morphants

Overexpression of LARGE is sufficient to synthesize glycan-enriched alpha-DG and is sufficient to improve laminin binding activity in multiple dystroglycanopathy patient cell lines (Barresi et al., 2004). Muscle-specific expression of *Large* is sufficient to rescue muscle structure, neurotransmission, and NMJs in *Large/myd* mutant mice (Gumerson et al., 2013). NMJ defects in *Large/myd* mutant mice were observed after birth (Herbst et al., 2009). The above data suggest that, in the context of Large-associated Dystroglycanopathy, NMJ defects are secondary to muscle disruption. Given that we observed very early developmental disruption of NMJs, we couldn't necessarily conclude that NMJ disruption in Fkrp-deficient embryos is secondary to the muscle phenotype. Thus, we tested whether muscle-specific expression of Fkrp would be sufficient to rescue neuromuscular function in *fkrp* morphant embryos. We first showed that global expression of Fkrp (under control of the heat shock promoter) is sufficient to rescue *fkrp* morphant embryos. This result indicates that the Fkrp-EGFP fusion protein is functional.

Next, we expressed Fkrp in muscle under control of the muscle specific *-503unc* promoter (Berger and Currie, 2013). We found that muscle-specific expression of Fkrp was sufficient to slightly, but significantly, reduce MTJ angles. However, muscle-specific expression of Fkrp was not sufficient to reduce muscle degeneration or improve the escape response (Fig. 2.8). We do not know why our results differ from the *Large* study. We do not believe that timing of expression is the key factor because muscle creatine kinase (*Large* study) and *Unc45b* (our study) are expressed at similar times during myotome development. In the DG glycosylation pathway, FKRPs works in concert with Fukutin (FKTN) to synthesize a tandem ribitol phosphate that connects a core o-linked glycan with matriglycan, the ligand for laminin and other ECM

proteins (Gerin et al., 2016; Kanagawa et al., 2016). This step precedes the completion of matriglycan synthesis by LARGE. Roles for LARGE or FKRPs in other glycosylation reactions have not been identified. However, the fact that muscle-specific expression of Fkrp is not sufficient to rescue muscle homeostasis may suggest that Fkrp is required to glycosylate proteins other than DG. Regardless, our data indicate that Fkrp is required outside of skeletal muscle to reduce muscle degeneration. In the future it will be interesting to determine in which tissues and cells Fkrp is required to rescue neuromuscular function in Fkrp-deficient embryos.

2.4. Conclusion

The myomatrix is critical for muscle development and homeostasis and is disrupted in many dystroglycanopathies studied thus far (Di Costanzo et al., 2014; Lin et al., 2011; Marchese et al., 2016; Roscioli et al., 2012; Stevens et al., 2013). Here, we primarily focused on two specialized junctions within the myomatrix: the MTJ and NMJ. MTJ and NMJ development are disrupted in *fkrp* morphants. NAD⁺ supplementation prior to muscle development, which improves myomatrix organization in DG-deficient zebrafish, was sufficient to improve muscle homeostasis, MTJ structure, and NMJ formation in *fkrp* morphant zebrafish. However, NAD⁺ did not improve vascular or UPR phenotypes in *fkrp* morphants, and NAD⁺ supplementation after initial muscle development was not particularly efficacious. There was a slight improvement in MTJ structure and a reduced variation in muscle degeneration. These data are similar to previous studies showing that earlier intervention has improved outcomes in *FKRP* mutant mice (Cataldi et al., 2018; Vannoy et al., 2017). Interestingly, in contrast to muscle-specific expression of Large in *Large/myd* mutant mice, muscle-specific overexpression of Fkrp was not sufficient to improve muscle structure/function in *fkrp* morphants. Taken together, our data indicate that Fkrp plays an early and crucial role in muscle, MTJ, and NMJ development.

CHAPTER 3

PHENOTYPIC VARIATION AND PLASTICITY IN A ZEBRAFISH MODEL OF GMPPB-ASSOCIATED DYSTROGLYCANOPATHY

3.1. Introduction

Skeletal muscle is a tissue that is conserved among many organisms and is necessary for strength and locomotion. It is a highly plastic tissue that undergoes changes in size based on genetic and/or environmental cues. Skeletal muscle may grow in size (hypertrophy) in response to diet and exercise. However, aging (sarcopenia), cancer cachexia, a lack of exercise, and neuromuscular diseases such as muscular dystrophies can cause a loss of muscle mass (atrophy). Individuals with muscular dystrophies and similar conditions often possess remarkable variation in both the level of muscle atrophy and the ability to regenerate skeletal muscle, even when the molecular basis of their condition is similar. The mechanisms that contribute to this phenotypic variation among individuals with the same type of muscular dystrophy remain poorly understood.

One group of muscular dystrophies where phenotypic variation is common are the dystroglycanopathies. These are a suite of molecularly distinct conditions that result from mutations in genes responsible for glycosylating Dystroglycan (DG) (Godfrey et al., 2011; Inamori et al., 2012; Muntoni et al., 2011). DG is a major component of the dystrophin-glycoprotein complex (DGC) that helps link the actin cytoskeleton of muscle fibers with laminin and other extracellular matrix (ECM) proteins. It contains a transmembrane beta subunit and an extracellular alpha subunit that binds to laminin and other ECM proteins (Muntoni et al., 2011). Alpha-DG must be glycosylated by a team of glycosyltransferases in order to bind to its ligands. Patients with dystroglycanopathies often present with either limb-girdle muscular dystrophies (LGMDs) or with congenital muscular dystrophies (CMDs) (Muntoni et al., 2008; Taniguchi-Ikeda

et al., 2016). Central nervous system defects are sometimes present in dystroglycanopathy patients with CMDs (Nickolls and Bönnemann, 2018); however, the role of alpha-DG glycosylation in the peripheral nervous system in dystroglycanopathies is less understood. Neuromuscular junction (NMJ) disruption has been reported in mouse models of dystroglycanopathy (Côté et al., 1999; Herbst et al., 2009; Levedakou et al., 2005; Saito et al., 2007). Additionally, alpha-DG glycosylation is necessary for NMJ formation in regenerating skeletal muscle (Goddeeris et al., 2013). We recently found that zebrafish deficient for DG or Fkrp exhibit NMJ defects during the late embryonic stages (Chapter 2). These data suggest that DG glycosylation enzymes are essential for NMJ formation. Despite these findings, the timing and mechanisms behind disrupted NMJ development remain unclear.

GMPPB-associated dystroglycanopathy is associated with phenotypes in both muscle and NMJs. This condition results from mutations in GDP-Mannose Pyrophosphorylase B (GMPPB), an enzyme that participates in DG glycosylation. GMPPB converts mannose-1-phosphate to GDP-mannose, which is subsequently used in several glycosylation reactions such as C-mannosylation and N-glycosylation (Carss et al., 2013). Patients with GMPPB-associated dystroglycanopathy present with phenotypic variation. Similar to other dystroglycanopathies, individuals with *GMPPB* mutations develop milder, adolescent- or adult-onset limb-girdle muscular dystrophies or severe congenital muscular dystrophies with central nervous system involvement (Bharucha-Goebel et al., 2015; Cabrera-Serrano et al., 2015; Carss et al., 2013; Jensen et al., 2015; Oestergaard et al., 2016; Raphael et al., 2014). Although genotype-phenotype correlations have emerged in regard to these phenotypes (Jensen et al., 2015), there is still phenotypic variation within individuals with the same molecular *GMPPB* variants, even within families (Bharucha-Goebel et al., 2015). For example, individuals with the common c.79 G>C mutation associated with limb-girdle muscular dystrophy may also develop congenital

myasthenic syndrome (CMS) (Belaya et al., 2015; Luo et al., 2017; Rodríguez Cruz et al., 2016). CMS is a neuromuscular disorder characterized by poor neuromuscular transmission at the NMJ (Finsterer, 2019). The age of symptomatic onset in individuals with the c.79 G>C variant is highly variable (Bharucha-Goebel et al., 2015; Montagnese et al., 2017). Cases of epilepsy (Astrea et al., 2018; Raphael et al., 2014), one case of autism spectrum disorder (Astrea et al., 2018), pseudometabolic myopathy (Panicucci et al., 2018), and rhabdomyolysis (Cabrera-Serrano et al., 2015) have also been reported in individuals with *GMPPB* mutations. These clinical studies suggest that the phenotypic diversity observed with these disorders may be a result of genetic and/or environmental factors. The above studies also suggest the importance of studying neural features associated with these disorders and indicate that it is critical to examine how muscle phenotypes develop or change over the course of one's illness.

Most of the research concerning *GMPPB*-associated dystroglycanopathy has been clinical and does not address the biological mechanisms underlying this disorder. Animal model studies regarding *GMPPB* are limited. *Gmppb* morphant zebrafish exhibit sarcolemmal damage, MTJ abnormalities, bent tails, and hypoglycosylated alpha-DG (Carss et al., 2013). There are currently no published genomic models for this disorder in mouse, zebrafish, *Drosophila*, or any other model organism. Zebrafish offer many advantages for studying neuromuscular diseases such as *GMPPB*-associated dystroglycanopathy. They are externally fertilized, possess high fecundity and rapid development, and are transparent for the first several days of life (reviewed by (Gibbs et al., 2013)). This allows for visualization of their muscle and/or nerves via immunofluorescence microscopy. Recently, genome editing techniques such as TALENs and CRISPR/Cas9 have made genomic manipulations more precise and accessible in zebrafish (reviewed by (Cornet et al., 2018; Liu et al., 2019; Rafferty and Quinn, 2018; Simone et al., 2018)). Zebrafish have been especially advantageous in elucidating the cell behaviors in the

context of neuromuscular disorders, including muscle cell-ECM adhesion mechanisms. We previously found that Nr2b-mediated NAD⁺ production potentiates laminin organization at the MTJ during zebrafish muscle development (Goody et al., 2010). We then determined that exogenous NAD⁺ is sufficient to improve laminin organization, muscle structure, and function two zebrafish models of dystroglycanopathy ((Goody et al., 2012), Chapter 2). However, whether NAD⁺ remains beneficial for GMPPB-associated dystroglycanopathy has not been investigated.

To address questions regarding cell-ECM adhesion and neuromuscular phenotypic variation in GMPPB-associated dystroglycanopathy, we used CRISPR/Cas9 mutagenesis to engineer a *gmppb* mutant zebrafish line. Programmed DNA was inserted near the 3' end of intron 2. RNA-seq analyses revealed the presence of multiple splice variants in *gmppb* mutants that are predicted to result in premature stop codons. We determined that *gmppb* mutants have abnormal beta-DG localization. Surprisingly, we found that NAD⁺ supplementation is not sufficient to rescue muscle and MTJ phenotypes. Additionally, *gmppb* mutants exhibited phenotypic variation, and “severe” embryos had wider MTJ angles and increased levels of dystrophy compared to “mild” embryos. We detected defects in early primary motoneuron development in *gmppb* mutants. Although *gmppb* mutants exhibited NMJ defects, these were not significantly different between “mild” and “severe” *gmppb* mutants. We subsequently found that *gmppb* mutants can be quantitatively separated into mild and severe phenotypes based on birefringence image analysis at 2 dpf. Longitudinal experiments revealed that a portion of *gmppb* mutants initially presenting with severe phenotypes recovered to milder phenotypes by 7 dpf. Taken together, these results suggest that *gmppb* mutants exhibit a degree of phenotypic variability similar to that of humans and undergo phenotypic shifts throughout the first several days of life.

3.2. Results

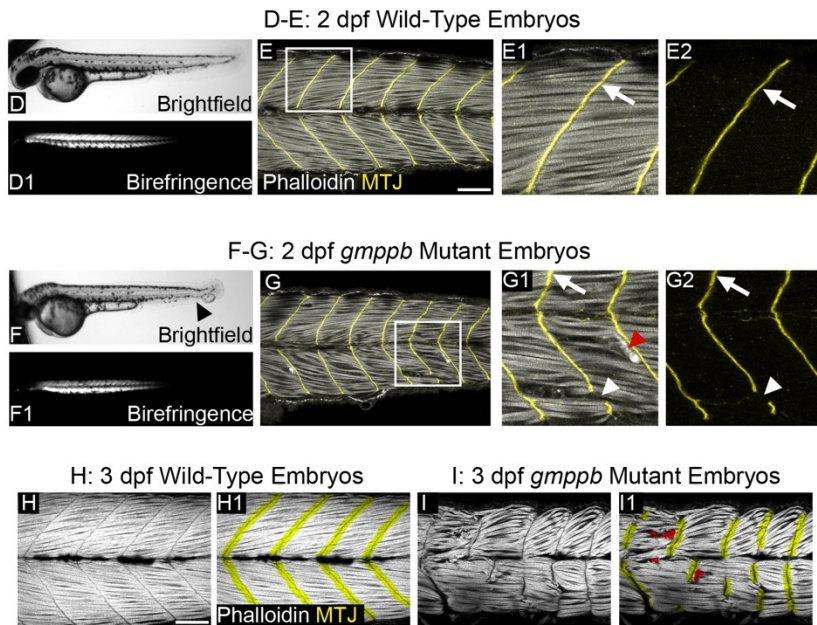
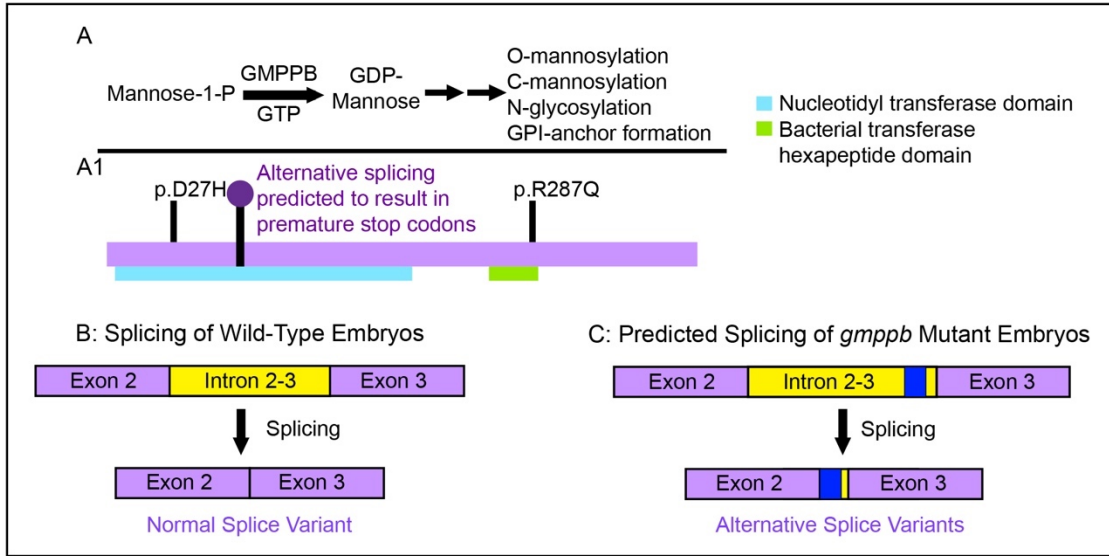
3.2.1. Characterization of *gmppb* mutants

In humans, the most commonly reported *GMPPB* mutation is single-nucleotide substitution associated with phenotypic variation: c.79 G>C (Bharucha-Goebel et al., 2015; Cabrera-Serrano et al., 2015; Carss et al., 2013; Jensen et al., 2015; Montagnese et al., 2017; Oestergaard et al., 2016; Raphael et al., 2014). To answer questions regarding cell-ECM adhesion and phenotypic variation in the context of *GMPPB*-associated dystroglycanopathy, we used CRISPR/Cas9 mutagenesis (Gagnon et al., 2014) to engineer a zebrafish *gmppb* mutant. A preliminary RNA-seq experiment was performed on a pool of wild-type and *gmppb* mutants. This experiment revealed that programmed DNA was inserted near the junction of intron 2 and exon 3 of *gmppb* as expected (Appendix B). In addition to detecting correctly spliced *gmppb* transcripts, we detected four alternative splice variants in the *gmppb* mutant samples (Fig. 3.1B-C, Appendix B). At least three of these variants are predicted to result in premature stop codons (Fig. 3.1A1, Appendix B). These data suggest that *gmppb* mutants are hypomorphic in nature.

The zebrafish *gmppb* morphant exhibits reduced body size, smaller eyes, and disorganized muscle fibers that cross the myotome boundaries at 48 hpf (Carss et al., 2013). We found that *gmppb* mutant embryos had abnormal tail morphology (Fig. 3.1F), as well as muscle fibers spanning multiple myotomes (MTJ failure) and fiber detachment (Fig. 3.1G-G2, I-I1). These data show that aberrant muscle phenotypes are present in this model, suggesting that *gmppb* mutants an attractive model for studying cell-matrix adhesion in the context of *GMPPB*-associated dystroglycanopathy.

Figure 3.1. Characterization of *gmppb* mutant zebrafish embryos. **(A)** Biochemical function of GMPPB. Note that GMPPB synthesizes GDP-mannose from mannose-1-phosphate and this product is used in several glycosylation reactions. Adapted from *Carss et al. (2013)*. **(A1)** Predicted location of the *gmppb* mutation relative to two common mutations in human populations. Based on RNA-seq data, the *gmppb* mutation is predicted to introduce premature stop codons in the nucleotidyl transferase domain of the protein due to alternative splicing. Schematic adapted from *Carss et al. (2013)*. **(B-C)** Proposed mechanisms of RNA splicing in wild-type (B) and mutant (C) embryos. The insertion of the stop cassette (blue) in intron 2-3 (yellow) introduces alternative splice sites that generate alternative RNA transcripts. **(D-E)** Anterior left, dorsal top, side-mounted 2 dpf wild-type embryos. **(D-D1)** Live brightfield (D) and birefringence (D1) images of 2 dpf wild-type embryo. **(E-E2)** Wild-type embryo stained for f-actin (phalloidin, gray). Note normal MTJ morphology (white arrow) and lack of fiber detachment. **(F-G)** Anterior left, dorsal top, side-mounted 2 dpf *gmppb* mutant embryos. **(F-F1)** Live brightfield (F) and birefringence (F1) images of 2 dpf *gmppb* mutants. Note abnormal posterior morphology (black arrowhead). **(G-G2)** Mutant embryo stained for f-actin (phalloidin, gray). Note breaks in MTJ (white arrowhead) and fiber detachment (red arrowhead) that are not present in the wild-type embryo. **(H-I1)** Anterior left, dorsal top, side-mounted 3 dpf embryos stained for f-actin (phalloidin, gray). **(H-H1)** Wild-type embryo. Note lack of fiber detachments or crossings. **(I-I1)** *gmppb* mutant embryo. Note muscle fibers crossing the MTJ boundaries. Scalebars are 50 micrometers.

Figure 3.1.



3.2.2. NAD⁺ is not sufficient to improve muscle phenotypes in *gmppb* mutants

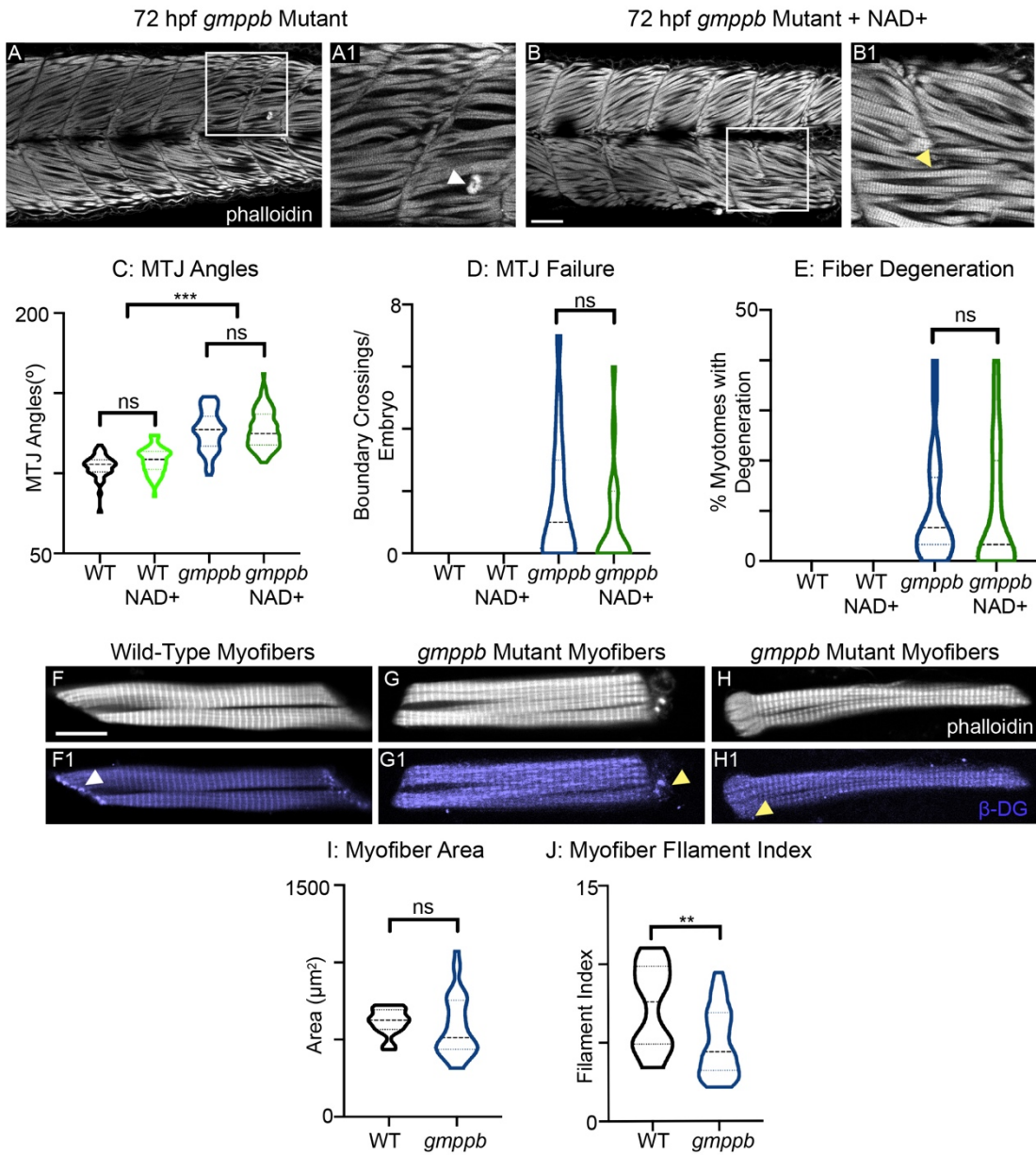
NAD⁺/EmergenC supplementation prior to muscle development is sufficient to improve muscle phenotypes in both *dag1* morphant (Goody et al., 2012) and *fkrp* morphant zebrafish (Fig. 2.1). Given that exogenous NAD⁺ reduces muscle degeneration in both of these circumstances and that *gmppb* mutants exhibit muscle and MTJ phenotypes, we hypothesized that NAD⁺ would improve muscle phenotypes in *gmppb* mutant embryos. Surprisingly, NAD⁺ supplementation was not sufficient to significantly improve MTJ angles, MTJ failure, and dystrophy in *gmppb* mutant embryos (Fig. 3.2A-E). Patients with *GMPPB* mutations exhibit variability in sarcolemmal beta-DG accumulation (Bharucha-Goebel et al., 2015; Cabrera-Serrano et al., 2015; Jensen et al., 2015; Oestergaard et al., 2016) and sometimes present with Western blot mobility shifts in beta-DG (Sarkozy et al., 2018). We asked if beta-DG localization was disrupted in *gmppb* mutants and found that isolated myofibers exhibited mislocalized beta-DG and abnormal clustering of beta-DG on the edges of the fibers (Fig. 3.2G-H1) compared to WT embryos (Fig. 3.2F-F1). Additionally, *gmppb* mutant myofibers were more circular in shape than wild-type myofibers (Fig. 3.2J). Our results suggest that beta-DG mislocalization occurs in *gmppb* mutants.

3.2.3. *Gmppb* mutants exhibit phenotypic variation in muscle

Humans harboring *GMPPB* mutations exhibit a broad range of symptoms and severities, even when individuals have identical genetic variants (Belaya et al., 2015; Cabrera-Serrano et al., 2015; Luo et al., 2017). *Gmppb* mutant zebrafish are an ideal model to address questions regarding neuromuscular phenotypic variation. We imaged 72 hpf wild-type and *gmppb* mutant embryos labeled for f-actin (phalloidin) to quantify MTJ angles, MTJ failure, and dystrophy at this stage. We determined that compared to wild-type embryos (Fig. 3.3A), *gmppb* mutants exhibit differences overall in terms of muscle (Fig. 3.3B, C). Additionally, we observed

Figure 3.2. *Gmppb* mutants are not rescued by NAD⁺ supplementation and have abnormal beta-DG localization. (A-B1) Anterior left, dorsal top, side-mounted embryos stained for f-actin (phalloidin, gray). **(A-A1)** 72 hpf *gmppb* mutant. Note fiber detachment in the myotome (white arrowhead). **(B-B1)** 72 hpf *gmppb* mutant treated with 0.1 mM NAD⁺ at 6 hpf. Note the muscle fibers spanning multiple myotomes (yellow arrowhead). **(C)** MTJ angles are significantly increased in *gmppb* mutant embryos (n=107 MTJs) compared to untreated (n=49 MTJs) and NAD⁺-treated (n=58 MTJs) wild-type embryos. MTJ angles are not significantly reduced in NAD⁺-treated *gmppb* mutants (n=84 MTJs) compared to untreated mutants. **(D)** There is not a significant difference in MTJ failure between *gmppb* mutants treated with NAD⁺ (n=19 embryos) and untreated *gmppb* mutants (n=19 embryos). **(E)** There is no significant difference in the percent of myotomes with degeneration between *gmppb* mutants treated with (n=19 embryos) and without (n=19 embryos) NAD⁺. **(F-H1)** Individual myofibers purified from 48 hpf embryos stained for phalloidin (lettered panels, gray) and beta-DG (numbered panels, blue). **(F-F1)** Control myofiber. Note that beta-DG localizes to the terminal edges of the myofibers (white arrowhead). **(G-H1)** *Gmppb* mutant myofibers. Note how beta-DG is aggregated along the myofibers (yellow arrowhead) and does not localize to the terminal ends. **(I)** There is no significant difference in myofiber area between control (n=16 myofibers) and *gmppb* mutant (n=38 myofibers) myofibers. **(J)** Myofiber shape was quantified in control (n=16 myofibers) and *gmppb* mutant myofibers (n=38 myofibers) using the filament index. This metric quantifies how much an object deviates from a circular shape: a lower filament index corresponds with a more circular shape (Snow et al., 2008b). There is a significant reduction in the filament index in *gmppb* mutants compared with controls. This suggests that *gmppb* mutant myofibers are more circular. Myofiber scalebars are 10 micrometers, other scalebars are 50 micrometers, * $p < 0.05$, ** $p < 0.01$, *** $p < 0.001$, ns non-significant.

Figure 3.2.

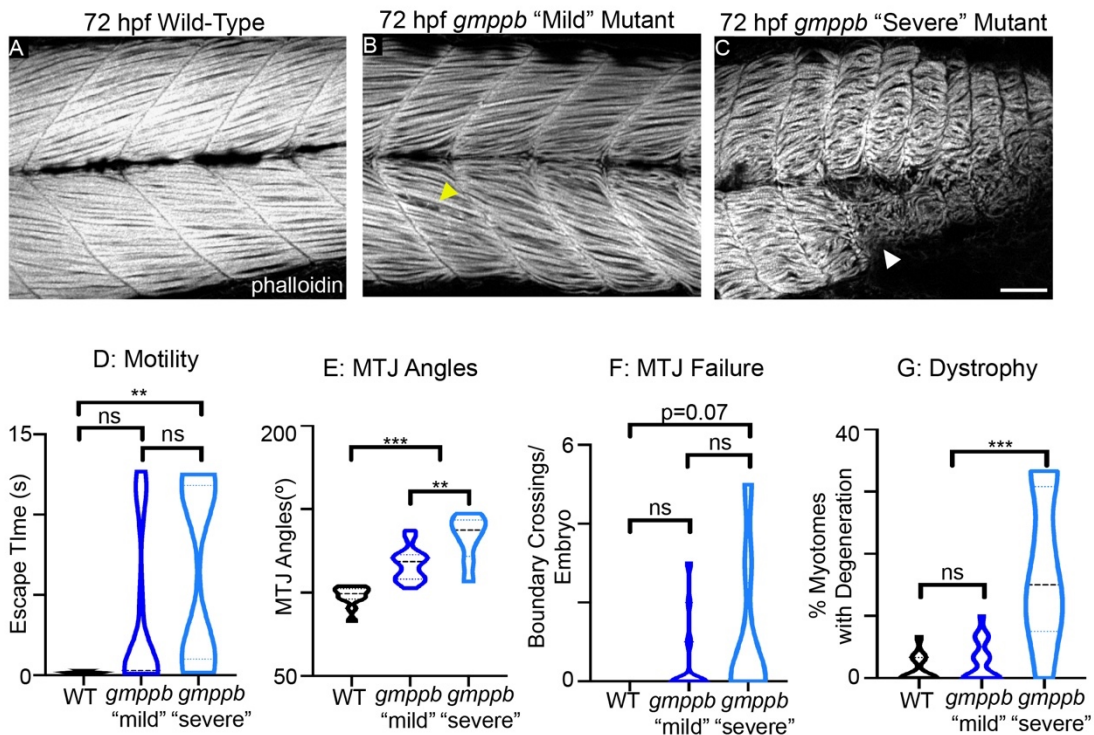


phenotypic variation within *gmppb* mutants, with embryos appearing “mild” or “severe” (Fig. 3.3B, C, Chapter 5, Section 5.10.2). Prior to staining our embryos, we performed a motility assay and found that “severe” and “mild” *gmppb* mutants did not have statistically significant differences in motility (Fig. 3.3D). We quantified MTJ angles, MTJ failure, and levels of dystrophy in “mild” and “severe” *gmppb* mutants. “Severe” mutants had significantly worse MTJ angles and increased levels of dystrophy compared to “mild” *gmppb* mutants (Fig. 3.3E, G). Although we observed a trend in increased MTJ failure that correlated with phenotypic severity, this trend was not significantly different between either class of mutant or wild-type embryos (Fig. 3.3F, $p=0.07$ for wild-type and “severe” mutants). Taken together, these data suggest *gmppb* mutants exhibit phenotypic variation in muscle.

3.2.4. *Gmppb* mutants exhibit neural phenotypes

Neuromuscular junction (NMJ) development requires tight coordination between both motoneurons and muscle cells. Congenital myasthenic syndromes that affect the NMJ have been documented in a number of patients with GMPPB-associated dystroglycanopathy (Belaya et al., 2015; Luo et al., 2017; Rodríguez Cruz et al., 2016). We asked if motor axon pathfinding and initial NMJ development are disrupted in *gmppb* mutants and if “mild” and “severe” embryos exhibit differences in NMJ morphology. We found that CaP (ventral) primary motor axon development was disrupted in 24 hpf *gmppb* mutant embryos compared to wild-type embryos (Fig. 3.4A-C). A lower percentage of primary motor axons exited the spinal cord (Fig. 3.4D) and extended past the choice point (Fig. 3.4F) in *gmppb* mutants compared to controls. However, we did not observe any significant differences in the axon length to the choice point (Fig. 3.4E) or the length of the axons that extend beyond the choice point (Fig. 3.4G) between either group. These data suggest that initial motoneuron development is disrupted in *gmppb* mutants.

Figure 3.3. *Gmppb* mutants exhibit phenotypic variation in muscle. (A-C) Anterior left, dorsal top, side-mounted 72 hpf embryos stained for f-actin (phalloidin, gray). **(A)** Control embryo. **(B)** “Mild” *gmppb* mutant embryo. Note subtle fiber degeneration within the myotome (yellow arrowhead) and wider MTJs. **(C)** “Severe” *gmppb* mutant embryo. Note abnormal myotome shape (white arrowhead), fiber disorganization, and wider MTJs. **(D)** Motility in 72 hpf “severe” *gmppb* mutant (n=8 embryos) embryos is significantly worsened compared to wild-type (n=12 embryos) embryos. However, there are no significant differences in motility between “mild” mutants (n=21 embryos) and “severe” mutants. **(E)** “Severe” *gmppb* mutants (n=8 embryos) exhibit significantly increased MTJ angles compared to “mild” *gmppb* mutants (n=21 embryos) and wild-type (n=12 embryos). **(F)** MTJ failure is not significantly between wild-type (n=12 embryos), “mild” *gmppb* mutant (n=21 embryos), or “severe” *gmppb* mutant (n=8 embryos) embryos ($p=0.07$ between wild-type and “severe” *gmppb* mutants). **(G)** “Severe” *gmppb* mutants (n=8 embryos) exhibit a significantly greater percentage of myotomes with degeneration than wild-type (n=12 embryos) or “mild” *gmppb* mutant (n=21 embryos) embryos. Scalebars are 50 micrometers. * $p<0.05$, ** $p<0.01$, *** $p<0.001$, ns = non-significant.



We next asked if NMJ formation was disrupted in *gmppb* mutants and if mutants exhibited variation in NMJ morphology. We analyzed NMJ structure at 72 hpf by staining for presynaptic synaptic vesicle protein (SV2) and postsynaptic acetylcholine receptors (alpha-bungarotoxin), focusing on innervation of fast-twitch fibers (distributed innervation, Fig. 3.4). Despite disruptions in initial motor axon development, *gmppb* embryos still formed synapses (Fig. 3.4I-J4). In contrast to wild-type embryos, *gmppb* “mild” and “severe” mutants exhibited reduced distributed innervation within the myotome (Fig. 3.4H-J4). We used a semi-automated MATLAB protocol (Chapter 5, Section 5.10.8) to quantify the degree of distributed innervation. We found that skeleton length was reduced in both classes of *gmppb* mutants compared to wild-type embryos; however, there were no significant differences between “mild” and “severe” *gmppb* embryos. On average, “mild” *gmppb* mutant skeleton length was 49.2% of that of the wild-type, and “severe” *gmppb* mutant skeleton length was 49.1% that of the wild-type (Fig. 3.4K). Taken together these results suggest that although NMJ morphology is disrupted in *gmppb* mutants, NMJs are not significantly different between “mild” and “severe” mutants.

3.2.5 *Gmppb* mutants can be quantitatively separated into mild and severe phenotypes

The above data suggest that *gmppb* mutants have “mild” and “severe” phenotypes that exhibit significant differences in terms of fiber degeneration and MTJ angles. However, it is key to classify the phenotypic severity of *gmppb* mutants with a non-biased approach. To achieve this, we captured birefringence images of wild-type and *gmppb* mutant embryos at 2 dpf and calculated the percent area and percent mean gray value (MGV) (Berger et al., 2012) relative to wild-type embryos at this stage. We found that *gmppb* mutants can be quantitatively separated into mild and severe phenotypes (Fig. 3.5) based on their percent area of birefringence

Figure 3.4. *Gmppb* mutants exhibit neural phenotypes. **(A-C1)** Anterior left, dorsal-top side-mounted 24 hpf embryos stained for *znp-1* (white) labeling primary motoneurons. **(A-A1)** Wild-type embryos. Note how primary motor axons extend past the choice point (white arrow). **(B-B1)** *gmppb* mutant embryos predicted to be “mild”. Some primary motor axons are truncated and do not extend past the choice point (yellow arrowhead). **(C-C1)** *gmppb* mutant embryos predicted to be “severe”. Note that many motor axons are truncated. **(D)** A significantly lower percentage of 24 hpf *gmppb* mutant motor axons (n=29 embryos) exit the spinal compared to wild-type (n=27 embryos) embryos. **(E)** Axon length to the choice point is not significantly different between 24 hpf wild-type (n=93 axons) and *gmppb* mutant (n= 115 axons) embryos. **(F)** The percent of axons that extend past the choice point is significantly lower in 24 hpf *gmppb* mutant (n=15 embryos) than in wild-type (n=13 embryos) embryos. **(G)** The length of axons that extend past the choice point does not significantly differ between wild-type (n=45 axons) and *gmppb* mutant (n=21 axons) embryos. **(H-J4)** Anterior left, dorsal top, side-mounted embryos labeled with acetylcholine receptors (AChRs) and synaptic vesicle protein 2 (SV2). **(Lettered panels)** Merged channels of AChR and SV2. **(1)** Skeletonized images. **(2)** Magnification of AChR channel. **(3)** Magnification of SV2 channel. **(4)** Magnification of skeletonized image. **(H-H4)** Control embryo. **(I-I4)** “Mild” *gmppb* mutant embryo exhibiting a reduced degree of distributed innervation within the myotome. **(J-J4)** “Severe” *gmppb* mutant embryo exhibiting reduced distributed innervation within the myotome. **(K)** Percent of wild-type skeleton length per muscle segment in wild-type (n=72 half-myotomes) and *gmppb* mutant (“mild” n=78 half-myotomes; “severe” n=106 half-myotomes) embryos. These percentages are significantly lower in both classes of *gmppb* mutants compared to wild-type but are not significantly different between either class of mutants. Scalebars are 50 micrometers. Error bars in (K) are standard error of the mean (L). * $p < 0.05$, ** $p < 0.01$, *** $p < 0.001$, ns= non-significant.

Figure 3.4.

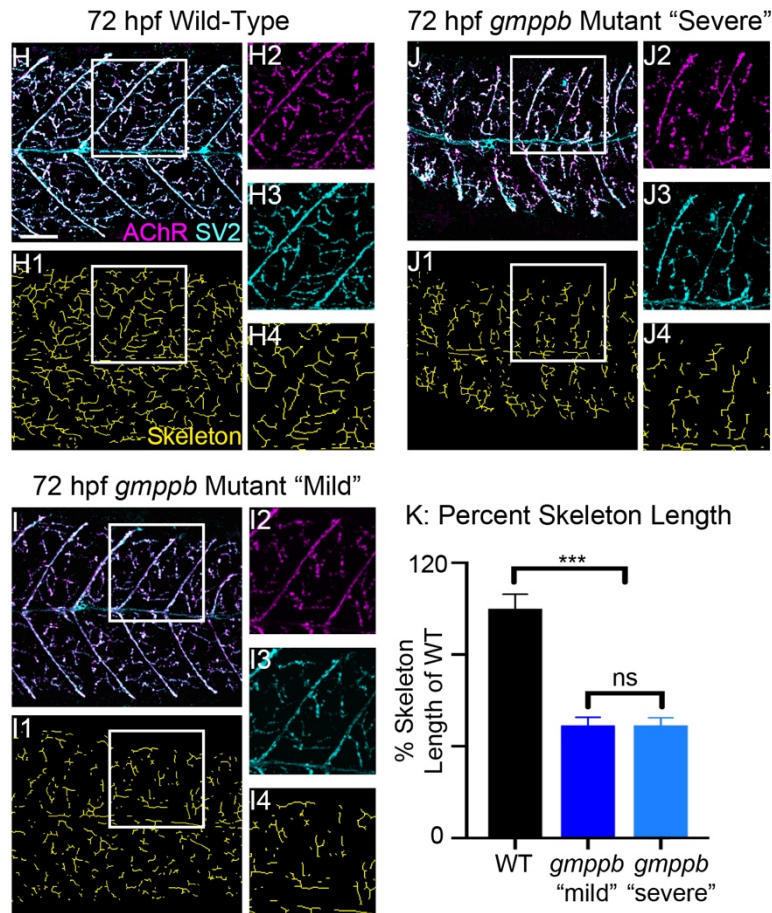
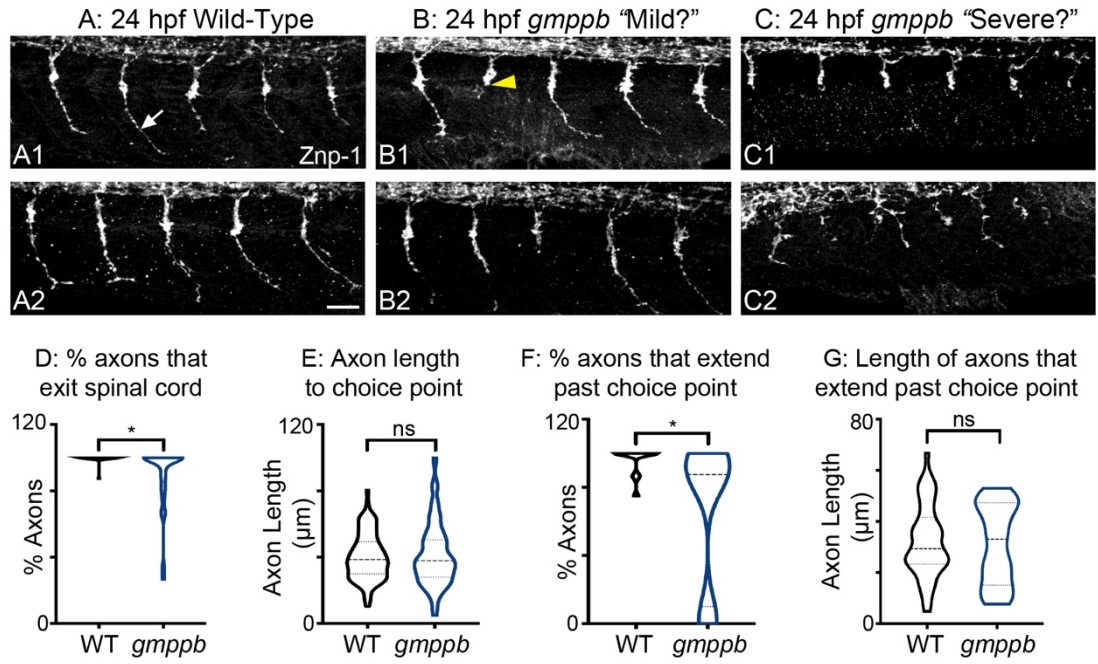


(Fig. 3.5D) and percent MGV (Fig. 3.5E). In mild *gmppb* mutants, both of these values were 85% or higher (see Chapter 5, Section 5.10.2). These results suggest that in terms of muscle, *gmppb* mutants exhibit phenotypic variation that is similar to the variability that is in patients with GMPPB-associated dystroglycanopathy.

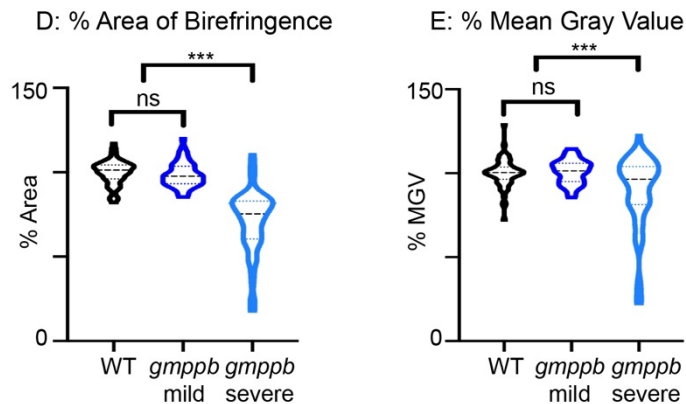
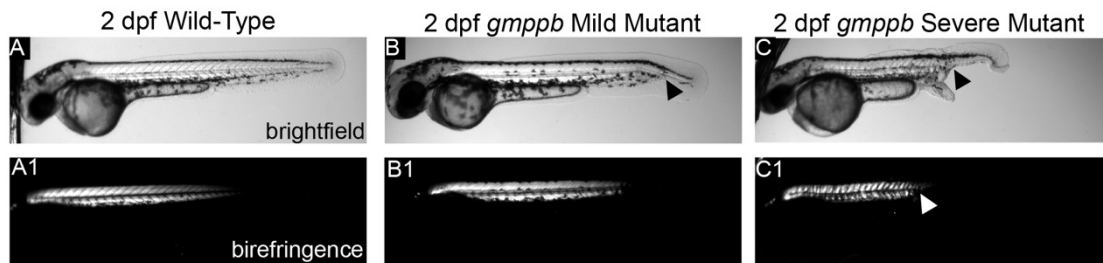
3.2.6. A portion of severe *gmppb* mutants recover to milder phenotypes

Gmppb mutant embryos exhibit phenotypic variation in terms of muscle degeneration and MTJ angles (Fig. 3.3E, G) and can be quantitatively separated into mild and severe phenotypes based on birefringence image analysis at 2 dpf (Fig. 3.5). As this variation is detectable at an early stage in life, we asked if such variation in *gmppb* mutants persists into the early larval stages. We performed longitudinal birefringence assays and analyzed birefringence images of wild-type and *gmppb* mutant zebrafish at 2 dpf and 7 dpf (Fig. 3.6A-D4). Surprisingly, by 7 dpf, a portion of *gmppb* mutants that initially had severe phenotypes presented with mild phenotypes (Fig. 3.6C-C4, F-I). The average percent area in severe-mild *gmppb* mutants increased to levels similar to those of mild *gmppb* mutant and wild-type zebrafish at 7 dpf (Fig. 3.6H). Between 2 dpf and 7 dpf, the average severe-mild *gmppb* mutant percent MGV increased, whereas the average percent MGV of *gmppb* mutants that remained severe decreased (Fig. 3.6I). The reverse of this was rare: we only observed two embryos/larvae that had a mild phenotype at 2 dpf that were severe at 7 dpf (one embryo/larva was just under the threshold, data not shown). Taken together, these results suggest that *gmppb* mutants exhibit phenotypic plasticity throughout the first several days of life.

3.3. Discussion

Individuals with GMPPB-associated dystroglycanopathy present with a broad range of symptoms that vary in terms of age of onset, severity, and involvement of the nervous system. A

Figure 3.5. *Gmppb* mutants can be quantitatively separated into mild and severe phenotypes at 2 dpf. (A-C1) Anterior left, dorsal top, side-mounted 2 dpf embryos imaged live for brightfield (lettered panels) and birefringence (numbered panels). (A-A1) Control embryo. (B-B1) Mild *gmppb* mutant embryo. Note abnormal tail morphology (black arrowhead). (C-C1) Severe *gmppb* mutant embryo. Note abnormal tail morphology (black and white arrowheads) and segments with reduced brightness. (D) Quantification of the percent area of birefringence for 2 dpf control (n=71 embryos), mild, (n=50 embryos) and severe (n=60 embryos) *gmppb* embryos. There is not a significant difference in the percent area of birefringence between controls and mild *gmppb* mutants. Severe *gmppb* mutant embryos have a significant reduction in the percent area of birefringence compared with mild *gmppb* mutants and control embryos. (E) Quantification of percent mean gray value (MGV) for 2 dpf wild-type (n=71 embryos), mild (n=50 embryos), and severe (n=60 embryos) *gmppb* embryos. Severe *gmppb* mutant embryos have a significant reduction in the percent MGV compared with mild *gmppb* mutants and controls. * $p < 0.05$, ** $p < 0.01$, * $p < 0.001$, ns= non-significant.**



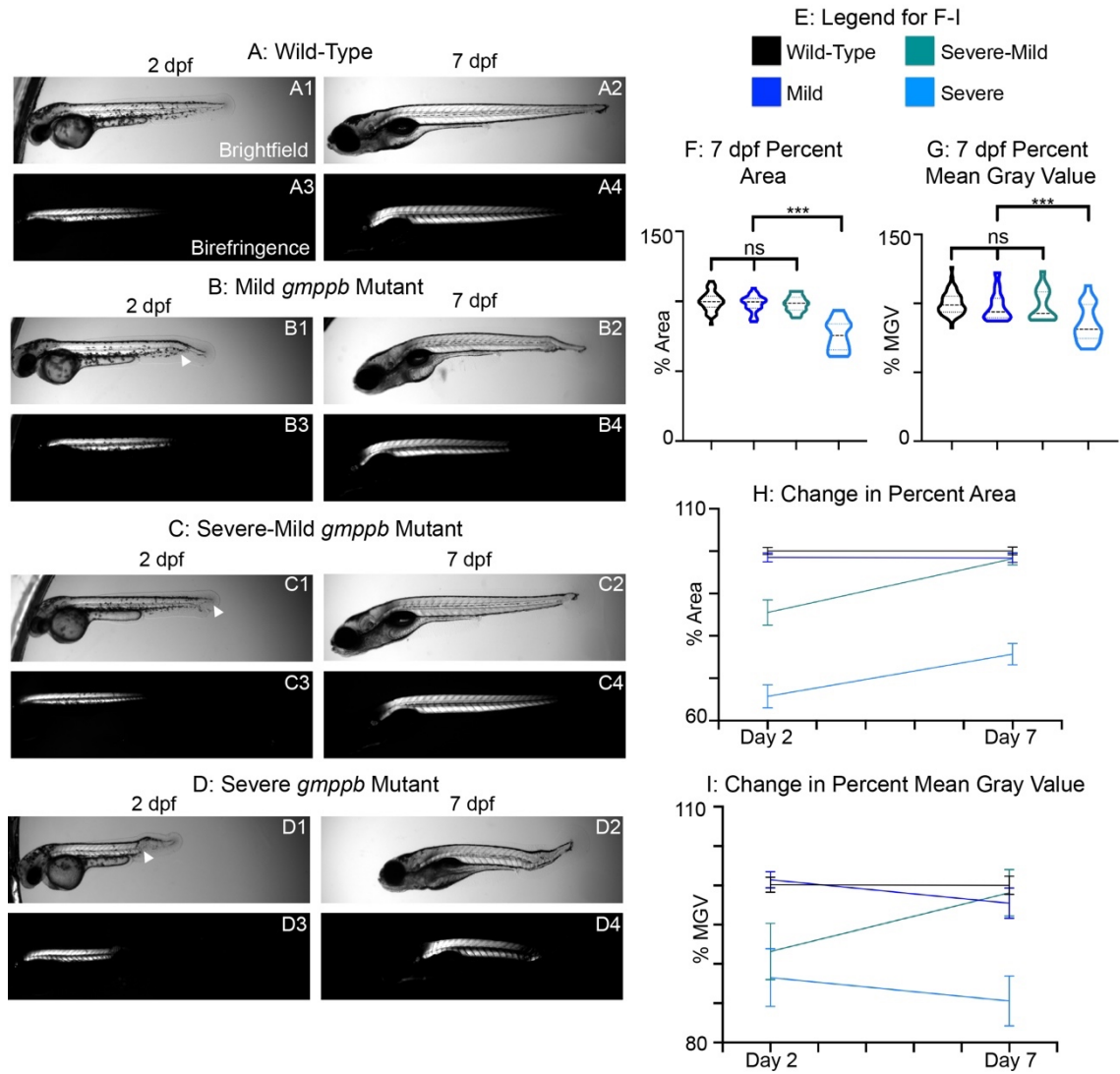
major gap in our understanding of GMPPB-associated disorders is how one mutated *GMPPB* allele can result in multiple phenotypes. Using CRISPR/Cas9 mutagenesis, we designed a *gmppb* mutant zebrafish line to investigate the mechanisms underlying phenotypic variation in GMPPB-associated dystroglycanopathy. To our knowledge, this is the first animal model of this condition that has been engineered at the genomic level. In contrast to previous studies in our lab regarding NAD⁺ and dystroglycanopathy, NAD⁺ supplementation failed to rescue *gmppb* mutants. We found that 72 hpf *gmppb* mutants exhibit phenotypic variation. Specifically, we showed that embryos appearing more severe had significant differences in MTJ angles and fiber degeneration compared to milder embryos. We uncovered a novel defect in motor axon development in 24 hpf *gmppb* mutants. Although we detected NMJ abnormalities in *gmppb* mutants, these were not significantly variable between “mild” and “severe” mutants. At 2 dpf, we detected mild and severe *gmppb* mutant phenotypes based on birefringence image analysis. Longitudinal studies revealed that *gmppb* mutants exhibited phenotypic plasticity. Our data indicate that zebrafish *gmppb* mutants exhibit a spectrum of phenotypic variation similar to that of human populations. This suggests that *gmppb* mutant zebrafish are a suitable model for studying the mechanisms underlying phenotypic variation in GMPPB-associated dystroglycanopathy.

3.3.1. Alternative splicing in *gmppb* mutants

Gmppb morphant zebrafish have been superficially characterized at 48 hpf and possess abnormal muscle structure, curved tails, motility defects, smaller body size, and smaller eyes (Carss et al., 2013). There are currently no other published animal models of GMPPB-associated dystroglycanopathy. Here, we showed that *gmppb* mutant zebrafish engineered via CRISPR/Cas9 mutagenesis exhibit abnormal tail morphology, as well as MTJ failure and muscle degeneration (Fig. 3.1). Preliminary RNA-seq analysis revealed that *gmppb* mutants have an insertion near the

Figure 3.6. A portion of severe *gmppb* mutants recover to mild phenotypes by 7 dpf. (A1-D4) Anterior left, dorsal top, side-mounted embryos and larvae live-imaged for brightfield (1-2) and birefringence (3-4) at 2 dpf (odd panels) and 7 dpf (even panels). **(A1-A4)** Control embryo/larva. **(B1-B4)** Mild *gmppb* mutant embryo/larva. **(C1-C4)** Severe-mild *gmppb* mutant embryo/larva. **(D1-D4)** Severe *gmppb* mutant embryo/larva. Note abnormal posterior morphology (white arrowhead) in 7 dpf larva. **(E)** Legend for (F-I) graphs for control (black), mild (dark blue), severe-mild (teal) and severe (light blue) larvae. **(F)** Quantification of percent area of birefringence between control (n=51 larvae), mild (n=28 larvae), severe-mild (n=15 larvae), and severe (n=18 larvae) larvae at 7 dpf. Percent area is significantly lower in severe larvae compared to all other groups. **(G)** Quantification of percent mean gray value (MGV) between control (n=51 larvae), mild (n=28 larvae), severe-mild (n=15 larvae), and severe (n=18 larvae) larvae at 7 dpf. Severe larvae have a significant reduction in percent MGV compared to all other groups. **(H)** Average percent area of birefringence between control, mild, severe-mild, and severe larvae at 2 dpf and 7 dpf. Severe-mild *gmppb* mutant percent area is above 85% at 7 dpf, whereas severe *gmppb* mutant percent area remains below 85% on average. **(I)** Average percent MGV between control, mild, severe-mild, and severe embryos at 2 dpf and 7 dpf. Severe-mild *gmppb* mutant percent MGV is higher at 7 dpf than at 2 dpf, whereas severe *gmppb* mutant percent MGV is lower at 7 dpf than at 2 dpf on average. Since data are only shown for 2 dpf and 7 dpf, a linear relationship should not be assumed for the data presented in (H) and (I). Error bars in (H) and (I) are standard error of the mean, * $p < 0.05$, ** $p < 0.01$, *** $p < 0.001$, ns= non-significant.

Figure 3.6.



end of intron 2 and have mis-spliced *gmppb* transcripts in addition to correctly spliced transcripts. Four classes of mis-spliced variants were detected (Appendix B). Three of these variants have been predicted to shift the reading frame and result in premature stop codons in the protein sequence (Fig. 3.1, Appendix B). This hypomorphic mutant is well-suited to study the basic biological mechanisms in the context of GMPPB-associated dystroglycanopathy.

Gmppb mutant zebrafish exhibiting RNA mis-splicing are just one example of alternative splicing in the context of neuromuscular disease. Alternative RNA splicing has been reported in the context of MDC1A (Kemaladewi et al., 2017; Sunada et al., 1995), Fukuyama Congenital Muscular Dystrophy (Taniguchi-Ikeda et al., 2011), molecular variants of Duchenne and Becker Muscular Dystrophies (Bérout et al., 2004; Takeshima et al., 2010; Todeschini et al., 2016) and Limb-Girdle Muscular Dystrophy Type 1B (LGMD1B) (Ito et al., 2017; Luo et al., 2014) (reviewed by (Montes et al., 2019; Scotti and Swanson, 2016)). LGMD1B is associated with *LMNA* mutations. Depending on the molecular basis of the *LMNA* mutation, individuals can also develop other conditions, including Emery-Dreifuss Muscular Dystrophy (EDMD), progeria syndromes, and lipodystrophy (Scotti and Swanson, 2016). *Gmppb* mutants have multiple classes of incorrectly spliced *gmppb* reads and exhibit phenotypic variation; thus, it would be interesting to determine whether different phenotypic classes of *gmppb* mutants have different mis-spliced *gmppb* reads.

3.3.2 Cell-matrix adhesion and GMPPB-associated dystroglycanopathy

Muscle fibers must adhere to the myotendinous junction (MTJ) for proper development and homeostasis. We previously identified a pathway that contributes to this process and determined that Nr2b-mediated NAD⁺ synthesis drives laminin organization at the MTJ during zebrafish muscle development (Goody et al., 2010). We subsequently showed that NAD⁺ supplementation is sufficient to improve laminin organization, muscle structure, and muscle

function in the absence of either DG or Itga7 (Goody et al., 2012), or in the absence of Fkrp (Chapter 2). Based on this information, we hypothesized that NAD⁺ would be sufficient to improve muscle structure in *gmppb* mutants. Surprisingly, we found that NAD⁺ supplementation prior to muscle development is not sufficient to improve muscle in *gmppb* mutant embryos. We subsequently found that beta-DG fails to localize to the terminal ends of individual *gmppb* mutant muscle fibers and is mislocalized along the myofibers.

DG clustering is highly variable among patients with GMPPB-associated dystroglycanopathy (Bharucha-Goebel et al., 2015; Cabrera-Serrano et al., 2015; Jensen et al., 2015; Oestergaard et al., 2016). A recent study has suggested that beta-DG may also be a marker of disease and determined that the mobility of beta-DG shifts on Western blots analyzing this protein in a subset of patients with GMPPB-associated dystroglycanopathy and that GMPPB is required for N-linked glycosylation of beta-DG (Sarkozy et al., 2018). This is not surprising, given that beta-DG contains 1 N-linked glycosylation site (Barresi and Campbell, 2006). N-glycans are also found on all integrin heterodimers (Janik et al., 2010) and cleavage of N-linked glycans on Integrinalpha5beta1 prevents its binding to fibronectin in the ECM (Zheng et al., 1994). It is currently unknown whether N-glycosylation of integrins promotes either laminin binding affinity or membrane localization of Integrinalpha6beta1 or Integrinalpha7beta1. Determining whether GMPPB and/or N-glycosylation are necessary for either of these processes to occur would be an interesting avenue to explore in the future.

3.3.3. Primary motoneuron disruption in GMPPB-associated dystroglycanopathy

Dystroglycan (DG) is associated with the NMJ through the utrophin glycoprotein complex (Deconinck et al., 1997). Thus, it is not surprising that NMJ morphology is disrupted in dystroglycanopathies. Fukutin- and Large- deficient mice have abnormal NMJs shortly after birth (Herbst et al., 2009; Saito et al., 2007). In Chapter 2, we show that NMJ development is

disrupted in *fkpr* morphants at 3 dpf (Fig. 2.5, 2.6). Congenital myasthenic syndrome, a disease that affects neuromuscular transmission at the NMJ, has been documented in patients with GMPPB-associated dystroglycanopathy (Belaya et al., 2015; Luo et al., 2017; Rodríguez Cruz et al., 2016). However, it is unclear when exactly NMJ development becomes disrupted. Early in development, primary motoneurons exit the spinal cord and innervate myotomes (Panzer et al., 2005). Here, we showed that primary motoneuron development is disrupted in *gmppb* mutant zebrafish at 24 hpf. To our knowledge, we are the first to report this in the context of dystroglycanopathy. Several ECM proteins implicated in various stages of motoneuron development are glycosylated, including plexin3A, collagen XV, collagen XIII, and sema5a (Feldner et al., 2007; Guillon et al., 2016; Hilario et al., 2009; Schneider and Granato, 2006). Therefore, it is possible that some of these ECM components have altered glycosylation and/or function in *gmppb* mutants. We found that a lower percentage of motor axons exit the spinal cord in *gmppb* mutants (Fig. 3.4D). We hypothesize that impaired glycosylation of one or more of the aforementioned guidance proteins could inhibit motor axon growth in *gmppb* mutants. Specifically, we would test whether expression and/or localization of any of these guidance proteins are altered in *gmppb* mutant embryos and if levels of abnormal expression and/or localization correlate with mild and severe phenotypes detected via birefringence.

Although early motoneuron defects and disrupted NMJ morphology are present, we also showed that synapses still form in *gmppb* mutants (Fig. 3.4H-J). Although NMJ morphology was disrupted in *gmppb* mutants, we did not detect any significant differences in skeleton length between “mild” and “severe” *gmppb* mutant embryos. These results were somewhat surprising, given the range of variability we observed in primary motor axon phenotypes in *gmppb* mutants (Fig. 3.4). In the future, it will be interesting to determine if NMJ formation in

gmppb mutants is facilitated by recovery of primary motor axon pathfinding, compensatory secondary axon pathfinding, or cycles of regeneration following degeneration.

3.3.4. Phenotypic variation and plasticity in *gmppb* mutants

Phenotypic variation is common in neuromuscular diseases, including GMPPB-associated dystroglycanopathy. Although genotype-phenotype correlations are starting to emerge, individuals still present with a broad spectrum of symptoms and severities. This is especially true for the c.79 G>C variant associated with Limb-Girdle Muscular Dystrophy Type 2T (LGMD2T) and Congenital Myasthenic Syndrome. Individuals with this specific mutation have highly variable symptoms and ages of onset (Bharucha-Goebel et al., 2015; Cabrera-Serrano et al., 2015; Carss et al., 2013; Jensen et al., 2015; Montagnese et al., 2017; Oestergaard et al., 2016; Raphael et al., 2014). We currently do not understand how individuals with the same mutant allele can experience drastically different symptoms and severities. *Gmppb* mutants exhibited a similar degree of phenotypic variation. These embryos can be categorized into mild and severe phenotypes based on birefringence image analysis at 2 dpf. By 7 dpf, a portion of *gmppb* mutants initially presenting with severe phenotypes recovered to milder phenotypes. Conversely, we only observed two *gmppb* mutants initially presenting as mild that became severe by 7 dpf (one was just under the threshold). Our data do not resolve the mechanisms underlying phenotypic variation and plasticity in this model. We hypothesize that this phenotypic variation is driven by one or more distinct molecular and/or cellular mechanisms. Several potential mechanisms include differences in RNA mis-splicing, muscle regeneration and/or degeneration, motor axon pathfinding, and cell adhesion strength (detailed in Chapter 4). These future studies aim to provide insight regarding the cell behaviors underlying phenotypic variation and plasticity in *gmppb* mutants.

3.4. Conclusion

Phenotypic variation is common in many neuromuscular disorders, including the dystroglycanopathies. We took advantage of CRISPR/Cas9 technology to engineer a zebrafish model of GMPPB-associated dystroglycanopathy, a neuromuscular disorder with highly variable clinical presentation. We found that the *gmppb* mutant allele is hypomorphic and mutants present with alternatively spliced *gmppb* RNA reads. *Gmppb* mutants also exhibited abnormal muscle and MTJ structure. In contrast to previous studies concerning other zebrafish models of dystroglycanopathies, these attributes are not improved with NAD⁺ supplementation prior to muscle development. We found that at 72 hpf, *gmppb* mutants exhibited “mild” and “severe” phenotypes, particularly in regard to muscle degeneration and MTJ angles. Although motoneuron development and NMJ morphology were abnormal in *gmppb* mutants, we did not find significant differences in NMJ morphology between “mild” and “severe” *gmppb* mutants. We determined that *gmppb* mutants can be quantitatively separated into mild and severe phenotypes at 2 dpf. Longitudinal birefringence imaging revealed that a portion of *gmppb* mutants initially presenting with severe phenotypes presented with milder phenotypes by 7 dpf. Taken together, our data indicate that *gmppb* mutants are well-suited to study the molecular and cellular behaviors underlying phenotypic variation in dystroglycanopathies.

CHAPTER 4

FUTURE DIRECTIONS

4.1. Introduction

The journey to elucidating the developmental and cellular behaviors evident in dystroglycanopathies is far from complete. While the work described herein has provided valuable insight regarding neuromuscular development and phenotypic variation in these conditions, it has also led to new and important questions. This chapter provides examples of exciting future directions to explore regarding zebrafish models of dystroglycanopathy. The following experiments are only a microcosm of possibilities. Other potential areas of exploration that will not be discussed in this chapter include the design of humanized *gmppb* mutant zebrafish, determining whether ECM proteins that participate in motoneuron guidance are impaired in *gmppb* mutants, elucidating intrinsic compensatory mechanisms present in *gmppb* mutants, and longitudinal studies of zebrafish models of FKRP-associated dystroglycanopathy. It is important to note that our preliminary experiments analyzing muscle and NMJs should be repeated with *gmppb* mutants that have been classified as mild or severe via birefringence analysis and should be repeated with a larger sample size. It is also essential to determine the exact molecular basis of *gmppb* mutants, particularly the genomic DNA sequence of intron 2.

4.2. New zebrafish models of FKRP-associated dystroglycanopathy

Zebrafish embryos have been advantageous in determining the cellular and molecular mechanisms governing disease phenotypes in muscular dystrophies, including dystroglycanopathies. While *fkrp* morphants are a respectable model for exploring FKRP-associated dystroglycanopathy, it would be useful to leverage novel *fkrp* mutant zebrafish in future research projects. Repeating experiments described in Chapter 2, especially NAD⁺, laminin, and NMJ experiments, with *fkrp* mutant zebrafish is ideal in order to confirm that our

observations also occur in *fkrp* mutants. Second, these models would be important for performing any longitudinal studies regarding FKRP-associated dystroglycanopathy in zebrafish, as the efficacy of morpholinos fades by 5 dpf.

Our lab has recently obtained two *fkrp* mutant zebrafish models (kind gifts from Dr. James Dowling and Dr. Matthew Alexander). One of these mutants is listed in the Sanger database contains a single nucleotide substitution which results in a premature stop codon at amino acid 169 (Kettleborough et al., 2013) but remains uncharacterized. The additional model we obtained contains a 13 bp deletion generated by TALENs and also carries a heat-shock inducible promoter for human FKRP carrying the L276I mutation (Serafini et al., 2018). When heat-shocked, this line exhibits a milder phenotype (Serafini et al., 2018). These mutant lines would be ideal to use for future studies regarding FKRP-associated dystroglycanopathy.

4.3. What are the tissue-specific requirements of Fkrp?

In Chapter 2, we determined that muscle-specific overexpression of Fkrp improved MTJ morphology; however, it was not sufficient to improve fiber resiliency and mobility in *fkrp* morphant zebrafish. Given that previous studies demonstrated that this enzyme resides in the perinucleus, sarcolemma, and Golgi cisternae (Alhamidi et al., 2011) and that muscle-specific expression of LARGE improves muscle pathology in large mutant mice (Gumerson et al., 2013), these results are surprising and intriguing. Our work is the first to indicate that Fkrp is required outside of muscle fibers for normal muscle development and homeostasis.

We also showed that Fkrp in zebrafish is required for homeostasis of two specialized muscle junctions that are necessary for proper muscle function: the myotendinous junction (MTJ) and the neuromuscular junction (NMJ). These interfaces link muscle with tendons and motoneurons, respectively. We speculate that Fkrp activity may be required in tendons and/or motoneurons, either independently or concurrently with activity in muscle, for proper MTJ and

neuromuscular development. Experiments that take advantage of additional tissue-specific promoters are an important first step in determining the tissue-specific requirements of Fkrp. We would drive Fkrp expression under motoneuron-specific promoters such as *mnx:1* (primary motoneurons) (Zelenchuk and Brusés, 2011) or *gata2* (secondary motoneurons) (Meng et al., 1997) and a tenocyte-specific promoter such as *scxa* (Chen and Galloway, 2014) and perform experiments with transgenics similar to those described in Chapter 2. These promoters would be fused to non-GFP fluorophores such as mCherry or mKate in order to create double transgenics in which Fkrp is overexpressed simultaneously in multiple tissues. If any of these combinations of tissue-specific overexpression rescued mobility or fiber degeneration in *fkrp* morphants or mutants, it would suggest that Fkrp is sufficient in those tissues for proper muscle development and homeostasis. Generating tissue-specific *fkrp* mutants to determine where Fkrp is necessary for proper muscle development and homeostasis is another possible avenue to explore. Experiments that elucidate the tissue-specific roles of Fkrp are key for providing insight for clinical researchers considering gene therapy as an avenue for improving muscle disease in patients with FKRP-associated dystroglycanopathy.

4.4. Functional rescue of *gmppb* mutants

When a novel genetic mutant is generated with a clear phenotype, it is important to determine if that mutant can be improved via mRNA rescue or chemical interventions. Injection of mRNA constructs designed to induce overexpression of Gmppb is one approach. Several transgenic gateway constructs designed for this purpose are currently under construction. These include *Tg(bact2:gmppb-EGFP)* and *Tg(hsp70l:gmppb-EGFP)*. These vectors can be injected into 1-cell stage *gmppb* mutant embryos. We would expect *Tg(bact2:gmppb-EGFP)* embryos to constitutively express Gmppb-EGFP without the need for additional manipulation. *Tg(hsp70l:gmppb-EGFP)* embryos would require heat shock at 38°C for 2 hours during an early

developmental stage (likely 15 somites or earlier, see Chapter 2) to induce *Gmppb*-EGFP expression. Successfully injected embryos would be raised to adulthood, and transgenic F1 progeny will be used for subsequent experiments. One outcome is that *Gmppb*-EGFP expressing embryos would exhibit improved muscle phenotypes. However, this approach might not rescue *gmppb* mutant phenotypes because our *gmppb* mutants are splice mutants.

An alternative method for rescuing *gmppb* mutants is to supplement embryos with exogenous GDP-mannose. Previous studies demonstrated that mannose supplementation improved phenotypes in cultured fibroblasts from individuals with congenital disorders of glycosylation (Rush et al., 2000). GMPPB synthesizes GDP-mannose from mannose-1-phosphate (Fig. 3.1A; (Carss et al., 2013)); therefore, we hypothesize that exogenous GDP-mannose can restore functional glycosylation to *gmppb* mutants. We would supplement *gmppb* mutants at several developmental stages with GDP-mannose in a manner similar to NAD⁺ supplementation. Designing experiments this way would allow us to determine if GDP-mannose supplementation is necessary prior to muscle development in *gmppb* mutants. Additionally, it would be interesting carry out these experiments longitudinally to determine if GDP-mannose repletion after muscle development gradually improves phenotypes in *gmppb* mutations. If GDP-mannose repletion experiments successfully rescued *gmppb* mutants, these results would have translational implications as a potential therapeutic for patients with GMPPB-associated dystroglycanopathy.

4.5. Elucidating the mechanisms underlying phenotypic variation in *gmppb* mutants

In Chapter 3, we showed that *gmppb* mutant zebrafish exhibit phenotypic variation. *Gmppb* mutants presenting with more “severe” phenotypes (not classified by birefringence image analysis) on average exhibited greater degrees of muscle degeneration. We also found that primary motor axon pathfinding was disrupted in *gmppb* mutants at 1 dpf (Fig. 3.4A-C). We

determined that *gmppb* mutants can be quantitatively classified as mild or severe based on birefringence image analysis at 2 dpf (Fig. 3.5) and that a portion of *gmppb* mutants initially presenting with severe phenotypes recover to mild phenotypes by 7 dpf (Fig. 3.6). These results beget the question of how these phenotypes, and their variability, originate in *gmppb* mutants. Such variation could occur via several mechanisms at the molecular and cellular levels (Fig. 4.1) and will be discussed in the following subsections.

4.5.1. Do levels of RNA mis-splicing correlate between mild and severe *gmppb* mutant phenotypes?

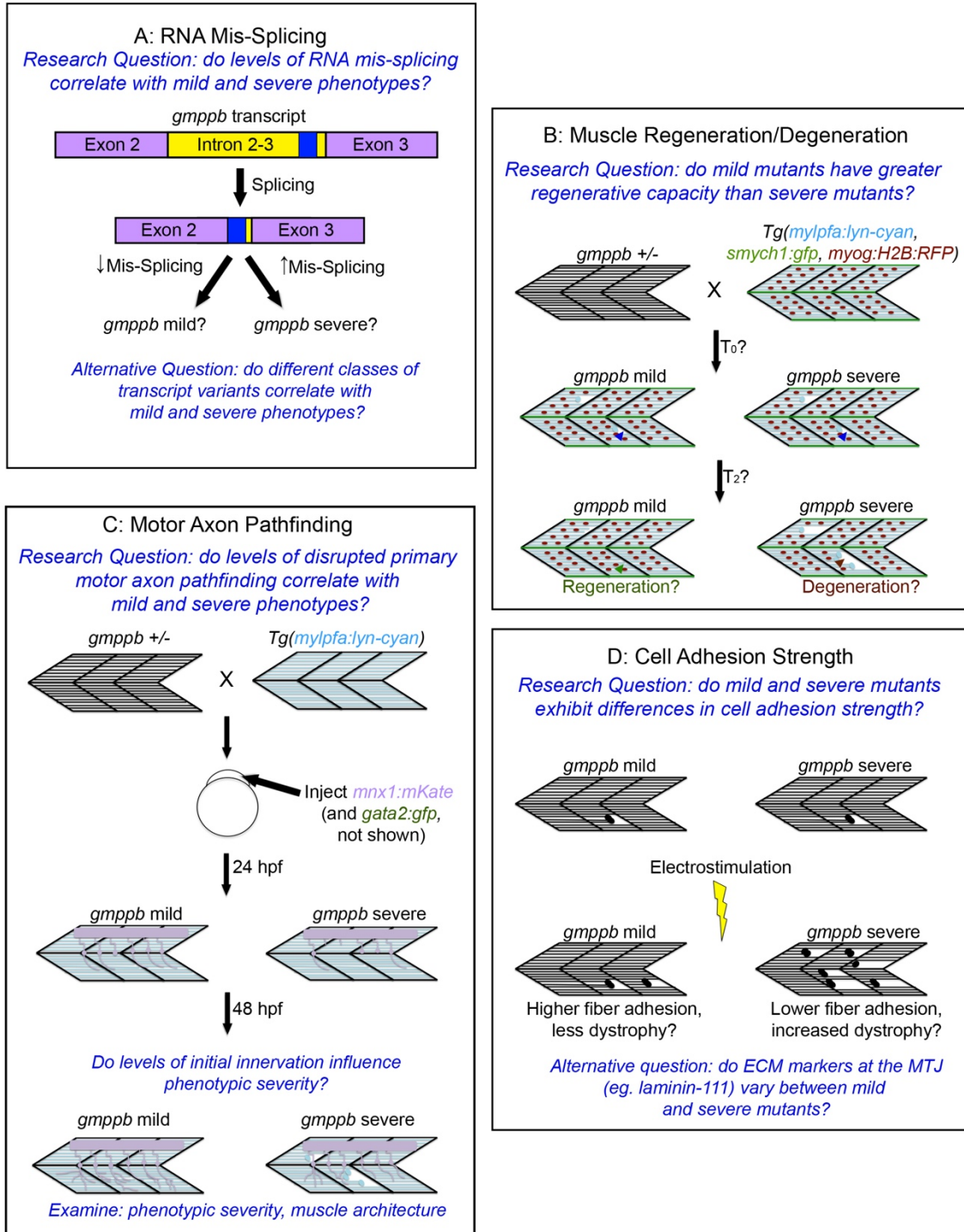
The *gmppb* mutant zebrafish described in Chapter 3 have an insertion in intron 2 that leads to alternative RNA splicing. These variants are predicted to generate truncated protein products based on the location of the open reading frame (Fig. 3.1A, Appendix B). In Chapter 3, we revealed that *gmppb* mutant zebrafish exhibit mild and severe phenotypes and that a portion of mutants initially presenting as severe recover to mild. Although there are likely cell behaviors that accompany these observations, it is also critical that we consider the role that alternative splicing levels could play in phenotypic variation and plasticity.

A collaborative study between the labs of Dr. Clarissa Henry and Dr. Benjamin King at the University of Maine is currently underway to answer this question. Longitudinal birefringence imaging was performed on control and *gmppb* mutant embryos at 2 dpf, 4 dpf, and 7 dpf, and birefringence images were analyzed immediately after each time point. Representative control, *gmppb* mild, and *gmppb* severe embryos at 4 dpf and 7 dpf were pooled together for deep sequencing (RNA-Seq). Data analysis of the deep sequencing data is currently in progress. When complete, this study is expected to determine whether levels of incorrectly spliced *gmppb* RNA correlate with mild and severe phenotypes (Fig. 4.1A). Another potential

Figure 4.1. Potential mechanisms underlying phenotypic variation in *gmppb* mutant zebrafish.

(A) One possible mechanism of phenotypic variation is different levels of RNA mis-splicing of the GMPPB transcript between mild and severe mutants. We hypothesize that severe *gmppb* mutants would exhibit higher levels of RNA mis-splicing. **(B)** It is also possible that mild and severe *gmppb* mutants have differences in regenerative capacity of their muscle. Our hypothesis is that severe *gmppb* mutants experience more muscle degeneration (red arrowhead) than mild *gmppb* mutants (green arrowhead) and that mild *gmppb* mutants could regenerate muscle. **(C)** We must also consider the possibility that the severity of primary motor axon pathfinding predicts phenotypic severity in the muscle of *gmppb* mutants. We hypothesize that severe *gmppb* mutants exhibit more severe disruptions of motor axon pathfinding early in development. **(D)** An additional mechanism to test is whether mild and severe *gmppb* mutants have differences in cell adhesion strength. We hypothesize that mild mutants will have greater cell adhesion and fiber resiliency and will be less prone to muscle wasting upon electrostimulation.

Figure 4.1.



outcome of this study is that different *gmppb* RNA splice variants correspond with different phenotypic classes of *gmppb* mutants.

4.5.2. Examining differences in muscle regeneration in *gmppb* mutants

In Chapter 3, we found that *gmppb* mutant zebrafish exhibit mild and severe phenotypes based on birefringence image analysis at 2 dpf (Fig. 3.5). Additionally, we showed that *gmppb* mutants that appear “severe” exhibit a greater degree of muscle degeneration than those that do not. A birefringence experiment that examined embryos on a day-by-day basis found that while severe *gmppb* mutants experienced more muscle degeneration, mild *gmppb* mutants with muscle degeneration experienced recovery (data not shown). Taken together, these data raise the possibility mild and severe *gmppb* mutants possess differences in regenerative capacity. While immunohistochemistry and fixing embryos at various stages can provide initial insight into this question, longitudinal birefringence and confocal imaging of *gmppb* mutants is a more ideal approach to address this. These rigorous techniques would also allow us to image *gmppb* mutants earlier than 2 dpf while still accurately classifying their phenotypic severity.

To address questions regarding regeneration in mild and severe *gmppb* mutants, we must cross *gmppb* mutants with a transgenic line. We would cross *gmppb* mutants with *Tg(mylpfa:lyn-cyan, smych1:GFP, myog:H2B:RFP)* transgenic fish (a kind gift from Dr. Jared Talbot) that label fast-twitch muscle fibers (cyan), slow-twitch muscle fibers (green), and myonuclei (red). Next, we would screen for heterozygous carriers that express these transgenes of interest. Beginning at 24 hpf, wild-type and *gmppb* mutant transgenics would be live-imaged via confocal microscopy daily. From 2 dpf to 7 dpf, these same fish would be imaged via birefringence immediately before confocal imaging. Such rigorous live imaging of muscle fibers and myonuclei would allow us to determine whether differences in muscle regeneration and/or

degeneration drive phenotypic variation and plasticity in *gmppb* mutants (Fig. 4.1B). These experiments would also allow us to examine other attributes of muscle development and homeostasis over time.

4.5.3. Does early motor axon pathfinding influence phenotypic severity?

In addition to muscle phenotypes, *gmppb* mutants also have delayed motor axon pathfinding and reduced fast-twitch fiber innervation (Fig. 3.4). Although levels of distributed innervation did not significantly differ between *gmppb* embryos that appeared mild or severe, it is still possible that motor axon pathfinding varies between mutants classified as mild or severe via birefringence image analysis. A number of ECM molecules that participate in motor axon pathfinding are glycosylated (Feldner et al., 2007; Guillon et al., 2016; Hilario et al., 2009; Schneider and Granato, 2006). Therefore, levels of primary motor axon pathfinding early in development is another potential mechanism underlying phenotypic variation in *gmppb* mutants. To answer this question, we can identify *gmppb* mutants crossed with *Tg(mylpfa:lyn-cyan, smych1:GFP, myog:H2B:RFP)* transgenic fish that only carry *Tg(mylpfa:lyn-cyan)* and establish a *Tg(mylpfa:lyn-cyan);gmppb* mutant line. Embryos from this line would be injected with transgenic *mnx1:mKate* (Gribble et al., 2018) and *gata2:GFP* (Meng et al., 1997) constructs in order to also study motor axon pathfinding in *gmppb* mutants. These embryos would be imaged via confocal microscopy daily beginning at 24 hpf, and for birefringence daily beginning at 48 hpf. These experiments would allow us to longitudinally image motoneurons in *gmppb* mutants and determine if differences in motor axon pathfinding, neurodegeneration, or compensatory innervation mechanisms drive phenotypic variation in *gmppb* mutants (Fig. 4.1C). We are especially interested in determining if levels of motor axon pathfinding influence muscle architecture or muscle degeneration and/or regeneration.

4.5.4. Investigating differences in cell adhesion strength

Our results presented in Chapter 3, particularly regarding fiber detachment, suggest that differences in cell-matrix adhesion may exist between mild and severe *gmppb* mutants. In zebrafish, muscle fibers can detach either due to sarcolemmal damage or detachment from the MTJ prior to sarcolemmal damage (Hall et al., 2007). A preliminary experiment that used Evan's Blue Dye (EBD) to examine this in *gmppb* mutants found that fibers primarily detach from the MTJ prior to loss of sarcolemmal integrity (data not shown). This suggests that cell-ECM adhesion is disrupted in *gmppb* mutants; thus, it would be useful to determine if *gmppb* mutants exhibit variability in terms of cell adhesion strength.

Questions regarding this topic in *gmppb* mutants can be approached in multiple ways. One straightforward approach involves using electrostimulation to test cell adhesion strength. This technique has been previously used in zebrafish to induce muscle contraction and to test muscle strength (Subramanian and Schilling, 2014) and can be employed to determine whether severe *gmppb* mutants experience greater fiber loss than mild *gmppb* mutants when stimulated (Fig. 4.1D). We plan to perform experiments where control, mild, and severe *gmppb* embryos are imaged for birefringence at 2 dpf. Embryos will immediately receive two rounds of electrostimulation followed by subsequent birefringence imaging, and we will determine whether severe *gmppb* mutant embryos experience a greater reduction in birefringence after two rounds of electrostimulation than mild *gmppb* mutant embryos. If this were the case, this outcome would suggest that severe *gmppb* mutants have reduced cell adhesion and fiber resiliency compared to mild *gmppb* mutants. Fixing and staining embryos for phalloidin and for cell adhesion/MTJ markers such as laminin after electrostimulation should also be considered in when performing these experiments.

4.6. Concluding remarks

This dissertation highlights the importance of viewing dystroglycanopathies as individual conditions. Specifically, our work suggests that this mindset is important in regard to distinct dystroglycanopathy genes *and* the same dystroglycanopathy gene. The experiments described in this chapter are designed to elucidate the mechanisms of disrupted neuromuscular development, cell-matrix adhesion, and phenotypic variation in dystroglycanopathies. Research regarding the tissue-specific requirements of Fkrp will determine where Fkrp is required for neuromusculoskeletal development and homeostasis. Analysis of RNA-seq data examining mild and severe *gmppb* mutant phenotypes, cell adhesion experiments, and longitudinal studies involving both birefringence and confocal microscopy will yield valuable information regarding the molecular and cellular mechanisms that contribute to phenotypic variation and plasticity in the context of dystroglycanopathy. As mentioned, there are many additional approaches to teasing apart these mechanisms. Studies that incorporate different perspectives and examine these conditions at the molecular and cellular levels have the greatest potential to broaden our understanding of dystroglycanopathies and provide insight for other basic researchers, translational scientists, clinicians, and patients and their families.

CHAPTER 5

MATERIALS AND METHODS

5.1. Zebrafish husbandry and lines

5.1.1. Zebrafish husbandry

All embryos were obtained from natural spawnings of adult zebrafish maintained on a 14 hour light/10 hour dark cycle at 28.5°C. Embryos were reared in 1X Embryo Rearing Medium (ERM) with methylene blue and staged according to (Kimmel et al., 1995). The following strains were utilized/generated: AB, *Tg(fli1:EGFP)* (Lawson and Weinstein, 2002), *Tg(ef1α:xbp1δ-GFP)* (Li et al., 2015) (a kind gift from Dr. Shao Jun Du), *Tg(hsp70l:pxn-EGFP)* (Coffey et al., 2018), *Tg(hsp70l:fkfp-EGFP)*, and *Tg(-503unc:fkfp-EGFP)*.

5.1.2. Construction of new transgenic lines

The *Tg(hsp70l:fkfp-EGFP)* and *Tg(-503unc:fkfp-EGFP)* lines were generated via the gateway cloning system. A sequence surrounding the *fkfp* gene was amplified with NCBI-verified primers was gated and inserted into the pDONR221 vector (Invitrogen). The heat shock gateway 222 5' vector, GFP gateway 366 3' vector, and the gateway 394 destination vector (Kwan et al., 2007) were used along with the donor vector and LR clonase II for the *Tg(hsp70l:fkfp-EGFP)* line. Components remained the same for the *Tg(-503unc:fkfp-EGFP)* line with the exception of the -503unc zebrafish muscle-specific promoter (Berger and Currie, 2013), which was used in place of the heat shock gateway 222 5' vector. Plasmids were injected at the single cell stage as previously described (Goody et al., 2010).

5.1.3. Construction of *gmppb* mutants

The single guide RNA (sgRNA) targeting the *gmppb* sequence (NCBI gene ID: 445097) was selected using CHOPCHOP (Montague et al., 2014). SgRNA synthesis was performed as previously described (Gagnon et al., 2014) with the following modifications. Oligonucleotide

annealing reactions were doubled and incubated for 40-60 minutes at 12°C. The sgRNA transcription reaction was doubled and synthesized using a MaxiScript Kit, and clean-up was performed in 4 µl lithium chloride and 150 µl 100% ethanol. Cas9 mRNA was synthesized as previously described (Gagnon et al., 2014). *Gmppb* sgRNA, Cas9, and a stop-cassette oligonucleotide (Table 5.1) were injected into one-cell stage AB embryos. F0 embryos with successful stop-cassette insertions were raised to adulthood and crossed to generate F1 embryos. F1 embryos were raised to adulthood and outcrossed with ABs to generate F2 embryos. All experiments described in Chapter 3 were performed using spawns of the F2 generation or later.

Table 5.1. Sequences used to construct *gmppb* mutants via CRISPR/Cas9 mutagenesis.

Sequences used to construct *gmppb* mutants with CRISPR/Cas9 mutagenesis technology. Note the target site is not a synthesized nucleotide and that the protospacer adjacent motif (PAM) sequence is underlined.

Nucleotide or Sequence Name	Sequence
GMPPB Target Site (not a synthesized nucleotide)	GGACTCCAGCCTGAACACAG <u>AGG</u>
GMPPB Gene-Specific Oligonucleotide	ATTTAGGTGACACTATAGGACTCCAGCCTGAACACAGGTTTTAGAGCTAGAAATAGCAAG
GMPPB Stop-Cassette Oligonucleotide	ACCATCCAACGGTGCCTCTGGTCATGGCGTTAAACCTTAATTAAGCTGTTGTAGTGTTCCAGGCTGGAGTCCGTC
Left Homology Sequence	ACCATCCAACGGTGCCTCTG
Right Homology Sequence	TGTTCCAGGCTGGAGTCCGTC

5.2. Morpholino injections

Antisense MOs were obtained from Gene Tools, LLC, and hydrated at 65°C for 10 minutes with sterile water to generate 1 mM stocks. For *fkpr* morphant experiments, the previously published *fkpr* MO2 (5'-CTTGTGGTTTTATGGCAGAAAGAGT-3') (Kawahara et al., 2010) was utilized and injected into the yolk of 1-2 cell stage embryos so that embryos received

approximately 3.2 ng of MO. For *dag1* morphant experiments, the previously published *dag1* MO (*dag1* MO1) (5'-CATGCCTGCTTTTATTTCCCTCGC-3' (Parsons et al., 2002) and an additional slightly overlapping *dag1* MO (*dag1* MO2) (5'-CCCTCGCTCGTACAAAAGAGGACGT-3') were co-injected into the yolk of 1-2 cell stage embryos so that embryos received approximately 12 ng of each *dag1* MO1 and *dag1* MO2. Embryos utilized in experiments alongside NAD⁺ and EmergenC treated embryos were placed in 60 mm Petri dishes with 25 embryos per dish in 10 mL 1X ERM.

5.3. NAD⁺ and EmergenC supplementation

Embryos receiving EmergenC treatment (Alacer Corp) were separated into 60 mm Petri dishes with 25 embryos per dish in 10 mL 1X ERM-EmergenC solution. The NAD⁺ solution was prepared as previously described (Goody et al., 2010) except in sterile water. The EmergenC solution was diluted in 1X ERM so that the level of niacin in the solution was equal to 7.61 μM. Supplementation began at 6 hpf or 24 hpf depending on the experiment and the solution was changed every 24 hours until embryo fixation.

5.4. Expression of constructs with the heat shock promoter

To constitutively overexpress Fkrp, uninjected and injected *Tg(hsp70l:fkpr-EGFP)* embryos were heat shocked at 38°C for 1.25-2 hours at the 15 somite stage. To overexpress Paxillin, *Tg(hsp70l:pxn-EGFP)* were heat shocked at 38°C for 1.5 hours at 12 hpf, then for 1.5-2 hours daily until fixation. Heat-shocked fish were immediately transferred to 28°C.

5.5. Mobility assays

To assess mobility in *fkpr* morphants, touch response analysis was performed at 3 dpf. Embryos were placed in 1X ERM and stimulated at the posterior end with fishing wire. The number of touches to evoke an escape response was recorded. For embryos that did not respond after 50 touches, 50 was recorded as their touches to response. Mobility in *gmppb* mutants was assessed as previously described (Goody et al., 2012).

5.6. Immunohistochemistry

All embryos were fixed in 4% Paraformaldehyde (PFA) for 2-4 hours at room-temperature, depending on the stage. After fixation, embryos received five rinses in PBS-0.1% Tween 20. For all embryos not stained with alpha-Bungarotoxin or anti-znp-1, embryos were permeabilized for 1.5 hours in PBS-2% Triton-X-100, followed by incubation in 1/20 phalloidin-546 (Invitrogen) overnight at 4°C. Embryos were then subjected to five rinses for five minutes in PBS-0.1% Tween 20, followed by an overnight incubation in antibody block (5%BSA, 1% DMSO, 1% Triton-X-100, 0.2% saponin in 1X PBS) for embryos receiving subsequent immunohistochemistry treatments. Primary antibodies were added at a concentration of 1:50 (anti-laminin, anti-paxillin, anti-beta-dystroglycan) in antibody block and incubated for 2-8 hours at room temperature followed by overnight at 4°C. All embryos were then treated with antibody block for 8 hours at room temperature or overnight at 4°C, followed by an overnight incubation in 1:200 secondary antibody (GAR488 and GAR633 for polyclonal; GAM488 and GAM633 for monoclonal), either preceded or succeeded by a 2-6 hour incubation at room temperature, depending on the antibody. Embryos were rinsed out of secondary antibody with PBS-0.1% Tween 20 prior to deyolking, mounting, and imaging.

NMJ staining was performed as mentioned above with the following changes. After rinsing embryos out of 4% PFA, embryos were permeabilized in 1 mg/ml collagenase in 1X PBS for 1.25-1.5 hours. Embryos were stained with 1/500 α -Bungarotoxin-647 for 2-4 hours at room temperature or overnight at 4°C. For co-staining, 1/20 phalloidin-546 was added to the alpha-Bungarotoxin solution in antibody block. Embryos were then rinsed as described above. Primary SV2 antibody was added at a concentration of 1:50 in antibody block and embryos were incubated in this solution for 2-8 hours at room temperature followed by 3 days at 4°C. Staining then proceeded as described above.

For anti-znp-1 staining, embryos were rinsed out of PFA as described above. Embryos were then dehydrated and rehydrated with methanol (MeOH) with 5 minute incubations (10 minutes for 100% MeOH) in the following series: 0%, 33%, 66%, 100%, 66%, 33%, 0% MeOH. Embryos were immediately blocked in antibody block for 2 hours at room temperature, and then were incubated in primary anti-znp-1 antibody at a concentration of 1:50 in antibody block overnight at 4°C. Staining then proceeded as described above.

5.7. Myofiber purification and staining

Individual myofibers from control and *gmppb* mutant zebrafish embryos were purified at 48 hpf as previously described (Horstick et al., 2013). Purified myofibers were then fixed in 4% PFA for fifteen minutes, rinsed three times for five minutes with PBS-0.1% Tween 20. Myofibers were permeabilized for three minutes in PBS-2% Triton-X-100, subsequently rinsed once with PBS-0.1% Tween 20, and stained with 1:40 phalloidin-546 in PBS-0.1% Tween 20 overnight at 4°C. Myofibers were rinsed the following morning three times for five minutes with PBS-0.1% Tween 20, were blocked overnight in antibody block at 4°C, then stained for beta-dystroglycan overnight at 4°C. Myofibers were rinsed three times for five minutes with PBS-0.1% Tween 20, blocked for three hours at room temperature, and then incubated in secondary antibody (GAM488) overnight at 4°C. Embryos were then rinsed five times for five minutes with PBS-0.1% Tween 20.

5.8. Imaging

For live brightfield and birefringence imaging, embryos were anesthetized in Tricaine, placed into a glass-bottomed dish, and imaged on a Leica screening microscope with camera attachment. For birefringence images, a polarized light filter attachment was placed onto the microscope. All live brightfield and birefringence images were taken at 2.5X and 3.2X. Fixed and stained embryos were deyolked, mounted, and imaged in 80% glycerol as previously described

(Goody et al., 2012). Fluorescent images of embryos were captured at 20X with a Zeiss Axio Imager Z1 microscope with a Zeiss ApoTome attachment, at 20X with an Olympus Fluoview IX-81 inverted microscope with FV1000 confocal system, or at 25X with a Leica DMI8 confocal microscope. Images for *Tg(ef1α:xbp1δ-GFP)* were acquired at 10X on a Zeiss Axio Imager Z1 microscope with a Zeiss ApoTome attachment or at 5X on a Zeiss microscope with Vivatome attachment. Exposure time was kept consistent between all embryo groups within an experiment for *Tg(ef1α:xbp1δ-GFP)* experiments.

5.9. Statistical analyses

All statistical analyses were performed in GraphPad PRISM 8. Quantitative data were log transformed before performing statistical comparisons. Statistical comparisons of quantitative data were performed using an unpaired two-tailed t-test for comparisons of two groups and an ordinary one-way ANOVA with Tukey's ad-hoc analysis for comparisons of three or more groups. Categorical MTJ staining intensity data were analyzed using Fisher's Exact Test for two categories and a Chi Square test for three or more categories.

5.10. Image analyses

5.10.1. Birefringence image analysis

Birefringence was quantified using FIJI as previously described (Berger et al., 2012) with the following modifications. For each experiment, a polygon was drawn around the fish body of a birefringence image between myotomes 6 and 26, and the area and mean gray value (MGV) were measured. This was repeated three times for each embryo, and the values were averaged. The average area and MGV for all controls were subsequently calculated. These values were used to determine the percent area and percent MGV for all embryos. Mutants with a percent area *and* a percent MGV at 85% or higher were classified as mild mutants.

5.10.2. Phenotypic classification

Embryos that received only phalloidin and/or NMJ staining (Fig. 3.3, 3.4) were retroactively classified as “mild” or “severe,” as these experiments were performed prior to our longitudinal studies. We initially planned to use *gmppb* mutants to study the relationship between muscle degeneration, MTJs, and NMJs; however, we observed remarkable phenotypic variation in the muscle of *gmppb* mutants in our confocal images. These observations were the basis for the longitudinal studies we conducted. For embryos imaged via birefringence, the percent area and MGV values described above were used to determine the phenotypic class of *gmppb* mutant embryos. Mutants with a percent area and a percent MGV at 85% or higher were classified as mild mutants. Embryos that did not meet these criteria were classified as severe mutants.

5.10.3. Myotome scoring

Muscle fiber degeneration was quantified by counting the number of muscle segments with degeneration per embryo and calculating the percent of myotomes with muscle degeneration. For laminin and beta-DG staining analyses, images were blinded using a Perl script and embryos were scored according to their relative staining intensity (Appendix A).

5.10.4. MTJ angles

Myotendinous junction angles were analyzed in FIJI (Schindelin et al., 2012; Schneider et al., 2012) (Schindelin et al., 2012; Schneider et al., 2012) by using the angle tool.

5.10.5. Anisotropy analysis

For anisotropy analysis, a polygon was drawn in eight myotomes per image analyzed using the polygonal lasso tool in Adobe Photoshop. The x,y coordinates of each polygon were recorded. Masks were generated from the coordinates, and 2DWTMM analysis was performed on each of these masks as previously described (Goody et al., 2010; Goody et al., 2012).

5.10.6. Fluorescence intensity

For analysis of *xbp1* transgenic embryos, fluorescence intensity was quantified using FIJI. A polygon was drawn around the dorsal muscle above the notochord for all embryos in the trunk region. The average pixel intensity (mean gray value) was calculated. The mean average pixel intensity for all controls was calculated. These values were used to determine the percent average pixel intensity for all embryos. Images for all *xbp1* transgenic embryos were blinded using a Perl script prior to analysis.

5.10.7. Intersegmental vessel and motoneuron lengths

Intersegmental vessel (ISV) lengths and primary motoneuron lengths were measured in FIJI using the segmented line tool.

5.10.8. NMJ analysis

Confocal images were processed into maximum intensity projections of distributed and myoseptal innervation using FIJI. Masks for the fish, horizontal myoseptum, and myoseptal innervation were generated in FIJI and were subsequently imported into MATLAB (Mathworks) for segmentation of the red (AChR) and green (SV2) fluorescence channels. Adaptive histogram equalization (MATLAB “*adaphstetq*” function) was used to enhance the images, and a 1 pixel radius Gaussian filter (MATLAB ‘*imguassfilt*’ function) was used to denoise the images. A threshold of 30 was used on each channel to generate single masks of fluorescence images, which were then combined with an or statement. Masks were skeletonized, and then cleaned and despurred using the “*bwmorph*” command in MATLAB. This command was also used to identify branchpoints. Muscle segments (half-myotomes) were defined using the masks for the fish, horizontal myoseptum, and myoseptal innervation. Measurements of skeleton length and branching frequency were then performed for each muscle segment (half-myotome) per embryo.

5.10.9. Myofiber analysis

For myofiber analysis, a polygon was drawn around each individual fiber in FIJI. The total area, perimeter, and Feret's diameter were measured for each individual fiber. The filament index (a measure of how much an object's shape deviates from circular) of the myofibers was calculated as previously described (Snow et al., 2008b).

BIBLIOGRAPHY

- Ackroyd, M. R., Skordis, L., Kaluarachchi, M., Godwin, J., Prior, S., Fidanboyly, M., Piercy, R. J., Muntoni, F. and Brown, S. C. (2009). Reduced expression of fukutin related protein in mice results in a model for fukutin related protein associated muscular dystrophies. *Brain* 132, 439–451.
- Alhamidi, M., Kjeldsen Buvang, E., Fagerheim, T., Brox, V., Lindal, S., Van Ghelue, M. and Nilssen, Ø. (2011). Fukutin-related protein resides in the Golgi cisternae of skeletal muscle fibres and forms disulfide-linked homodimers via an N-terminal interaction. *PLoS ONE* 6, e22968.
- Askari, J. A., Buckley, P. A., Mould, A. P. and Humphries, M. J. (2009). Linking integrin conformation to function. *J. Cell. Sci.* 122, 165–170.
- Astrea, G., Romano, A., Angelini, C., Antozzi, C. G., Barresi, R., Battini, R., Battisti, C., Bertini, E., Bruno, C., Cassandrini, D., et al. (2018). Broad phenotypic spectrum and genotype-phenotype correlations in GMPPB-related dystroglycanopathies: an Italian cross-sectional study. *Orphanet J Rare Dis* 13, 170.
- Bajanca, F., Luz, M., Raymond, K., Martins, G. G., Sonnenberg, A., Tajbakhsh, S., Buckingham, M. and Thorsteinsdóttir, S. (2006). Integrin alpha6beta1-laminin interactions regulate early myotome formation in the mouse embryo. *Development* 133, 1635–1644.
- Balcin, H., Palmio, J., Penttilä, S., Nennesmo, I., Lindfors, M., Solders, G. and Udd, B. (2017). Late-onset limb-girdle muscular dystrophy caused by GMPPB mutations. *Neuromuscul. Disord.* 27, 627–630.
- Barresi, R. and Campbell, K. P. (2006). Dystroglycan: from biosynthesis to pathogenesis of human disease. *J. Cell. Sci.* 119, 199–207.
- Barresi, R., Michele, D. E., Kanagawa, M., Harper, H. A., Dovico, S. A., Satz, J. S., Moore, S. A., Zhang, W., Schachter, H., Dumanski, J. P., et al. (2004). LARGE can functionally bypass alpha-dystroglycan glycosylation defects in distinct congenital muscular dystrophies. *Nat. Med.* 10, 696–703.
- Bassett, D. and Currie, P. D. (2004). Identification of a zebrafish model of muscular dystrophy. *Clin. Exp. Pharmacol. Physiol.* 31, 537–540.
- Beattie, C. E. (2000). Control of motor axon guidance in the zebrafish embryo. *Brain Res. Bull.* 53, 489–500.
- Belaya, K., Rodríguez Cruz, P. M., Liu, W. W., Maxwell, S., McGowan, S., Farrugia, M. E., Petty, R., Walls, T. J., Sedghi, M., Basiri, K., et al. (2015). Mutations in GMPPB cause congenital myasthenic syndrome and bridge myasthenic disorders with dystroglycanopathies. *Brain* 138, 2493–2504.

Beltran-Valero de Bernabé, D., Voit, T., Longman, C., Steinbrecher, A., Straub, V., Yuva, Y., Herrmann, R., Sperner, J., Korenke, C., Diesen, C., et al. (2004). Mutations in the FKRP gene can cause muscle-eye-brain disease and Walker-Warburg syndrome. *J. Med. Genet.* 41, e61.

Berger, J. and Currie, P. D. (2013). 503unc, a small and muscle-specific zebrafish promoter. *Genesis* 51, 443–447.

Berger, J., Sztal, T. and Currie, P. D. (2012). Quantification of birefringence readily measures the level of muscle damage in zebrafish. *Biochem. Biophys. Res. Commun.* 423, 785–788.

Bérout, C., Carrié, A., Beldjord, C., Deburgrave, N., Llense, S., Carelle, N., Peccate, C., Cuisset, J. M., Pandit, F., Carré-Pigeon, F., et al. (2004). Dystrophinopathy caused by mid-intronic substitutions activating cryptic exons in the DMD gene. *Neuromuscul. Disord.* 14, 10–18.

Bharucha-Goebel, D. X., Neil, E., Donkervoort, S., Dastgir, J., Wiggs, E., Winder, T. L., Moore, S. A., Iannaccone, S. T. and Bönnemann, C. G. (2015). Intrafamilial variability in GMPPB-associated dystroglycanopathy: Broadening of the phenotype. *Neurology* 84, 1495–1497.

Bieganowski, P. and Brenner, C. (2004). Discoveries of nicotinamide riboside as a nutrient and conserved NRK genes establish a Preiss-Handler independent route to NAD⁺ in fungi and humans. *Cell* 117, 495–502.

Blaeser, A., Keramaris, E., Chan, Y. M., Sparks, S., Cowley, D., Xiao, X. and Lu, Q. L. (2013). Mouse models of fukutin-related protein mutations show a wide range of disease phenotypes. *Hum. Genet.* 132, 923–934.

Briggs, D. C., Yoshida-Moriguchi, T., Zheng, T., Venzke, D., Anderson, M. E., Strazzulli, A., Moracci, M., Yu, L., Hohenester, E. and Campbell, K. P. (2016). Structural basis of laminin binding to the LARGE glycans on dystroglycan. *Nat. Chem. Biol.* 12, 810–814.

Brockington, M., Yuva, Y., Prandini, P., Brown, S. C., Torelli, S., Benson, M. A., Herrmann, R., Anderson, L. V., Bashir, R., Burgunder, J. M., et al. (2001). Mutations in the fukutin-related protein gene (FKRP) identify limb girdle muscular dystrophy 2I as a milder allelic variant of congenital muscular dystrophy MDC1C. *Hum. Mol. Genet.* 10, 2851–2859.

Bronner-Fraser, M., Artinger, M., Muschler, J. and Horwitz, A. F. (1992). Developmentally regulated expression of alpha 6 integrin in avian embryos. *Development* 115, 197–211.

Burden, S. J., Huijbers, M. G. and Remedio, L. (2018). Fundamental Molecules and Mechanisms for Forming and Maintaining Neuromuscular Synapses. *Int J Mol Sci* 19, .

Burkin, D. J. and Kaufman, S. J. (1999). The alpha7beta1 integrin in muscle development and disease. *Cell Tissue Res.* 296, 183–190.

- Cabrera-Serrano, M., Ghaoui, R., Ravenscroft, G., Johnsen, R. D., Davis, M. R., Corbett, A., Reddel, S., Sue, C. M., Liang, C., Waddell, L. B., et al. (2015). Expanding the phenotype of GMPPB mutations. *Brain* 138, 836–844.
- Carss, K. J., Stevens, E., Foley, A. R., Cirak, S., Riemersma, M., Torelli, S., Hoischen, A., Willer, T., van Scherpenzeel, M., Moore, S. A., et al. (2013). Mutations in GDP-mannose pyrophosphorylase B cause congenital and limb-girdle muscular dystrophies associated with hypoglycosylation of α -dystroglycan. *Am. J. Hum. Genet.* 93, 29–41.
- Cataldi, M. P., Lu, P., Blaeser, A. and Lu, Q. L. (2018). Ribitol restores functionally glycosylated α -dystroglycan and improves muscle function in dystrophic FKRP-mutant mice. *Nat Commun* 9, 3448.
- Chan, Y. M., Keramaris-Vrantsis, E., Lidov, H. G., Norton, J. H., Zinchenko, N., Gruber, H. E., Thresher, R., Blake, D. J., Ashar, J., Rosenfeld, J., et al. (2010). Fukutin-related protein is essential for mouse muscle, brain and eye development and mutation recapitulates the wide clinical spectrums of dystroglycanopathies. *Hum. Mol. Genet.* 19, 3995–4006.
- Charvet, B., Ruggiero, F. and Le Guellec, D. (2012). The development of the myotendinous junction. A review. *Muscles Ligaments Tendons J* 2, 53–63.
- Chen, J. W. and Galloway, J. L. (2014). The development of zebrafish tendon and ligament progenitors. *Development* 141, 2035–2045.
- Coffey, E. C., Pasquarella, M. E., Goody, M. F. and Henry, C. A. (2018). Ethanol Exposure Causes Muscle Degeneration in Zebrafish. *J Dev Biol* 6,.
- Cohn, R. D., Mayer, U., Saher, G., Herrmann, R., van der Flier, A., Sonnenberg, A., Sorokin, L. and Voit, T. (1999). Secondary reduction of α 7B integrin in laminin α 2 deficient congenital muscular dystrophy supports an additional transmembrane link in skeletal muscle. *J. Neurol. Sci.* 163, 140–152.
- Cong, L., Ran, F. A., Cox, D., Lin, S., Barretto, R., Habib, N., Hsu, P. D., Wu, X., Jiang, W., Marraffini, L. A., et al. (2013). Multiplex genome engineering using CRISPR/Cas systems. *Science* 339, 819–823.
- Constantin, B. (2014). Dystrophin complex functions as a scaffold for signalling proteins. *Biochim. Biophys. Acta* 1838, 635–642.
- Cornet, C., Di Donato, V. and Terriente, J. (2018). Combining Zebrafish and CRISPR/Cas9: Toward a More Efficient Drug Discovery Pipeline. *Front Pharmacol* 9, 703.
- Côté, P. D., Moukhles, H., Lindenbaum, M. and Carbonetto, S. (1999). Chimaeric mice deficient in dystroglycans develop muscular dystrophy and have disrupted myoneural synapses. *Nat. Genet.* 23, 338–342.

Crawford, B. D., Henry, C. A., Clason, T. A., Becker, A. L. and Hille, M. B. (2003). Activity and distribution of paxillin, focal adhesion kinase, and cadherin indicate cooperative roles during zebrafish morphogenesis. *Mol. Biol. Cell* 14, 3065–3081.

de Bernabé, D. B.-V., van Bokhoven, H., van Beusekom, E., Van den Akker, W., Kant, S., Dobyns, W. B., Cormand, B., Currier, S., Hamel, B., Talim, B., et al. (2003). A homozygous nonsense mutation in the fukutin gene causes a Walker-Warburg syndrome phenotype. *J. Med. Genet.* 40, 845–848.

Deakin, N. O. and Turner, C. E. (2008). Paxillin comes of age. *J. Cell. Sci.* 121, 2435–2444.

Deconinck, A. E., Potter, A. C., Tinsley, J. M., Wood, S. J., Vater, R., Young, C., Metzinger, L., Vincent, A., Slater, C. R. and Davies, K. E. (1997). Postsynaptic abnormalities at the neuromuscular junctions of utrophin-deficient mice. *J. Cell Biol.* 136, 883–894.

Devoto, S. H., Melançon, E., Eisen, J. S. and Westerfield, M. (1996). Identification of separate slow and fast muscle precursor cells in vivo, prior to somite formation. *Development* 122, 3371–3380.

Di Costanzo, S., Balasubramanian, A., Pond, H. L., Rozkalne, A., Pantaleoni, C., Saredi, S., Gupta, V. A., Sunu, C. M., Yu, T. W., Kang, P. B., et al. (2014). POMK mutations disrupt muscle development leading to a spectrum of neuromuscular presentations. *Hum. Mol. Genet.* 23, 5781–5792.

Ervasti, J. M. and Campbell, K. P. (1993). A role for the dystrophin-glycoprotein complex as a transmembrane linker between laminin and actin. *J. Cell Biol.* 122, 809–823.

Fashena, D. and Westerfield, M. (1999). Secondary motoneuron axons localize DM-GRASP on their fasciculated segments. *J. Comp. Neurol.* 406, 415–424.

Feldner, J., Reimer, M. M., Schweitzer, J., Wendik, B., Meyer, D., Becker, T. and Becker, C. G. (2007). PlexinA3 restricts spinal exit points and branching of trunk motor nerves in embryonic zebrafish. *J. Neurosci.* 27, 4978–4983.

Finsterer, J. (2019). Congenital myasthenic syndromes. *Orphanet J Rare Dis* 14, 57.

Flanagan-Steet, H., Fox, M. A., Meyer, D. and Sanes, J. R. (2005). Neuromuscular synapses can form in vivo by incorporation of initially aneural postsynaptic specializations. *Development* 132, 4471–4481.

Frost, A. R., Böhm, S. V., Sewduth, R. N., Josifova, D., Ogilvie, C. M., Izatt, L. and Roberts, R. G. (2010). Heterozygous deletion of a 2-Mb region including the dystroglycan gene in a patient with mild myopathy, facial hypotonia, oral-motor dyspraxia and white matter abnormalities. *Eur. J. Hum. Genet.* 18, 852–855.

- Gagnon, J. A., Valen, E., Thyme, S. B., Huang, P., Akhmetova, L., Ahkmetova, L., Pauli, A., Montague, T. G., Zimmerman, S., Richter, C., et al. (2014). Efficient mutagenesis by Cas9 protein-mediated oligonucleotide insertion and large-scale assessment of single-guide RNAs. *PLoS ONE* 9, e98186.
- Gasiunas, G., Barrangou, R., Horvath, P. and Siksnys, V. (2012). Cas9-crRNA ribonucleoprotein complex mediates specific DNA cleavage for adaptive immunity in bacteria. *Proc. Natl. Acad. Sci. U.S.A.* 109, E2579-2586.
- Gawlik, K., Miyagoe-Suzuki, Y., Ekblom, P., Takeda, S. and Durbeej, M. (2004). Laminin alpha1 chain reduces muscular dystrophy in laminin alpha2 chain deficient mice. *Hum. Mol. Genet.* 13, 1775–1784.
- Gee, S. H., Montanaro, F., Lindenbaum, M. H. and Carbonetto, S. (1994). Dystroglycan-alpha, a dystrophin-associated glycoprotein, is a functional agrin receptor. *Cell* 77, 675–686.
- Gerin, I., Ury, B., Breloy, I., Bouchet-Seraphin, C., Bolsée, J., Halbout, M., Graff, J., Vertommen, D., Muccioli, G. G., Seta, N., et al. (2016). ISPD produces CDP-ribitol used by FKTN and FKRP to transfer ribitol phosphate onto α -dystroglycan. *Nat Commun* 7, 11534.
- Gibbs, E. M., Horstick, E. J. and Dowling, J. J. (2013). Swimming into prominence: the zebrafish as a valuable tool for studying human myopathies and muscular dystrophies. *FEBS J.* 280, 4187–4197.
- Goddeeris, M. M., Wu, B., Venzke, D., Yoshida-Moriguchi, T., Saito, F., Matsumura, K., Moore, S. A. and Campbell, K. P. (2013). LARGE glycans on dystroglycan function as a tunable matrix scaffold to prevent dystrophy. *Nature* 503, 136–140.
- Godfrey, C., Foley, A. R., Clement, E. and Muntoni, F. (2011). Dystroglycanopathies: coming into focus. *Curr. Opin. Genet. Dev.* 21, 278–285.
- Goody, M. F. and Henry, C. A. (2010). Dynamic interactions between cells and their extracellular matrix mediate embryonic development. *Mol. Reprod. Dev.* 77, 475–488.
- Goody, M. F., Kelly, M. W., Lessard, K. N., Khalil, A. and Henry, C. A. (2010). Nr2b-mediated NAD⁺ production regulates cell adhesion and is required for muscle morphogenesis in vivo: Nr2b and NAD⁺ in muscle morphogenesis. *Dev. Biol.* 344, 809–826.
- Goody, M. F., Kelly, M. W., Reynolds, C. J., Khalil, A., Crawford, B. D. and Henry, C. A. (2012). NAD⁺ biosynthesis ameliorates a zebrafish model of muscular dystrophy. *PLoS Biol.* 10, e1001409.
- Goody, M. F., Sher, R. B. and Henry, C. A. (2015). Hanging on for the ride: adhesion to the extracellular matrix mediates cellular responses in skeletal muscle morphogenesis and disease. *Dev. Biol.* 401, 75–91.

- Goody, M. F., Carter, E. V., Kilroy, E. A., Maves, L. and Henry, C. A. (2017). “Muscling” Throughout Life: Integrating Studies of Muscle Development, Homeostasis, and Disease in Zebrafish. *Curr. Top. Dev. Biol.* 124, 197–234.
- Gribble, K. D., Walker, L. J., Saint-Amant, L., Kuwada, J. Y. and Granato, M. (2018). The synaptic receptor Lrp4 promotes peripheral nerve regeneration. *Nature Communications* 9, 2389.
- Guillon, E., Bretaud, S. and Ruggiero, F. (2016). Slow Muscle Precursors Lay Down a Collagen XV Matrix Fingerprint to Guide Motor Axon Navigation. *J. Neurosci.* 36, 2663–2676.
- Gullberg, D., Tiger, C. F. and Velling, T. (1999). Laminins during muscle development and in muscular dystrophies. *Cell. Mol. Life Sci.* 56, 442–460.
- Gumerson, J. D., Davis, C. S., Kabaeva, Z. T., Hayes, J. M., Brooks, S. V. and Michele, D. E. (2013). Muscle-specific expression of LARGE restores neuromuscular transmission deficits in dystrophic LARGE(myd) mice. *Hum. Mol. Genet.* 22, 757–768.
- Gupta, V., Kawahara, G., Gundry, S. R., Chen, A. T., Lencer, W. I., Zhou, Y., Zon, L. I., Kunkel, L. M. and Beggs, A. H. (2011). The zebrafish dag1 mutant: a novel genetic model for dystroglycanopathies. *Hum. Mol. Genet.* 20, 1712–1725.
- Gupta, V. A., Kawahara, G., Myers, J. A., Chen, A. T., Hall, T. E., Manzini, M. C., Currie, P. D., Zhou, Y., Zon, L. I., Kunkel, L. M., et al. (2012). A splice site mutation in laminin- α 2 results in a severe muscular dystrophy and growth abnormalities in zebrafish. *PLoS ONE* 7, e43794.
- Guyon, J. R., Mosley, A. N., Zhou, Y., O’Brien, K. F., Sheng, X., Chiang, K., Davidson, A. J., Volinski, J. M., Zon, L. I. and Kunkel, L. M. (2003). The dystrophin associated protein complex in zebrafish. *Hum. Mol. Genet.* 12, 601–615.
- Hall, T. E., Bryson-Richardson, R. J., Berger, S., Jacoby, A. S., Cole, N. J., Hollway, G. E., Berger, J. and Currie, P. D. (2007). The zebrafish candyfloss mutant implicates extracellular matrix adhesion failure in laminin α 2-deficient congenital muscular dystrophy. *Proc. Natl. Acad. Sci. U.S.A.* 104, 7092–7097.
- Hara, Y., Balci-Hayta, B., Yoshida-Moriguchi, T., Kanagawa, M., Beltrán-Valero de Bernabé, D., Gündeşli, H., Willer, T., Satz, J. S., Crawford, R. W., Burden, S. J., et al. (2011). A dystroglycan mutation associated with limb-girdle muscular dystrophy. *N. Engl. J. Med.* 364, 939–946.
- Hayashi, Y. K., Chou, F. L., Engvall, E., Ogawa, M., Matsuda, C., Hirabayashi, S., Yokochi, K., Ziober, B. L., Kramer, R. H., Kaufman, S. J., et al. (1998). Mutations in the integrin α 7 gene cause congenital myopathy. *Nat. Genet.* 19, 94–97.
- Helbling-Leclerc, A., Zhang, X., Topaloglu, H., Cruaud, C., Tesson, F., Weissenbach, J., Tomé, F. M., Schwartz, K., Fardeau, M. and Tryggvason, K. (1995). Mutations in the laminin α 2-chain gene (LAMA2) cause merosin-deficient congenital muscular dystrophy. *Nat. Genet.* 11, 216–218.

- Henry, C. A. and Amacher, S. L. (2004). Zebrafish slow muscle cell migration induces a wave of fast muscle morphogenesis. *Dev. Cell* 7, 917–923.
- Herbst, R., Iskratsch, T., Unger, E. and Bittner, R. E. (2009). Aberrant development of neuromuscular junctions in glycosylation-defective Large(myd) mice. *Neuromuscul. Disord.* 19, 366–378.
- Hilario, J. D., Rodino-Klapac, L. R., Wang, C. and Beattie, C. E. (2009). Semaphorin 5A is a bifunctional axon guidance cue for axial motoneurons in vivo. *Dev. Biol.* 326, 190–200.
- Hinits, Y. and Hughes, S. M. (2007). Mef2s are required for thick filament formation in nascent muscle fibres. *Development* 134, 2511–2519.
- Holmberg, J. and Durbeej, M. (2013). Laminin-211 in skeletal muscle function. *Cell Adh Migr* 7, 111–121.
- Horstick, E. J., Gibbs, E. M., Li, X., Davidson, A. E. and Dowling, J. J. (2013). Analysis of embryonic and larval zebrafish skeletal myofibers from dissociated preparations. *J Vis Exp* e50259.
- Inamori, K., Yoshida-Moriguchi, T., Hara, Y., Anderson, M. E., Yu, L. and Campbell, K. P. (2012). Dystroglycan function requires xylosyl- and glucuronyltransferase activities of LARGE. *Science* 335, 93–96.
- Ito, K., Patel, P. N., Gorham, J. M., McDonough, B., DePalma, S. R., Adler, E. E., Lam, L., MacRae, C. A., Mohiuddin, S. M., Fatkin, D., et al. (2017). Identification of pathogenic gene mutations in LMNA and MYBPC3 that alter RNA splicing. *Proc. Natl. Acad. Sci. U.S.A.* 114, 7689–7694.
- Jacob, A. E., Amack, J. D. and Turner, C. E. (2017). Paxillin genes and actomyosin contractility regulate myotome morphogenesis in zebrafish. *Dev. Biol.* 425, 70–84.
- Janik, M. E., Lityńska, A. and Vereecken, P. (2010). Cell migration-the role of integrin glycosylation. *Biochim. Biophys. Acta* 1800, 545–555.
- Jayasinha, V., Nguyen, H. H., Xia, B., Kammesheidt, A., Hoyte, K. and Martin, P. T. (2003). Inhibition of dystroglycan cleavage causes muscular dystrophy in transgenic mice. *Neuromuscul. Disord.* 13, 365–375.
- Jenkins, M. H., Alrowaished, S. S., Goody, M. F., Crawford, B. D. and Henry, C. A. (2016). Laminin and Matrix metalloproteinase 11 regulate Fibronectin levels in the zebrafish myotendinous junction. *Skelet Muscle* 6, 18.
- Jensen, B. S., Willer, T., Saade, D. N., Cox, M. O., Mozaffar, T., Scavina, M., Stefans, V. A., Winder, T. L., Campbell, K. P., Moore, S. A., et al. (2015). GMPPB-Associated Dystroglycanopathy: Emerging Common Variants with Phenotype Correlation. *Hum. Mutat.* 36, 1159–1163.

- Jinek, M., Chylinski, K., Fonfara, I., Hauer, M., Doudna, J. A. and Charpentier, E. (2012). A programmable dual-RNA-guided DNA endonuclease in adaptive bacterial immunity. *Science* 337, 816–821.
- Johnson, K., Bertoli, M., Phillips, L., Töpf, A., Van den Bergh, P., Vissing, J., Witting, N., Nafissi, S., Jamal-Omidi, S., Łusakowska, A., et al. (2018). Detection of variants in dystroglycanopathy-associated genes through the application of targeted whole-exome sequencing analysis to a large cohort of patients with unexplained limb-girdle muscle weakness. *Skelet Muscle* 8, 23.
- Kanagawa, M., Kobayashi, K., Tajiri, M., Manya, H., Kuga, A., Yamaguchi, Y., Akasaka-Manyu, K., Furukawa, J.-I., Mizuno, M., Kawakami, H., et al. (2016). Identification of a Post-translational Modification with Ribitol-Phosphate and Its Defect in Muscular Dystrophy. *Cell Rep* 14, 2209–2223.
- Kawahara, G., Guyon, J. R., Nakamura, Y. and Kunkel, L. M. (2010). Zebrafish models for human FKRP muscular dystrophies. *Hum. Mol. Genet.* 19, 623–633.
- Kemaladewi, D. U., Maino, E., Hyatt, E., Hou, H., Ding, M., Place, K. M., Zhu, X., Bassi, P., Baghestani, Z., Deshwar, A. G., et al. (2017). Correction of a splicing defect in a mouse model of congenital muscular dystrophy type 1A using a homology-directed-repair-independent mechanism. *Nature Medicine* 23, 984–989.
- Kettleborough, R. N. W., Busch-Nentwich, E. M., Harvey, S. A., Dooley, C. M., de Bruijn, E., van Eeden, F., Sealy, I., White, R. J., Herd, C., Nijman, I. J., et al. (2013). A systematic genome-wide analysis of zebrafish protein-coding gene function. *Nature* 496, 494–497.
- Kimmel, C. B., Ballard, W. W., Kimmel, S. R., Ullmann, B. and Schilling, T. F. (1995). Stages of embryonic development of the zebrafish. *Dev. Dyn.* 203, 253–310.
- Kwan, K. M., Fujimoto, E., Grabher, C., Mangum, B. D., Hardy, M. E., Campbell, D. S., Parant, J. M., Yost, H. J., Kanki, J. P. and Chien, C.-B. (2007). The Tol2kit: a multisite gateway-based construction kit for Tol2 transposon transgenesis constructs. *Dev. Dyn.* 236, 3088–3099.
- Lawson, N. D. and Weinstein, B. M. (2002). In vivo imaging of embryonic vascular development using transgenic zebrafish. *Dev. Biol.* 248, 307–318.
- Levedakou, E. N., Chen, X.-J., Soliven, B. and Popko, B. (2005). Disruption of the mouse Large gene in the enr and myd mutants results in nerve, muscle, and neuromuscular junction defects. *Mol. Cell. Neurosci.* 28, 757–769.
- Lewis, K. E. and Eisen, J. S. (2003). From cells to circuits: development of the zebrafish spinal cord. *Prog. Neurobiol.* 69, 419–449.
- Li, J., Mayne, R. and Wu, C. (1999). A novel muscle-specific beta 1 integrin binding protein (MIBP) that modulates myogenic differentiation. *J. Cell Biol.* 147, 1391–1398.

- Li, J., Rao, H., Burkin, D., Kaufman, S. J. and Wu, C. (2003). The muscle integrin binding protein (MIBP) interacts with alpha7beta1 integrin and regulates cell adhesion and laminin matrix deposition. *Dev. Biol.* 261, 209–219.
- Li, J., Chen, Z., Gao, L.-Y., Colorni, A., Ucko, M., Fang, S. and Du, S. J. (2015). A transgenic zebrafish model for monitoring xbp1 splicing and endoplasmic reticulum stress in vivo. *Mech. Dev.* 137, 33–44.
- Lin, Y.-Y., White, R. J., Torelli, S., Cirak, S., Muntoni, F. and Stemple, D. L. (2011). Zebrafish Fukutin family proteins link the unfolded protein response with dystroglycanopathies. *Hum. Mol. Genet.* 20, 1763–1775.
- Liu, K., Petree, C., Requena, T., Varshney, P. and Varshney, G. K. (2019). Expanding the CRISPR Toolbox in Zebrafish for Studying Development and Disease. *Front Cell Dev Biol* 7, 13.
- Luo, Y.-B., Mastaglia, F. L. and Wilton, S. D. (2014). Normal and aberrant splicing of LMNA. *J. Med. Genet.* 51, 215–223.
- Luo, S., Cai, S., Maxwell, S., Yue, D., Zhu, W., Qiao, K., Zhu, Z., Zhou, L., Xi, J., Lu, J., et al. (2017). Novel mutations in the C-terminal region of GMPPB causing limb-girdle muscular dystrophy overlapping with congenital myasthenic syndrome. *Neuromuscul. Disord.* 27, 557–564.
- Mali, P., Yang, L., Esvelt, K. M., Aach, J., Guell, M., DiCarlo, J. E., Norville, J. E. and Church, G. M. (2013). RNA-guided human genome engineering via Cas9. *Science* 339, 823–826.
- Manya, H., Chiba, A., Yoshida, A., Wang, X., Chiba, Y., Jigami, Y., Margolis, R. U. and Endo, T. (2004). Demonstration of mammalian protein O-mannosyltransferase activity: coexpression of POMT1 and POMT2 required for enzymatic activity. *Proc. Natl. Acad. Sci. U.S.A.* 101, 500–505.
- Marchese, M., Pappalardo, A., Baldacci, J., Verri, T., Doccini, S., Cassandrini, D., Bruno, C., Fiorillo, C., Garcia-Gil, M., Bertini, E., et al. (2016). Dolichol-phosphate mannose synthase depletion in zebrafish leads to dystrophic muscle with hypoglycosylated α -dystroglycan. *Biochem. Biophys. Res. Commun.* 477, 137–143.
- Martin, P. T. (2006). Mechanisms of disease: congenital muscular dystrophies-glycosylation takes center stage. *Nat Clin Pract Neurol* 2, 222–230.
- Mayer, U., Saher, G., Fässler, R., Bornemann, A., Echtermeyer, F., von der Mark, H., Miosge, N., Pöschl, E. and von der Mark, K. (1997). Absence of integrin alpha 7 causes a novel form of muscular dystrophy. *Nat. Genet.* 17, 318–323.
- Meng, A., Tang, H., Ong, B. A., Farrell, M. J. and Lin, S. (1997). Promoter analysis in living zebrafish embryos identifies a cis-acting motif required for neuronal expression of GATA-2. *Proc. Natl. Acad. Sci. U.S.A.* 94, 6267–6272.

- Michele, D. E. and Campbell, K. P. (2003). Dystrophin-glycoprotein complex: post-translational processing and dystroglycan function. *J. Biol. Chem.* 278, 15457–15460.
- Millay, D. P., Goonasekera, S. A., Sargent, M. A., Maillet, M., Aronow, B. J. and Molkentin, J. D. (2009). Calcium influx is sufficient to induce muscular dystrophy through a TRPC-dependent mechanism. *Proc. Natl. Acad. Sci. U.S.A.* 106, 19023–19028.
- Miner, J. H. and Yurchenco, P. D. (2004). Laminin functions in tissue morphogenesis. *Annu. Rev. Cell Dev. Biol.* 20, 255–284.
- Montagnese, F., Klupp, E., Karampinos, D. C., Biskup, S., Gläser, D., Kirschke, J. S. and Schoser, B. (2017). Two patients with GMPPB mutation: The overlapping phenotypes of limb-girdle myasthenic syndrome and limb-girdle muscular dystrophy dystroglycanopathy. *Muscle Nerve* 56, 334–340.
- Montague, T. G., Cruz, J. M., Gagnon, J. A., Church, G. M. and Valen, E. (2014). CHOPCHOP: a CRISPR/Cas9 and TALEN web tool for genome editing. *Nucleic Acids Research* 42, W401.
- Montes, M., Sanford, B. L., Comiskey, D. F. and Chandler, D. S. (2019). RNA Splicing and Disease: Animal Models to Therapies. *Trends in Genetics* 35, 68–87.
- Moore, C. J., Goh, H. T. and Hewitt, J. E. (2008). Genes required for functional glycosylation of dystroglycan are conserved in zebrafish. *Genomics* 92, 159–167.
- Muntoni, F., Torelli, S. and Brockington, M. (2008). Muscular dystrophies due to glycosylation defects. *Neurotherapeutics* 5, 627–632.
- Muntoni, F., Torelli, S., Wells, D. J. and Brown, S. C. (2011). Muscular dystrophies due to glycosylation defects: diagnosis and therapeutic strategies. *Curr. Opin. Neurol.* 24, 437–442.
- Myers, P. Z., Eisen, J. S. and Westerfield, M. (1986). Development and axonal outgrowth of identified motoneurons in the zebrafish. *J. Neurosci.* 6, 2278–2289.
- Nickolls, A. R. and Bönnemann, C. G. (2018). The roles of dystroglycan in the nervous system: insights from animal models of muscular dystrophy. *Dis Model Mech* 11,.
- Odenthal, J., Haffter, P., Vogelsang, E., Brand, M., van Eeden, F. J., Furutani-Seiki, M., Granato, M., Hammerschmidt, M., Heisenberg, C. P., Jiang, Y. J., et al. (1996). Mutations affecting the formation of the notochord in the zebrafish, *Danio rerio*. *Development* 123, 103–115.
- Oestergaard, S. T., Stojkovic, T., Dahlqvist, J. R., Bouchet-Seraphin, C., Nectoux, J., Leturcq, F., Cossée, M., Solé, G., Thomsen, C., Krag, T. O., et al. (2016). Muscle involvement in limb-girdle muscular dystrophy with GMPPB deficiency (LGMD2T). *Neurol Genet* 2, e112.
- Ogawa, M., Nakamura, N., Nakayama, Y., Kurosaka, A., Manya, H., Kanagawa, M., Endo, T., Furukawa, K. and Okajima, T. (2013). GTDC2 modifies O-mannosylated α -dystroglycan in the

- endoplasmic reticulum to generate N-acetyl glucosamine epitopes reactive with CTD110.6 antibody. *Biochem. Biophys. Res. Commun.* 440, 88–93.
- Panicucci, C., Fiorillo, C., Moro, F., Astrea, G., Brisca, G., Trucco, F., Pedemonte, M., Lanteri, P., Sciarretta, L., Minetti, C., et al. (2018). Mutations in GMPPB Presenting with Pseudometabolic Myopathy. *JIMD Rep* 38, 23–31.
- Panzer, J. A., Gibbs, S. M., Dosch, R., Wagner, D., Mullins, M. C., Granato, M. and Balice-Gordon, R. J. (2005). Neuromuscular synaptogenesis in wild-type and mutant zebrafish. *Dev. Biol.* 285, 340–357.
- Parsons, M. J., Campos, I., Hirst, E. M. A. and Stemple, D. L. (2002). Removal of dystroglycan causes severe muscular dystrophy in zebrafish embryos. *Development* 129, 3505–3512.
- Pevzner, A., Schoser, B., Peters, K., Cosma, N.-C., Karakatsani, A., Schalke, B., Melms, A. and Kröger, S. (2012). Anti-LRP4 autoantibodies in AChR- and MuSK-antibody-negative myasthenia gravis. *J. Neurol.* 259, 427–435.
- Pilgram, G. S. K., Potikanond, S., Baines, R. A., Fradkin, L. G. and Noordermeer, J. N. (2010). The roles of the dystrophin-associated glycoprotein complex at the synapse. *Mol. Neurobiol.* 41, 1–21.
- Postel, R., Vakeel, P., Topczewski, J., Knöll, R. and Bakkers, J. (2008). Zebrafish integrin-linked kinase is required in skeletal muscles for strengthening the integrin-ECM adhesion complex. *Dev. Biol.* 318, 92–101.
- Powell, G. T. and Wright, G. J. (2011). Jamb and jamc are essential for vertebrate myocyte fusion. *PLoS Biol.* 9, e1001216.
- Praissman, J. L., Willer, T., Sheikh, M. O., Toi, A., Chitayat, D., Lin, Y.-Y., Lee, H., Stalnaker, S. H., Wang, S., Prabhakar, P. K., et al. (2016). The functional O-mannose glycan on α -dystroglycan contains a phospho-ribitol primed for matriglycan addition. *Elife* 5,.
- Pratt, S. J. P., Valencia, A. P., Le, G. K., Shah, S. B. and Lovering, R. M. (2015). Pre- and postsynaptic changes in the neuromuscular junction in dystrophic mice. *Front Physiol* 6, 252.
- Qiao, C., Wang, C.-H., Zhao, C., Lu, P., Awano, H., Xiao, B., Li, J., Yuan, Z., Dai, Y., Martin, C. B., et al. (2014). Muscle and heart function restoration in a limb girdle muscular dystrophy 2I (LGMD2I) mouse model by systemic FKRP gene delivery. *Mol. Ther.* 22, 1890–1899.
- Rafferty, S. A. and Quinn, T. A. (2018). A beginner's guide to understanding and implementing the genetic modification of zebrafish. *Prog. Biophys. Mol. Biol.* 138, 3–19.
- Raphael, A. R., Couthouis, J., Sakamuri, S., Siskind, C., Vogel, H., Day, J. W. and Gitler, A. D. (2014). Congenital muscular dystrophy and generalized epilepsy caused by GMPPB mutations. *Brain Res.* 1575, 66–71.

- Rodríguez Cruz, P. M., Belaya, K., Basiri, K., Sedghi, M., Farrugia, M. E., Holton, J. L., Liu, W. W., Maxwell, S., Petty, R., Walls, T. J., et al. (2016). Clinical features of the myasthenic syndrome arising from mutations in GMPPB. *J. Neurol. Neurosurg. Psychiatry* 87, 802–809.
- Rooney, J. E., Gurpur, P. B. and Burkin, D. J. (2009). Laminin-111 protein therapy prevents muscle disease in the mdx mouse model for Duchenne muscular dystrophy. *Proc. Natl. Acad. Sci. U.S.A.* 106, 7991–7996.
- Rooney, J. E., Knapp, J. R., Hodges, B. L., Wuebbles, R. D. and Burkin, D. J. (2012). Laminin-111 Protein Therapy Reduces Muscle Pathology and Improves Viability of a Mouse Model of Merosin-Deficient Congenital Muscular Dystrophy. *Am J Pathol* 180, 1593–1602.
- Roscioli, T., Kamsteeg, E.-J., Buysse, K., Maystadt, I., van Reeuwijk, J., van den Elzen, C., van Beusekom, E., Riemersma, M., Pfundt, R., Vissers, L. E. L. M., et al. (2012). Mutations in ISPD cause Walker-Warburg syndrome and defective glycosylation of α -dystroglycan. *Nat. Genet.* 44, 581–585.
- Rost, F., Eugster, C., Schröter, C., Oates, A. C. and Brusch, L. (2014). Chevron formation of the zebrafish muscle segments. *J. Exp. Biol.* 217, 3870–3882.
- Rush, J. S., Panneerselvam, K., Waechter, C. J. and Freeze, H. H. (2000). Mannose supplementation corrects GDP-mannose deficiency in cultured fibroblasts from some patients with Congenital Disorders of Glycosylation (CDG). *Glycobiology* 10, 829–835.
- Rybakova, I. N., Patel, J. R. and Ervasti, J. M. (2000). The dystrophin complex forms a mechanically strong link between the sarcolemma and costameric actin. *J. Cell Biol.* 150, 1209–1214.
- Saito, F., Masaki, T., Saito, Y., Nakamura, A., Takeda, S., Shimizu, T., Toda, T. and Matsumura, K. (2007). Defective peripheral nerve myelination and neuromuscular junction formation in fukutin-deficient chimeric mice. *J. Neurochem.* 101, 1712–1722.
- Sarathy, A., Wuebbles, R. D., Fontelonga, T. M., Tarchione, A. R., Mathews Griner, L. A., Heredia, D. J., Nunes, A. M., Duan, S., Brewer, P. D., Van Ry, T., et al. (2017). SU9516 Increases α 7 β 1 Integrin and Ameliorates Disease Progression in the mdx Mouse Model of Duchenne Muscular Dystrophy. *Mol. Ther.* 25, 1395–1407.
- Sarkozy, A., Torelli, S., Mein, R., Henderson, M., Phadke, R., Feng, L., Sewry, C., Ala, P., Yau, M., Bertoli, M., et al. (2018). Mobility shift of beta-dystroglycan as a marker of GMPPB gene-related muscular dystrophy. *J. Neurol. Neurosurg. Psychiatry* 89, 762–768.
- Sasaki, T., Giltay, R., Talts, U., Timpl, R. and Talts, J. F. (2002). Expression and distribution of laminin alpha1 and alpha2 chains in embryonic and adult mouse tissues: an immunochemical approach. *Exp. Cell Res.* 275, 185–199.

- Schindelin, J., Arganda-Carreras, I., Frise, E., Kaynig, V., Longair, M., Pietzsch, T., Preibisch, S., Rueden, C., Saalfeld, S., Schmid, B., et al. (2012). Fiji: an open-source platform for biological-image analysis. *Nat. Methods* 9, 676–682.
- Schneider, V. A. and Granato, M. (2006). The myotomal diwanka (lh3) glycosyltransferase and type XVIII collagen are critical for motor growth cone migration. *Neuron* 50, 683–695.
- Schneider, C. A., Rasband, W. S. and Eliceiri, K. W. (2012). NIH Image to ImageJ: 25 years of image analysis. *Nat. Methods* 9, 671–675.
- Schweitzer, J., Becker, T., Lefebvre, J., Granato, M., Schachner, M. and Becker, C. G. (2005). Tenascin-C is involved in motor axon outgrowth in the trunk of developing zebrafish. *Dev. Dyn.* 234, 550–566.
- Scotti, M. M. and Swanson, M. S. (2016). RNA mis-splicing in disease. *Nat. Rev. Genet.* 17, 19–32.
- Serafini, P. R., Feyder, M. J., Hightower, R. M., Garcia-Perez, D., Vieira, N. M., Lek, A., Gibbs, D. E., Moukha-Chafiq, O., Augelli-Szafran, C. E., Kawahara, G., et al. (2018). A limb-girdle muscular dystrophy 2I model of muscular dystrophy identifies corrective drug compounds for dystroglycanopathies. *JCI Insight* 3,.
- Simone, B. W., Martínez-Gálvez, G., WareJoncas, Z. and Ekker, S. C. (2018). Fishing for understanding: Unlocking the zebrafish gene editor’s toolbox. *Methods* 150, 3–10.
- Singhal, N. and Martin, P. T. (2011). Role of extracellular matrix proteins and their receptors in the development of the vertebrate neuromuscular junction. *Dev Neurobiol* 71, 982–1005.
- Smith, S. J., Wang, J. C., Gupta, V. A. and Dowling, J. J. (2017). A novel early onset phenotype in a zebrafish model of merosin deficient congenital muscular dystrophy. *PLoS ONE* 12, e0172648.
- Snow, C. J. and Henry, C. A. (2009). Dynamic formation of microenvironments at the myotendinous junction correlates with muscle fiber morphogenesis in zebrafish. *Gene Expr. Patterns* 9, 37–42.
- Snow, C. J., Peterson, M. T., Khalil, A. and Henry, C. A. (2008a). Muscle development is disrupted in zebrafish embryos deficient for fibronectin. *Dev. Dyn.* 237, 2542–2553.
- Snow, C. J., Goody, M., Kelly, M. W., Oster, E. C., Jones, R., Khalil, A. and Henry, C. A. (2008b). Time-lapse analysis and mathematical characterization elucidate novel mechanisms underlying muscle morphogenesis. *PLoS Genet.* 4, e1000219.
- Song, W. K., Wang, W., Sato, H., Bielser, D. A. and Kaufman, S. J. (1993). Expression of alpha 7 integrin cytoplasmic domains during skeletal muscle development: alternate forms, conformational change, and homologies with serine/threonine kinases and tyrosine phosphatases. *J. Cell. Sci.* 106 (Pt 4), 1139–1152.

Stensland, E., Lindal, S., Jonsrud, C., Torbergesen, T., Bindoff, L. A., Rasmussen, M., Dahl, A., Thyssen, F. and Nilssen, Ø. (2011). Prevalence, mutation spectrum and phenotypic variability in Norwegian patients with Limb Girdle Muscular Dystrophy 2I. *Neuromuscul. Disord.* 21, 41–46.

Stevens, E., Carss, K. J., Cirak, S., Foley, A. R., Torelli, S., Willer, T., Tambunan, D. E., Yau, S., Brodd, L., Sewry, C. A., et al. (2013). Mutations in B3GALNT2 cause congenital muscular dystrophy and hypoglycosylation of α -dystroglycan. *Am. J. Hum. Genet.* 92, 354–365.

Subramanian, A. and Schilling, T. F. (2014). Thrombospondin-4 controls matrix assembly during development and repair of myotendinous junctions. *Elife* 3,.

Subramanian, A., Wayburn, B., Bunch, T. and Volk, T. (2007). Thrombospondin-mediated adhesion is essential for the formation of the myotendinous junction in *Drosophila*. *Development* 134, 1269–1278.

Sun, L., Shen, D., Xiong, T., Zhou, Z., Lu, X. and Cui, F. (2019). Limb-girdle muscular dystrophy due to GMPPB mutations: A case report and comprehensive literature review. *Bosn J Basic Med Sci.*

Sunada, Y., Bernier, S. M., Utani, A., Yamada, Y. and Campbell, K. P. (1995). Identification of a novel mutant transcript of laminin alpha 2 chain gene responsible for muscular dystrophy and dysmyelination in dy2J mice. *Hum. Mol. Genet.* 4, 1055–1061.

Takehima, Y., Yagi, M., Okizuka, Y., Awano, H., Zhang, Z., Yamauchi, Y., Nishio, H. and Matsuo, M. (2010). Mutation spectrum of the dystrophin gene in 442 Duchenne/Becker muscular dystrophy cases from one Japanese referral center. *J. Hum. Genet.* 55, 379–388.

Taniguchi-Ikeda, M., Kobayashi, K., Kanagawa, M., Yu, C., Mori, K., Oda, T., Kuga, A., Kurahashi, H., Akman, H. O., DiMauro, S., et al. (2011). Pathogenic exon-trapping by SVA retrotransposon and rescue in Fukuyama muscular dystrophy. *Nature* 478, 127–131.

Taniguchi-Ikeda, M., Morioka, I., Iijima, K. and Toda, T. (2016). Mechanistic aspects of the formation of α -dystroglycan and therapeutic research for the treatment of α -dystroglycanopathy: A review. *Mol. Aspects Med.* 51, 115–124.

Telfer, W. R., Busta, A. S., Bonnemann, C. G., Feldman, E. L. and Dowling, J. J. (2010). Zebrafish models of collagen VI-related myopathies. *Hum. Mol. Genet.* 19, 2433–2444.

Tempel, W., Rabeh, W. M., Bogan, K. L., Belenky, P., Wojcik, M., Seidle, H. F., Nedyalkova, L., Yang, T., Sauve, A. A., Park, H.-W., et al. (2007). Nicotinamide riboside kinase structures reveal new pathways to NAD⁺. *PLoS Biol.* 5, e263.

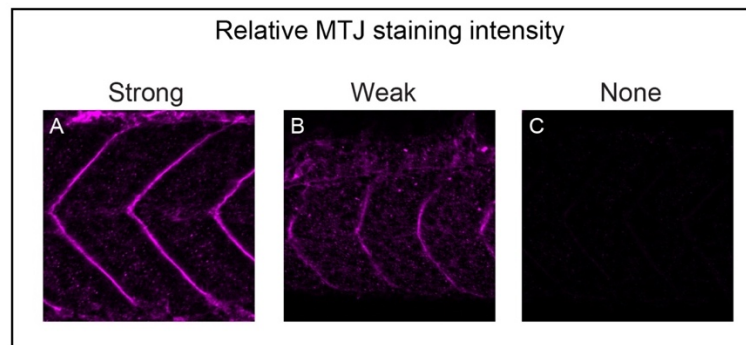
Thomas, P. J., Xu, R. and Martin, P. T. (2016). B4GALNT2 (GALGT2) Gene Therapy Reduces Skeletal Muscle Pathology in the FKR P448L Mouse Model of Limb Girdle Muscular Dystrophy 2I. *Am. J. Pathol.* 186, 2429–2448.

- Thornhill, P., Bassett, D., Lochmüller, H., Bushby, K. and Straub, V. (2008). Developmental defects in a zebrafish model for muscular dystrophies associated with the loss of fukutin-related protein (FKRP). *Brain* 131, 1551–1561.
- Tintignac, L. A., Brenner, H.-R. and Rüegg, M. A. (2015). Mechanisms Regulating Neuromuscular Junction Development and Function and Causes of Muscle Wasting. *Physiol. Rev.* 95, 809–852.
- Todeschini, A., Gualandi, F., Trabanelli, C., Armaroli, A., Ravani, A., Fanin, M., Rota, S., Bello, L., Ferlini, A., Pegoraro, E., et al. (2016). Becker muscular dystrophy due to an intronic splicing mutation inducing a dual dystrophin transcript. *Neuromuscul. Disord.* 26, 662–665.
- Tucker, J. D., Lu, P. J., Xiao, X. and Lu, Q. L. (2018). Overexpression of Mutant FKRP Restores Functional Glycosylation and Improves Dystrophic Phenotype in FKRP Mutant Mice. *Mol Ther Nucleic Acids* 11, 216–227.
- Turner, C. E., Glenney, J. R. and Burridge, K. (1990). Paxillin: a new vinculin-binding protein present in focal adhesions. *J. Cell Biol.* 111, 1059–1068.
- Van Reeuwijk, J., Olderode-Berends, M. J. W., Van den Elzen, C., Brouwer, O. F., Roscioli, T., Van Pampus, M. G., Scheffer, H., Brunner, H. G., Van Bokhoven, H. and Hol, F. A. (2010). A homozygous FKRP start codon mutation is associated with Walker-Warburg syndrome, the severe end of the clinical spectrum. *Clin. Genet.* 78, 275–281.
- Van Ry, P. M., Wuebbles, R. D., Key, M. and Burkin, D. J. (2015). Galectin-1 Protein Therapy Prevents Pathology and Improves Muscle Function in the mdx Mouse Model of Duchenne Muscular Dystrophy. *Mol. Ther.* 23, 1285–1297.
- van Tol, W., Michelakakis, H., Georgiadou, E., van den Bergh, P., Moraitou, M., Papadimas, G. K., Papadopoulos, C., Huijben, K., Alsady, M., Willemsen, M. A., et al. (2019). Towards understanding tissue-specific symptoms in dolichol-phosphate-mannose synthesis disorders; insight from DPM3-CDG. *J. Inherit. Metab. Dis.*
- Vannoy, C. H., Xiao, W., Lu, P., Xiao, X. and Lu, Q. L. (2017). Efficacy of Gene Therapy Is Dependent on Disease Progression in Dystrophic Mice with Mutations in the FKRP Gene. *Mol Ther Methods Clin Dev* 5, 31–42.
- Welser, J. V., Rooney, J. E., Cohen, N. C., Gurpur, P. B., Singer, C. A., Evans, R. A., Haines, B. A. and Burkin, D. J. (2009). Myotendinous junction defects and reduced force transmission in mice that lack alpha7 integrin and utrophin. *Am. J. Pathol.* 175, 1545–1554.
- Willer, T., Inamori, K.-I., Venzke, D., Harvey, C., Morgensen, G., Hara, Y., Beltrán Valero de Bernabé, D., Yu, L., Wright, K. M. and Campbell, K. P. (2014). The glucuronyltransferase B4GAT1 is required for initiation of LARGE-mediated α -dystroglycan functional glycosylation. *Elife* 3,.

- Wolff, C., Roy, S. and Ingham, P. W. (2003). Multiple muscle cell identities induced by distinct levels and timing of hedgehog activity in the zebrafish embryo. *Curr. Biol.* 13, 1169–1181.
- Wood, A. J., Müller, J. S., Jepson, C. D., Laval, S. H., Lochmüller, H., Bushby, K., Barresi, R. and Straub, V. (2011). Abnormal vascular development in zebrafish models for fukutin and FKRП deficiency. *Hum. Mol. Genet.* 20, 4879–4890.
- Wu, H., Xiong, W. C. and Mei, L. (2010). To build a synapse: signaling pathways in neuromuscular junction assembly. *Development* 137, 1017–1033.
- Wu, B., Shah, S. N., Lu, P., Bollinger, L. E., Blaeser, A., Sparks, S., Harper, A. D. and Lu, Q. L. (2018). Long-Term Treatment of Tamoxifen and Raloxifene Alleviates Dystrophic Phenotype and Enhances Muscle Functions of FKRП Dystroglycanopathy. *Am. J. Pathol.* 188, 1069–1080.
- Yoshida, A., Kobayashi, K., Many, H., Taniguchi, K., Kano, H., Mizuno, M., Inazu, T., Mitsushashi, H., Takahashi, S., Takeuchi, M., et al. (2001). Muscular dystrophy and neuronal migration disorder caused by mutations in a glycosyltransferase, POMGnT1. *Dev. Cell* 1, 717–724.
- Yoshida-Moriguchi, T., Willer, T., Anderson, M. E., Venzke, D., Whyte, T., Muntoni, F., Lee, H., Nelson, S. F., Yu, L. and Campbell, K. P. (2013). SGK196 is a glycosylation-specific O-mannose kinase required for dystroglycan function. *Science* 341, 896–899.
- Yurchenco, P. D., McKee, K. K., Reinhard, J. R. and Rüegg, M. A. (2018). Laminin-deficient muscular dystrophy: Molecular pathogenesis and structural repair strategies. *Matrix Biol.* 71–72, 174–187.
- Zelenchuk, T. A. and Brusés, J. L. (2011). In vivo labeling of zebrafish motor neurons using an mnx1 enhancer and Gal4/UAS. *Genesis* 49, 546–554.
- Zheng, M., Fang, H. and Hakomori, S. (1994). Functional role of N-glycosylation in alpha 5 beta 1 integrin receptor. De-N-glycosylation induces dissociation or altered association of alpha 5 and beta 1 subunits and concomitant loss of fibronectin binding activity. *J. Biol. Chem.* 269, 12325–12331.

APPENDIX A: CATEGORICAL SCORING OF MTJ STAINING INTENSITY

Figure A1. Scoring of relative MTJ staining intensity. (A-C) Anterior left, dorsal-side mounted zebrafish embryos at 26 hpf stained for laminin-111 at the MTJ (purple). **(A)** Example of an embryo with strong laminin staining intensity at the MTJ. **(B)** An embryo with weak laminin staining intensity at the MTJ. **(C)** An embryo lacking laminin staining at the MTJ.



APPENDIX B: PRELIMINARY RNA-SEQ DATA OF *GMPPB* MUTANTS

The following data are results of a collaboration with Dr. Benjamin King's laboratory at the University of Maine. The Henry laboratory sorted the wild-type and *gmppb* mutant embryos prior to RNA extraction; the King laboratory performed the RNA extraction, sent the samples for RNA sequencing, and compiled/analyzed the read data. RNA-seq was performed at the Hubbard Center for Genome Studies at the University of New Hampshire. These data indicate the presence of alternative splicing and differential gene expression in *gmppb* mutants. Analysis of a second RNA-seq experiment with control, mild *gmppb* mutants, and severe *gmppb* mutants is currently in progress (Kodey Silknitter and Dr. Benjamin King, personal communication).

Table B.1. RNA-seq reads of *gmppb* transcripts in *gmppb* mutants. Four distinct classes of splice variants were detected in *gmppb* mutants. Protein products were predicted using the Open Reading Frame (ORF) Viewer Tool. *Data provided by Dr. Benjamin King (personal communication).*

Category of Read	Predicted Protein Product
Properly spliced (normal)	Normal protein product
Unspliced	Currently Unknown
7 base pair insertion from intron	Frameshift with premature stop codon at amino acid 59
8 base pair cassette insertion and 8 base pair insertion from intron	Frameshift with premature stop codon at amino acid 58
24 base pair cassette insertion and 8 base pair insertion from intron	Frameshift with premature stop codon at amino acid 47

Figure B.1. Examples of RNA-seq reads of *gmppb* transcripts. (A) Correctly spliced read. **(B)** Mis-spliced read with 7 bp insertion from intron (red box). **(C)** Mis-spliced read with 8 bp cassette insertion (gray box) and 8 bp insertion from intron (red box). **(D)** Mis-spliced read with 24 bp cassette insertion (gray and blue boxes) and 8 bp insertion from intron (red box). Exon 2 sequences are in green font, exon 3 sequences are in blue font. The last base pair of exon 2 and first base pair of exon 3 are surrounded by a yellow box. *Data provided by Kodey Silkmitter and Dr. Benjamin King (personal communication).*

A

```
>PROPERLY_SPLICED_MUT_3_CGCTCATT-GGCTCTGA_L001_R2_005_paired.fastq
CCTCACTGTGCCAAACCACTCGTTGAGTTCTGCAACAAACCCATTCTGCTGCATCAGGTGGAGGCTTTGGTC
AAAGCTGGAGTCCGTCAGGTCATCCTTGCTGTGAGTTACATGTCTGAGCTATTGGAGCGAGAGATGAGAGCC
CAGGAG
```

B

```
>03_MISSPLICED_MUT_1_ATTACTCG-GGCTCTGA_L001_R2_001_paired.fastq
CTGACCTATAATGAAAGCTCTGATTCTTGTCCGGTGGCTATGGCACACGATTACGGCCGCTCACCCCTCACTGTGC
CCAAACCACTCGTTGAGTTCTGCAACAAACCCATTCTGCTGCATCAGGTGGAGGCTTTGGTCAAAGTGTTCAGG
CTGG
```

Insertion from intron →

C

```
>08_MISSPLICED_WITH_EXTRA_C_MUT_1_ATTACTCGGGCTCTGA_L001_R2_003_paired.fastq
TGGCACACGATTACGGCCGCTCACCCCTCACTGTGCCAAACCACTCGTTGAGTTCTGCAACAAACCCATTCTGC
TGCATAGGTGGAGGCTTTGGTCAAAGCTGTTGTAAGTGTTCAGGCTGGAGTCCGTCATGTCATCCTTGCTGTGAG
TTA
```

← insertion from intron

8bp additional insertion that is not contiguous intronic sequence

D

```
>49_STRANGE_MUT_3_CGCTCATT-GGCTCTGA_L001_R2_005_paired.fastq
AGTTCTGCAACAAACCCATTCTGCTGCATCAGGTGGAGGCTTTGGTCAAAGTGTAACTTAATTAAGCTGTTGTA
GTGTTCAGGCTGGAGTCCGTCATGTCATCCTTGCTGTGAGTTACATGTCTGAGCTATTGGAGCGAGAGATGAG
AGAG
```

← insertion from intron

24bp additional insertion that is not contiguous intronic sequence

BIOGRAPHY OF THE AUTHOR

Erin Bailey grew up in southern Maine and graduated with honors from Marshwood High School in 2009. She attended the University of Maine for undergraduate studies and graduated *summa cum laude* with Highest Honors in 2013 with a BS in Biochemistry, Molecular and Cellular Biology, and Microbiology. As an undergraduate, Erin studied the evolution of innate immune receptors to pathogenic fungi in Dr. Rob Wheeler's lab and was a 2012-2013 Goldwater Scholar. She returned to the University of Maine to earn a PhD in Biomedical Sciences in fall 2013 and officially joined Dr. Clarissa Henry's lab in July 2014. In addition to research, Erin served in Graduate Student Government for a year and a half, was a teaching assistant for laboratory courses in the School of Biology and Ecology and served as the 2016-2017 GSBSE monthly meeting coordinator. Erin received several awards as a PhD candidate: she was the 2017 recipient of the GSBSE service award, placed twice in the GSBSE annual meeting's oral presentation competition, and was a 2017-2018 Chase Distinguished Research Assistant. She is a co-author on three publications (she is second author on two of these) and recently re-submitted a revised first author manuscript. After graduation, Erin is switching to the *Drosophila* model system for her postdoctoral research to study wound-induced polyploidization in Dr. Vicki Losick's lab at Boston College. Erin is a candidate for the Doctor of Philosophy degree in Biomedical Science from the University of Maine in August 2019.